Spring 3-10-2014

Neural Correlates of Reach Planning and Execution

Thomas Pearce
Washington University in St. Louis

WASHINGTON UNIVERSITY IN ST. LOUIS

Division of Biology and Biomedical Sciences
Neurosciences

Dissertation Examination Committee:
Daniel W. Moran, Chair
Dennis L. Barbour
John P. Cunningham
Baranidharan Raman
Lawrence H. Snyder
Kurt A. Thoroughman

Neural Correlates of Reach Planning and Execution

by

Thomas Michael Pearce

A dissertation presented to the
Graduate School of Arts and Sciences
Of Washington University in
partial fulfillment of the
requirements for the degree
of Doctor of Philosophy

May 2014

St. Louis, Missouri

Contents

List of Figures

Acknowledgments

I would like to take this opportunity acknowledge the individuals and institutions that have supported me through the course of my education. First I'd like to thank my wife Sarah, who has given me her unconditional love and support throughout this process. She not only tolerated my long hours in lab and on the computer, and my preoccupation with science, she provided me with reasons to step back and enjoy the rest of life too. I would also like to thank my family – Bob, Margie, Tim, Amy and Christopher, as well as the extended clan. Being surrounded by your knowledge, love, and competitive spirit has made me who I am. I'd like to thank the Washington University Medical Scientist Training Program, the National Institute of Neurological Disorders and Stroke, and the Cognitive and Computational Systems Neuroscience training grant sponsored by the National Science Foundation for providing financial support for my education, without which this work would not have happened. My scientific and personal interactions with my colleagues in the Moran lab, particularly Adam Rouse, Jordan Williams and Jesse Wheeler, were the source of much pleasure, personal growth, and many excellent ideas. Thanks to Donna Reedy for her help training and caring for the monkeys. Thank you to my entire thesis committee for providing valuable advice and insight throughout this experience. Finally, without the mentorship, encouragement, guidance and support of my advisor Dan Moran, none of this would have been possible. Thank you.

ABSTRACT OF THE DISSERTATION

Neural Correlates of Reach Planning and Execution

by

Thomas Michael Pearce

Doctor of Philosophy in Biology and Biomedical Sciences
Neurosciences

Washington University in St. Louis, 2014

Professor Daniel W. Moran, Chair

Humans and other primates often interact with the world by reaching and grabbing objects with their hands. This seemingly simple activity is a challenging computational problem that requires the nervous system to transform sensory input into muscle activations that move the hand appropriately through space. This dissertation investigates neural activity in the dorsal premotor cortex of the macaque monkey while simple and complex reaching movements are planned and executed. A novel virtual-reality obstacle-avoidance task is used to decorrelate the direction of the initial segment of the trajectory from the direction of the final target. An unobstructed center-out task is used as a comparison. The firing rates of many neurons are modulated by kinematic factors including hand position and movement direction. During obstacle-avoidance reaching, both the initial segment and final target directions are represented in the firing of dorsal premotor neurons. Population decoders for position, velocity and target direction were built using the indirect optimal linear estimator method, a variant of the population vector algorithm. The decoding model constructed from the direct-reaching task ultimately predicts the direction of movement, not the final target, during the planning period before movement begins. A separate

decoding model predicts the target direction when the hand must move elsewhere initially. The time course of neural activity during planning suggests that the two monkeys utilized different preparatory strategies during the obstacle-avoidance task, leading to differences in performance on a subset of trials. A position-based population decoder predicts the hand trajectory during movement, anticipating the real hand position by approximately 200 ms. These findings demonstrate that multiple kinematic parameters of hand movement are represented in dorsal premotor cortex during planning and execution of voluntary reaching behavior. A simple linear decoding scheme based on roughly cosine-tuned spiking activity can extract relevant information from the population of neurons. This work contributes to the overall understanding of the factors that influence dorsal premotor cortical activity during complex reaching movements.

1 Introduction

1.1 Overview

In the dorsal premotor area of the cerebral cortex of primates, neural firing rates carry information about planned arm movements. This thesis examines neuronal activity in dorsal premotor cortex (PMd) during simple and complex reaching tasks. A novel obstacle-avoidance task was designed to induce rhesus macaque monkeys to move their hands along curved, indirect trajectories in a virtual environment. An unimpeded straight-line reaching task was used as a comparison. As the monkeys performed these tasks, penetrating intracortical electrodes were used to measure extracellular potential within PMd, including the electrical signatures of one or more spiking neurons. The data set for this thesis consists of the activity of over 1100 neurons from three hemispheres of two monkeys. For each neuron, the corresponding behavioral set comprises 300-500+ reaches in a virtual reality environment.

This document is organized as follows: Chapter 1 provides an introduction to the field of primate motor cortical neuroscience, specifically focusing on previous studies of primary motor and premotor cortical activity in nonhuman primates that provide the background and motivation for the current line of experiments. Chapter 2 details the methods that were used to generate the data, including training the monkeys in a virtual reality environment, recording hand kinematics and neural activity, and preprocessing the data. Chapter 3 examines the diverse and heterogeneous firing rate patterns displayed by individual neurons during a complex set of reaching movements. Chapter 4 focuses on population-level decoding of kinematic variables during planning and execution of reaching movements using the indirect optimal linear estimator, a variation of the basic population vector algorithm. Chapter 5 applies a recently-

developed dynamical systems framework to examine the neural data for evidence of intrinsic population dynamics. Chapter 6 concludes by a discussing these findings in the context of previous studies and proposes future directions of research.

1.2 Introduction

What makes an animal an animal? A humpback whale breaches the ocean surface, slapping the water with a fin. A lion perks an ear at the sound of a gazelle walking by. A human reaches for a sharpened stick at the sight of an unidentified intruder. An ant picks up a crumb of food and carries it back to the nest. With a few exceptions, a defining characteristic is the presence of a nervous system, which allows animals to detect and respond to their environments through appropriate actions. The abilities to escape from harm, travel in search of food and water, and seek out mates are fundamental aspects of animal life. These activities, and many others, are achieved through coordinated, time varying sequences of muscle contractions, controlled via innervation of the musculature. A control system to generate patterns of neural firing which lead to appropriate movement of the body is thus highly advantageous.

Movements can broadly be grouped into the general categories of voluntary and involuntary. Involuntary movements include reflexes, like the patellar tendon stretch reflex (knee jerk) tested by physicians during routine physical exams. Such reflexes require only that the circuitry from the limb to the spinal cord and back be functional - no input from the brain is required, though it does have a modulatory role; reflexes become hyperactive in the absence of descending input. In contrast, voluntary movements - like the doctor rapping your knee with the hammer during the physical - originate in the cerebral cortex and require an intact descending corticospinal tract to succeed. Primates, including humans, have highly evolved voluntary motor

control systems, and are particularly facile at making intentional arm and hand movements to interact with the environment.

From an engineering perspective, the everyday movements we take for granted, like drinking a glass of water, are staggeringly complex. Considering only the upper limb, to move ones hand toward a glass of water involves three degrees of freedom (DOF) at the shoulder, one at the elbow, and three at the wrist. Those seven DOF are used just to translate and rotate the hand through space - 17 additional DOF are involved in shaping the hand appropriately to grasp the glass. The system is underconstrained, meaning that there is no unique solution of muscle activations to achieve a particular desired movement. In addition, there is a substantial delay between sending a signal to move and receiving feedback about the resulting action, due to the relatively slow conduction velocity of even the largest axons. In spite of this, even a small child is vastly superior to the most sophisticated artificial system at performing at such a task.

The motor control system also must account for the dynamics of the external world. To continuing the example of reaching for a glass of water: Once the container has been grasped, the mass of the hand has, in effect, increased. This requires a compensatory change in the forces being generated, to avoid the unwanted outcome of the hand dropping and spilling the beverage. Once the hand and glass begin the return trip towards the mouth, another difficulty arises: The liquid in the glass can slosh around, producing moment-by-moment variability in the distribution of mass within the system. Perhaps this example action is occurring while the child is riding in a car, and inertial forces arise as the car is rounds a bend in the road. Finally, the system must be capable of both rapid adaptation and longer term learning, because both the environment and the body change over time. The car is not always going around a bend; the water glass may be heavier or lighter, or more or less full of liquid; the length of the arm changes as the child

matures; the muscles strengthen with exercise. Even the most routine of actions can pose immensely difficult computational problems, yet the nervous system is capable of generating elegant, precise, purposeful movements.

Losing the ability to make precise, purposeful movements is a devastating consequence of a variety of illnesses and injuries. These ailments often severely limit the ability of patients to lead "normal" lives, and effective treatments are a major research goal. Examples include Parkinson's disease, amyotrophic lateral sclerosis (ALS, aka Lou Gehrig's disease), spinal cord injury leading to para- or tetraplegia, and limb amputation. In each of these cases, motor cortical areas are intact, but the descending motor output system is compromised (or in the case of amputation, the effector has been lost). A developing therapeutic avenue for these disorders is a class of devices termed "brain-computer interfaces" (BCIs), which have the potential to restore lost functionality to these patient populations. BCI systems measure neural activity related to the intention to make a movement, decode the intended action, and perform the action artificially, bypassing the compromised output system. Through this process, direct control of external devices ranging from computer cursors to prosthetic limbs to robotic arms has been achieved.

The benefits of studying the motor control system are myriad. The knowledge that movement intentions can be decoded from neural activity is the basis for the development of BCI devices. A deeper understanding of the cortical circuitry responsible for generating naturalistic actions promises to further improve these systems. Beyond the therapeutic possibilities, a mechanistic description of how the nervous system solves the problems of generating movement could serve as inspiration for biomimetic control systems, in robotics or artificial intelligence applications. In particular, the ability to cope with noisy and incomplete information and to adapt to changes in the environment would be of great benefit. And in the domain of the

neurosciences, voluntary movement intersects with other important processes such as plasticity, adaptation, learning and memory; sensorimotor transformations; reward and decision making; attention and error processing; and many others. The neural circuitry responsible for generating purposeful actions is in some sense a window into all of these processes. After all, our actions are how we respond to events and influence our world.

1.3 Background

1.3.1 Model organism: the awake, behaving monkey

Much of our knowledge of the neuronal substrates of movement generation comes from invasive neurophysiological recordings taken from the motor systems of animals. For a number of reasons, the macaque monkey has long been the model organism of choice for studying voluntary motor control (Evarts, 1966). First, there exist substantial functional and structural homologies between macaque and human brains, particularly in the visuo-motor cortical networks. Like humans, macaques have well-developed visual systems, and regularly reach for visually-identified targets (such as food). Second, the musculoskeletal system of the upper limb is structurally similar to the human arm, and macaques make reaching movements very similarly to humans. This allows researchers to interrogate neural correlates of processes like motor adaptation and learning, which have been extensively studied via human psychophysical experimentation. Third, macaques can be trained to perform complex tasks, making it possible to experimentally manipulate the reaching behavior. The widespread use of this animal model is also advantageous in that well-developed neuroanatomical atlases are available for localization of cortical structures, and it allows a more direct comparison of experimental results with other studies in the scientific literature than if a variety of animal models were used.

1.3.2 Many motor cortical neurons broadly tune to movement

Building on Evarts' pioneering recordings of electrical activity from motor cortical neurons in conscious, behaving monkeys (Evarts, 1968, 1968), Georgopoulos introduced the widely-used "center-out" reaching task, which forms the basis for many subsequent studies including this thesis (Georgopoulos et al., 1982). In this paradigm, the subject's hand begins each reach at the same central location (the "center") and moves "out" to a peripheral target located on a circle centered on the start position. A set of reaches samples movements in all directions – for example, 8 targets spaced 45 degrees apart. Movement-related discharge of many primary motor (M1) neurons was found to vary as a function of hand direction: the highest firing rate occurred in one direction, the lowest in the opposite direction, and a smooth transition from high to low at intermediate directions. When the neural activity was plotted as against movement direction for each trial, the data were well-fit by a cosine function. This type of relationship between extrinsic parameters (such as direction or hand position) and neural firing rate is termed "cosine tuning," and the angle that generates the maximal firing rate is referred to as the "preferred direction" of a neuron.

Although cosine-tuned neurons are a common finding in the motor cortical literature, it should be noted that not all neurons can be categorized this way. The original center-out study found that ~75% of task-related neurons were cosine-tuned, while 25% had different, more complex activation patterns (Georgopoulos et al., 1982). In a 1978 study, Thach described a wrist-movement task that dissociated muscle activations, wrist position, and the direction of the upcoming movement (Thach, 1978). Roughly equal proportions of primary motor cortical neurons were categorized as being related to muscle, position, and direction. It was noted that while the muscle-related neurons formed an isolated group, there was substantial overlap in the

populations that correlated with the kinematic variables (position and direction). Similarly, in a 3D reaching task hand position and velocity were found to be represented in overlapping populations of M1 neurons (Wang et al., 2007). 36% of recorded units in that study did not significantly tune to either kinematic parameter. In addition, the fact that a linear model is statistically different than zero does not mean it is a thorough description of the response pattern of a neuron: additional, untested linear or nonlinear factors may also influence the firing rate. Nonetheless, simple linear tuning models provide a useful way to test for relationships between movements and neuronal activity.

1.3.3 Preparing and executing movement: Primary and premotor cortices

Movement-related modulation of neural firing rates in M1 neurons typically begins approximately 100-200 ms prior to movement onset and lasts through the action (Georgopoulos et al., 1982). In contrast, neural responses in the adjacent premotor (PM) cortices are not limited to the peri-movement time. Rather, the discharge rate shows evidence of cosine tuning shortly after an instruction to make a future movement, even if the physical action is not to be executed until a later time. This activity pattern is maintained for the duration of the so-called "instructed delay" period, and is one of the defining characteristics of premotor areas. Since neurons reflect the upcoming movement as soon as the relevant information is known, preparatory activity in premotor areas is considered to be a cortical substrate of motor planning. In general, PM areas are similar to M1 in that many cells are broadly tuned to various features of movement. In addition to neuronal modulation occurring earlier in PM, the modulation is thought to be driven by a mix of sensory and cognitive as well as motor functions (Wise et al., 1997).

Anatomically, PM is located just rostral to M1 and lateral to the supplementary motor area (SMA). Compared to M1, PM areas are less granular and more heavily interconnected with

sensory and association areas in prefrontal and posterior parietal cortex (Lu et al., 1994; Wise et al., 1997). These histological features exist along a gradient, transitioning smoothly along the rostral-caudal axis into M1. The lack of sharply-demarcated cytoarchitectural boundaries, both between PM and M1 and within PM, generated much historical disagreement over the definition of PM as a distinct cortical area. Beginning in the 1980s, single-unit delay period activity from reaching tasks was used to characterize the function of these areas, which helped further distinguish them from M1 (Godschalk et al., 1981, 1985; Weinrich and Wise, 1982; Weinrich et al., 1984; Kurata and Tanji, 1986). Based on anatomical studies (Muakkassa and Strick, 1979) and observations of functionally distinctive patterns of neural activity, researchers have subdivided PM into dorsal and ventral aspects (PMd and PMv, respectively). Some studies go a step further and describe differences between the rostral and caudal parts of each (Barbas and Pandya, 1987; Rizzolatti et al., 2002). Similarly, M1 itself has distinct functional differences along the rostral-caudal axis, with direct projections to alpha motoneurons in the spinal cord limited exclusively to the caudal portion in the bank of the central sulcus (Rathelot and Strick, 2006). Next, we review some of the experiments that helped refine the definitions of these cortical areas.

Dorsal premotor cortex (PMd) is strongly activated during sensory-guided reaching tasks. Many neurons are tuned to an instructed reach direction, regardless of whether the contralateral or ipsilateral arm is to be used (Cisek et al., 2003). If multiple possible targets are displayed, PMd neurons encode all targets initially, and change over time to represent only the chosen target (Cisek and Kalaska, 2005). Ebner showed that firing rates of PMd neurons depend not only on direction but also target location, distance, and movement speed, and that the representation can evolve in time over the course of a trial (Fu et al., 1993, 1995). Recent studies

have emphasized the role of PMd in abstract movement planning (Cisek et al., 2003; Cisek and Kalaska, 2004, 2005; Nakayama et al., 2008).

The evidence that PMd is an important region in reach planning is not limited to monkey electrophysiological experiments. Human imaging and transcranial magnetic stimulation studies have shown a similar organization and specialization of PMd for sensory-guided movements (Boussaoud, 2001; Simon et al., 2002). Microstimulation and somatosensory mapping studies have suggested a rough somatotopic organization within PMd: proximal forelimb movements were elicited more often medially and distal more laterally, though in overlapping regions (Raos et al., 2003). Using a long-duration pulse-train stimulation paradigm, Graziano elicited movements to specific postures, often with the arm extended into the space in front of the subject (Graziano et al., 2002). These studies and many others support the idea that PMd is intimately involved in the planning and control of reaching movements (see (Shadmehr and Wise, 2005) for a thorough review).

As with PMd, many ventral premotor (PMv) neurons are active during arm and hand movements (and the planning of such). In a visual illusion study, researchers gradually altered the relationship between visual feedback and hand movement during a drawing task in virtual reality. Population activity in PMv closely matched the visual movement on the screen, while a population from M1 was predictive of the hand path through space(Schwartz et al., 2004). In a different study, wrist movements were dissociated from arm posture, allowing classification of neurons in PMv as “extrinsic-like” or “muscle-like” depending on whether the preferred direction changed when the wrist was rotated 180 degrees from pronated to supinated. PMv neurons were overwhelmingly found to be “extrinsic-like” during both the planning and execution epochs (Kakei et al., 2001) Along the rostral-caudal PMv axis, the caudal subregion

appears to be more proximally-oriented, related to things like reaching movements, while rostral PMv is more closely associated with hand shape and grasping activities. The putative "mirror neuron" system was first identified in PMvr (also known as area F5), where researchers identified cells that responded both when grasping an object and when observing another individual performing the same action (Gallese et al., 1996). Another characteristic of PMv is that neurons respond strongly to objects in peripersonal space, irrespective of the sensory modality (vision, somatosensation, audition) that detects the stimulus (Graziano et al., 1997, 1999). Ongoing studies continue to characterize functional differences in the subregions that make up the premotor cortices (Fujii et al., 2000; Boussaoud, 2001; Picard and Strick, 2001; Hoshi and Tanji, 2002, 2007; Abe and Hanakawa, 2009). Although many of the neurophysiological experiments discussed here were designed to emphasize distinctions between subregions of premotor cortex, a unifying theme is that neural activity in PM areas provides a signature of (skeletal) movement planning.

1.3.4 Directional tuning: selecting a target, or planning a movement?

In PMd, like the neighboring M1, many neurons are broadly tuned during reaching to kinematic variables such as the hand position or velocity. One of the fundamental challenges of determining whether various parameters correlate with neural firing is that many of these factors correlate with each other as well. This is particularly true during the basic center-out task: in straight-line movements, the hand position, target direction, and velocity vectors are all highly correlated. Neural activity that correlates with one of these parameters necessarily also correlates with the others, and the true contribution of any one factor to the overall firing rate is difficult to determine. For this reason a common experimental strategy is to create tasks that dissociate various movement parameters from each other, making it possible to distinguish the

contribution of each to the overall neural activity. Bauswein and Fromm demonstrated that when an animal's hand is passively moved to a new starting location before movement is cued, delay-period PM activity shifts to reflect the new direction of the reach (Bauswein and Fromm, 1992). When the stimulus is divorced from the movement direction - that is, the target of the reach is located somewhere other than where the visual information was presented - neuronal activity reflects the direction of the upcoming movement, not the stimulus location (di Pellegrino and Wise, 1993; Crammond and Kalaska, 1994). These studies indicate that directional tuning is not exclusively representing target or stimulus locations in extrinsic coordinates, but rather relates to some feature of the planned hand movement. It is not clear from these studies, however, whether the tuning reflects the movement direction or the target direction relative to the hand.

1.3.5 Evidence for target encoding

An emerging view of the role of PMd in reach planning is that its directionally-tuned neurons encode a vector pointing from the hand to the desired endpoint or target of the reach. Based on a study which reported that a majority of PMd neurons during a remembered-target reach were both directionally tuned and modulated by target distance (Messier and Kalaska, 2000) , the Shenoy group reported a brain-computer interface which used PMd activity to predict a monkey's goal from a discrete set of possible targets, allowing the system to move the cursor directly to the intended target (Santhanam et al., 2006). The finding that goal information can be predicted from PMd activity is in agreement with another study that showed M1 activity was more suitable for decoding online movement while PMd firing was better predictive of discrete targets (Hatsopoulos et al., 2004). We find this result intuitive, given that M1 lies closer to the actual motor output than does PMd. These studies and others have been interpreted as indicating that PMd encodes the location of a target to be reached for, not the intended trajectory. As an

example, a 1997 study by Shen and Alexander used an elegant experimental design in which a monkey used a joystick to move a cursor in a center-out task. The critical aspect of the task was that two mappings of joystick position to cursor position were used, which differed by a 90 degree rotation about the center of the workspace, such that in some trials the animal moved its hand forward to move the cursor to an upward target, while in others it moved its hand to the right to achieve the upward target. The results of the study showed that the vast majority (> 90%) of directionally tuned PMd neurons reflected the visual target location, not the limb trajectory (Shen and Alexander, 1997).

1.3.6 The role of visual trajectory

Although there is evidence for target encoding, it remains plausible that PMd activity represents a trajectory plan, as the endpoint-only hypothesis has not been fully examined. When planning a reach, both the path and the end point can be important. We find it likely that PMd encodes multiple parameters of an intended movement, particularly when the trajectory of the hand is important as well as the target of the reach. However, the critical experiments needed to test this hypothesis have not been carried out because the standard center-out tasks used to study reaching in monkeys generate minimally curved trajectories which lead directly to the target. Under these circumstances, activity that is predictive of the target direction could also represent the intended trajectory of the end-effector in visual space. Actual reach trajectories that are not straight toward the target could result from a transformation from visual to limb coordinates downstream from PMd. Since the reach trajectory is not spatially constrained by the task, any solution which ultimately achieves the goal would be satisfactory even if it did not perfectly follow the intended path. In this case, even if the visual trajectory did not perfectly match the prediction, there would be little incentive to continue refining the motor output. In this manner,

a mismatch between planned and executed trajectories could persist, leading to the interpretation that trajectory planning is unimportant.

Viewed in a visual-trajectory framework, the results of Shen and Alexander's joystick remapping task (in which the hand direction changed, while the visual direction remained the same) can be interpreted as evidence for a trajectory plan in a visual reference frame as opposed to a limb-centric reference frame. Although this was not the authors' interpretation, it is consistent with a study which showed that during a tracing task with a distorted mapping of hand position to cursor location, a population vector from premotor cortex reflected visual cursor movement, while M1 activity reflected the actual hand movement (Schwartz et al., 2004). During the movement itself, a third possibility arises: directional tuning could reflect the instantaneous direction of movement, the original hand-target direction, or an instantaneous hand-target direction. Again, for unconstrained straight reaches, all three vectors are aligned so distinguishing which direction is encoded is difficult. During the movement, of course, the hand speed and distance to the target are changing, but the directional component remains the same. It is unclear how hand speed and target distance interact with directional tuning in PMd, making it difficult to unambiguously determine what aspects of the movement are encoded if the reach path is directly toward the target. Simply put, based on the current literature, PMd neurons can reasonably be interpreted to encode the intended visual trajectory of a reach or the direction and distance of an intended end-point. By dissociating initial trajectory and endpoint directions, the experiments in this thesis are designed to directly examine this distinction.

1.3.7 Direct and indirect trajectories

Why draw a distinction between neuronal encoding of target direction and hand direction (or velocity vector)? Because in real-world activities, unlike simplistic experiments, it is

common to move one's hand along a trajectory other than directly to the target. For example, a reach target might be a glass of water on a dining table, surrounded by dishes and candlesticks; disturbing the food or fire would be an undesirable consequence of an errant hand path. Later, while cleaning up after the meal, dirty utensils on a countertop could be placed into an under-counter dishwasher. Moving one's hand directly from above to below the countertop, however, is physically impossible – completing the task requires an alternative spatial strategy. Of course, other situations may occur when a straight-line movement is not only permissible, but desirable. And many times, there are only loose constraints; both direct and indirect trajectories would be acceptable. Ultimately, both the endpoint of a reach and the trajectory of the arm and hand through space are important to the success of many actions.

A number of human behavioral studies have examined the psychophysics of reaching in the presence of obstacles. In one experiment, subjects working on a virtual 2D task space were instructed to move a circle centered at their fingertip from one target to another, avoiding the tip of a visually presented obstacle located between the targets (Sabes and Jordan, 1997). One finding from this study was that subjects moved asymmetrically with respect to the obstacle, which contrasts with the symmetric trajectory predicted by a maximum-smoothness control system. Additionally, the reach trajectories were rotationally asymmetric, with near-point angles (a measure of the shape of the path as it passed the obstacle) differing with rotation of the entire target-obstacle-target workspace. The authors proposed a control mechanism which took the anisotropic sensitivity of the arm to uncertainty or perturbations into account, using postural information at least indirectly to inform the best trajectory. A subsequently published study expanded this paradigm into the 3D workspace (Sabes et al., 1998). The results of the 2D study were revisited in a 2002 theoretical paper, which simulated the task using a model which

minimizes mean-squared error at the target while keeping the probability of collision with the obstacle below a threshold value in the presence of signal-dependent noise (Hamilton and Wolpert, 2002). The model qualitatively reproduced some of the observed movement features, including asymmetric trajectories. Other studies have examined the impact of obstacles in the workspace on reaching kinematics. In one example, it was recently found that subjects react more slowly to moving obstacles than they do to moving targets, suggesting a difference in the visuomotor processing of these objects (Aivar et al., 2008). The results of these and other human behavioral studies highlight the importance of examining motor control in cases other than simple straight-line reaches.

Few studies have examined indirect reach trajectories in non-human primates. In 2006, Torres and Andersen reported the behavioral results of training monkeys to reach to targets in the presence of cylindrical obstacles (Torres and Andersen, 2006). The experimental setup involved a frontoparallel workspace containing buttons with light-emitting diodes (LEDs) indicating targets of delayed center-out reaches. During the reach itself, all LEDs were extinguished and the subject was in the dark. Blocks of unobstructed reaches were alternated with blocks with cylindrical obstacles protruding from the board. The monkeys had knowledge of the presence of the cylinders, as they could see the researchers placing them with the lights on. For some targets, the size and position of these obstacles precluded the animals from making straight-line reaches to the remembered location. Based on the observed motor output in these alternating blocks, the authors claim a dissociation of spatial and temporal components of movement planning. They note that the animals succeeded in avoiding the obstacles on the very first reach following obstacle placement, and over the course of the block the trajectory did not significantly change. What did change was the overall speed profile of the reach, which initially had multiple peaks,

indicating a halting, broken movement. Over time, the movements resolved to resemble a smooth, single-peaked speed profile. The authors interpreted their results as showing that "paths are anticipated before the movement takes place, show an immediate spatial strategy, the paths are time invariant, and that the first impulse of the motion is under cognitive control. The type of precomputation that best characterizes our data is geometric— i.e., independent of the motion dynamics—yet provides a signal ready for the execution system." Recently the Shenoy lab recorded from M1 and PMd during a task that required monkeys to navigate a "maze" with their hands, avoiding contact with "walls" in various configurations while making center-out reaches (Churchland et al., 2006, 2010). In that study, target location and initial velocity both correlated reasonably well with the neural data; however, they were not explicitly dissociated across conditions, and the analysis and interpretations were focused elsewhere. Other studies likewise provide some degree of electrophysiological evidence that neural firing in PMd is influenced by the movement path, and not simply the endpoint (Hocherman and Wise, 1991; Ajemian et al., 2001). For a number of reasons, however, including the presence of intermediate targets, the limited set of movements which were studied, and the lack of systematic characterization of tuning curves, it is difficult to draw strong conclusions based on these data.

1.3.8 Population decoding

The concept of a neuron "tuning" to a spatial parameter is essentially a description of a commonly observed phenomenon – a systematic relationship between discharge rate and some feature of the arm movement. Along with the initial description of cosine tuning in motor cortical neurons, Georgopoulos proposed that any direction of movement could be encoded at the population level via the discharge pattern of many such cells with overlapping directional response functions. A natural follow-up question was then asked: given the firing rates from a

population of neurons, can the direction of movement be *decoded*? A simple linear decoding scheme, the "population vector," did just that (Georgopoulos et al., 1986). The preferred direction was measured for each cell in a recorded population, and used as a vector which was scaled by the instantaneous discharge rate of that neuron. Vectorially summing all of the individual neuron contributions yielded a population-level estimate of the 3D movement direction that closely matched the actual direction of the hand as it translated through space.

When the spatial distributions of preferred directions (PDs) of a population of neurons is uniform, the population vector algorithm (PVA) provides a good mapping from firing rate onto a stimulus condition (hand movement, typically). Practically speaking, measuring a uniform distribution is not common; sampling effects and/or underlying non-uniformity in the total population lead to conditions where a PV is less than ideal. The optimal linear estimator (OLE) method uses weighted-least-squares linear regression over a whole population of neurons to generate a set of weights (vectors) that provide theoretically optimized decoding performance (Salinas and Abbott, 1994). These optimal weights are utilized equivalently to preferred direction in the original PVA; both methods are linear predictions of a stimulus based on measured neural activity (Kass et al., 2005). A further extension of the method, the indirect OLE, uses encoding vectors calculated separately for each neuron to compute the optimal set of decoding weights (Wang et al., 2007). This technique combines the improved decoding of the OLE with the advantage that, like the original PVA, it requires knowledge only of the PD of each neuron, not the full neural and kinematic training data sets. The PD can be determined for each neuron from a distinct set of kinematic conditions, allowing neurons recorded during different behaviors to be utilized in the population decoder.

PVA and its offshoots provide a way to determine a sort of average response over many neurons. From the earliest studies making use of cosine-like tuning and population vectors, these analysis techniques have generated controversy. The principle objection is that only a portion, and often a very small portion, of the variance in neural firing is explained using these analyses. This is a valid observation; it would be problematic if the goals of the studies were to fully account for the entirety of the rate function of these neurons. However, population decoding can generate very useful information nonetheless. For example, a functional difference in PMv and M1 was found during a visual illusion (Schwartz et al., 2004). Population decoders were created from cells in these two regions as a monkey moved his hand along an elliptical path in a virtual reality system. Over time, the feedback gain along the major axis of the ellipse was reduced, and ultimately the monkey was making circular hand movements to generate the elliptical trajectory on the screen. During this process, the population decoder from PMv continued to decode the elliptical trajectory of the cursor. In contrast, the M1 population activity predicted the circular trajectory of the hand. Obviously it is neither the exclusive function of PMv neurons to represent cursor trajectory, nor of M1 neurons to represent hand velocity. Nonetheless, PVA offered insights about the function of these areas during the transformation from visual instructions to hand movements.

The emerging field of brain-computer interface technology frequently takes advantage of the fact that kinematic parameters can be extracted from neural data using PVA-based decoding schemes. External actuators from computer cursors to robotic arms can be controlled directly via purposefully-modulated cortical activity, provided that a user's intentions can be accurately estimated. So far, devices based on intracortically-recorded single units and local field potentials, sub- and epidural electrocorticography, and surface electroencephalography have

been demonstrated. The simplicity of linear decoders is advantageous for applications like BCI devices. Knowledge of which variables can be linearly decoded from specific cortical areas, and when the information is available in that area, is therefore useful for device development as well as being a generally interesting scientific question.

1.3.9 Cortical circuitry, dynamic systems, and neuronal variability

Of course, the ability to decode a particular variable, such as hand direction, from a population of neurons does not mean that the function of those neurons is limited to simply encoding that variable. Decoding studies ask the question: how well can neural activity explain various features of a stimulus, such as the orientation of a bar on a screen or the direction of an upcoming hand movement? A different question is how well stimulus features can account for neural activity.

Over the past 40+ years, many experiments have revealed relationships between neuronal firing rate and a host of extrinsic parameters, including but not limited to hand position, hand direction, hand speed, isometric force, wrist orientation and angular velocity, target direction, and muscle activation. In virtually every study, although many neurons show tuning to one or more of these parameters, many others do not. Tuning to one parameter does not preclude a neuron from tuning to others; many neurons are significantly modulated by both position and velocity, for example. In addition, even when a cell's firing rate is statistically significantly modulated by extrinsic parameters, these variables do not fully account for the variability of the firing rate. Other observations also highlight the complicated and poorly understood nature of motor cortical circuitry. For example, Georgopoulos noted in the original center-out reaching study that modulation of many neurons by hand direction was stronger (or exclusive to) goal-directed movements such as reaches to a rewarded target or corrections to keep the

manipulandum centered over a target. These same neurons failed to respond equivalently during other types of movements (Georgopoulos et al., 1982).

Recently, a hypothesis has been put forth that a substantial amount of the activity in motor cortical neurons may be due to intrinsically dynamical activity of the cortical circuitry, and is inherently unrelated to extrinsic factors (Churchland et al., 2010, 2012). In this view, neurons "tune" to intrinsic variables such as the firing of other neurons, perhaps in addition to any relationship that exists to extrinsic parameters. As with the longstanding controversy regarding whether M1 neurons should be considered muscle-like or kinematic-like, the truth is likely to incorporate elements of both. An attractive possibility is that examining neural firing as it relates to the activity of other neurons in the population will provide a different and complementary view of the function of motor and premotor cortices in generating voluntary reaching movement.

1.3.10 Aims of this work

The neural underpinnings of voluntary motor control make up a vastly complex system; individual steps toward understanding this system must necessarily be limited in scope. In this thesis, the central question is: Does planning-related directional tuning of macaque dorsal premotor neurons relate to the direction of a reach target or the direction the monkey is planning to move his hand?

To answer this question, a novel reaching task was developed to dissociate the initial direction of movement from the final target direction using virtual obstacles. Neurons were recorded from PMd during the planning and execution of reaches in the novel obstacle-avoidance task and a simpler center-out-based task. In chapter 3, the activity of individual neurons is examined for cosine-like tuning that linearly relates firing rate to kinematic

parameters of the behavior. The results are in agreement with other studies in the literature that many neurons show statistically significant kinematic tuning. Interestingly, both the target direction and initial movement direction are represented during planning, and individual neurons can significantly tune to both parameters during the same time period within the task. An unexpected negative correlation between preferred directions to the two parameters is observed and discussed. In chapter 4, kinematic parameters are decoded from the neural population using PVA-based analyses. A decoder based on the simple center-out task is ultimately predictive of the initial hand direction, not the target direction, when planning indirect reaches. At the same time, a different set of decoding weights additionally predicted the direction of the target at the population level. These and other findings are discussed. In chapter 5, the neural data are considered from the perspective of a dynamical system. Similarities and differences between these findings and those of the original study are examined.

It is hoped that the results of these experiments can help clarify ambiguity about the effects of reach targets and hand movement directions on neural activity in PMd, and will contribute to our understanding of this cortical area in the planning and online control of voluntary reaching behaviors.

2 General Methods

2.1 Experimental setup

Two male rhesus macaques (*macaca mulatta*), monkey G (~8 years old, 10kg) and monkey H (~5 years old, 6 kg), were used in these experiments. The monkeys were trained to perform reaching movements in a virtual-reality simulator (fig 2.1). First, the animals were operantly conditioned to leave their home cages and sit in open-sided primate chairs for transport from the vivarium to the laboratory. Each chair was configured to allow the subject to sit comfortably upon a perch, with the rigid collar secured into a slanted neck-level protective shield. A waist-level plate (and optionally, a belt-like ring) enclosed the lower-limb section of the chair and ensured that the subject maintained a seated posture. Each arm was loosely restrained using an adjustable armrest and a clear, rigid plastic tube. The restraint on the "working arm" was removed once the subject was secured into the experimental apparatus.

The experimental apparatus ("rig") was constructed from modular extruded aluminum T-slot framing members (80/20 Inc., Columbia City, IN, USA). The rig contained a bay for a primate chair; an LCD computer monitor mounted facing downward; an angled mirror underneath the monitor; and hardware for mounting the electrophysiological recording equipment. Once they were properly restrained, subjects were transported to the recording room on a wheeled trundle and inserted into the bay facing the angled mirror. Slots in the chair were aligned to matching ones in the bay and the chair was securely bolted in place. A black canvas barrier attached to the lower edge of the mirror was connected to the bottom of the neck shield. This served two purposes:

it kept the subject from bringing his hand to his mouth, and also obscured from view the area in which he moved his hand during the experiment.

Within the experimental recording room, the rig was oriented so the monkey was facing perpendicular to a 3-camera motion capture system (Optotrak 3020, NDI, Waterloo, CA), with the working arm positioned toward the cameras. An infrared LED marker was securely taped to the dorsum of the working hand, with the connecting wire running up the arm. A U-shaped stainless steel drink tube was placed on the neck shield within easy reach of the subjects' lips. One end of the drink tube was connected via flexible tubing to a reservoir, and liquid flow was controlled by a solenoid valve. Rewards were dispensed through a small hole in the bottom of the "U", and the distal end of the "U" was uncapped. This ensured that the subjects could not generate suction on the tube and obtain extra unearned liquid.

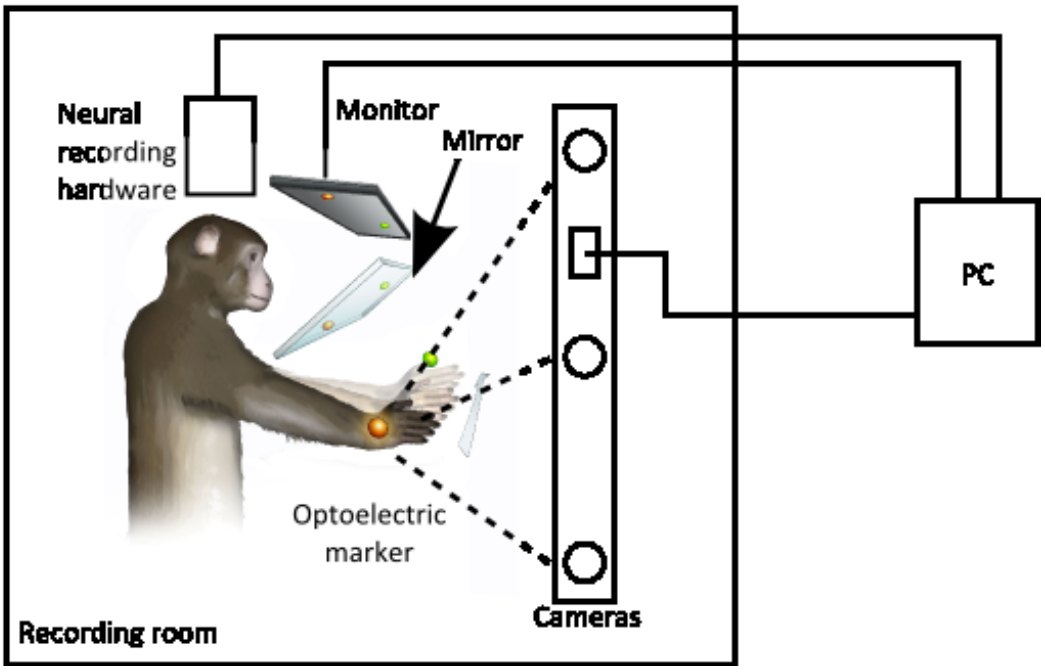

Figure 2.1: Schematic of the virtual reality setup.

2.2 Task control and kinematic data acquisition software

Behavioral tasks and training paradigms were controlled via custom C++ software. The software was developed in Microsoft Visual Studio 2005/2008 for use on the control PC, a Dell Precision T3400 workstation with an Intel Core2 Duo running 32-bit Microsoft Windows XP. A combination of proprietary C/C++ hardware interfaces and open-source C++ libraries were utilized in the control software. A multithreaded environment (via the OpenThreads library, www.openscenegraph.org) was developed to allow task logic to be continuously executed in a dedicated thread, uninterrupted by either the OpenGL rendering (OpenSceneGraph, www.openscenegraph.org) or the graphical user interface (Qt open-source libraries, Trolltech, Sweden. Available online at qt.digia.com).

The reaching tasks consisted of the subject moving his arm and hand freely in the space in front of him. The position of the infrared LED (on the back of the hand) was tracked in 3D space with a sampling frequency of 100 Hz by the Optotrak camera system. Position data were streamed to the control PC in "real time" for use controlling a spherical cursor, displayed simultaneously to the subject via the mirror/monitor located in the rig, and the experimenter in the next room. The real-time data stream was subject to occasional transmission delays and/or CPU slowdowns, leading to skipped frames and small perturbations in the timing of the incoming data points. For this reason, the measured position data were additionally buffered internally within the camera system, providing a higher-fidelity estimate of the marker position. During recording sessions, this buffered data was flushed to the PC between trials and saved for use in kinematic analyses.

2.3 Electrophysiological data acquisition hardware and software

Electrophysiological data were acquired using the Eckhorn Matrix 16-channel electrode drive (Thomas Recording, Germany), also referred to as the "Thomas drive". During recording sessions, multiple glass/tungsten microelectrodes (impedance = 1-2 MΩ at 1 kHz) were driven through the dura and into cortical tissue. Extracellular voltage was amplified via a 5x headstage amplifier (Thomas Recording), split, and digitized at 24,414Hz at two Medusa preamplifiers (TDT, Alachua, Fl). The spike-data preamplifier had a 1x gain and a 2.2Hz-7.7kHz bandpass filter, while the other had a 10x gain and a 3Hz-500Hz bandpass filter, and was used for LFP analysis (not presented in this thesis). From the preamps, the signals were fiber-optically transmitted to an RX5 Pentusa real-time processor (TDT). There, the signals were band-pass filtered on digital signal processors (0.3-5.0 kHz for spikes, 3-500 Hz for LFPs) and streamed to disk. To avoid this disk-IO-heavy process interfering with the task control and kinematic data acquisition procedures, the electrophysiological recordings were performed on a second PC. The electrophysiological data were synchronized to the task using a digital IO card (PCI-236, Amplicon, Brighton, UK). 1 ms pulses of high voltage were emitted from the task PC time-locked to trial events, detected by the TDT processor, and written to the data tank alongside the voltage streams. The durations of inter-pulse intervals was later used to synchronize the data from the two PCs.

2.4 Reward schedule

Food and beverage rewards were utilized to motivate the subjects during training and data recording sessions. Subjects were kept on a water-restricted diet, receiving a minimum of 15 ml/kg of water per day. In the rig, drops of water were delivered via the drink tube under computer control. Reward levels were continually monitored and adjusted to maintain subjects'

behavior and overall water consumption at appropriate levels. Between and after sessions in the rig, the subjects were rewarded with food treats and supplemental water or juice.

2.5 Behavioral tasks

Two variations of the basic center-out task (Georgopoulos et al., 1982) were used in this study. Although the hand was moving freely in three dimensions, in both tasks the hand position was projected onto a 2D frontal (coronal) plane and the third dimension (anterior/posterior) was irrelevant.

2.6 Center-out (with position)

This task, referred to in this thesis as simply as "center-out," involved direct point-to-point reaching, similar to the majority of previous experiments. Instead of a single starting position, a quincunx arrangement of possible centers was used (fig. 2.2a). This feature allowed the effects of hand position on neural firing to be determined during a time when the upcoming reach target was unknown, before a directional movement plan could influence neural activity. The sequence of events for each trial is below:

1) Center appears pseudo-randomly at one of 5 starting positions
2) Hand and cursor move to center location (duration: subject dependent)
3) Cursor-center contact; color change indicates contact
4) Delay period 1: target is invisible (duration: 500 ms)
5) Target appears pseudo-randomly in one of 8 directions from center
6) Delay period 2: target is visible (duration: 500-1300 ms, random uniform distribution)
7) Center disappears: go cue
8) Hand and cursor move to target location (duration: subject dependent)
9) Cursor-target contact; color change indicates contact

10) Hold period (duration: 500 ms)

11) Cursor freezes; color change indicates successful trial; reward delivered.

12) Reward and feedback period (duration: 500 ms)

13) Intertrial interval (duration: 600 ms [success] or 1100 ms [error])

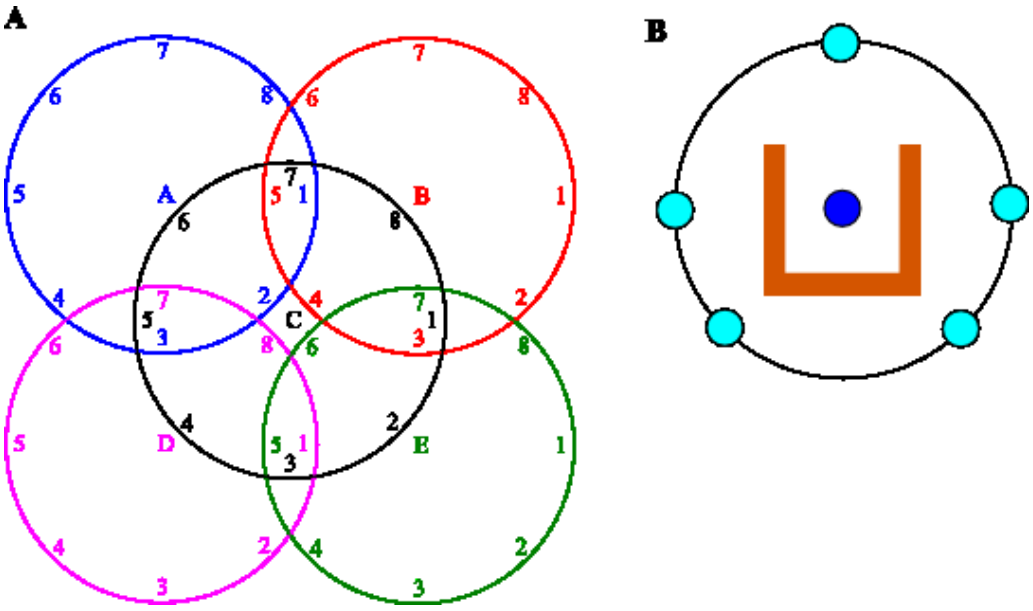

Figure 2.2: Task conditions. A) Direct center-out movements begin from 5 starting locations (A-E) with targets located in 8 directions (1-8). B) In obstacle-avoidance movements, 5 relative orientations of target and obstacle are possible. The configuration pictured here is rotated in 45^{o} increments such that the top target and obstacle opening are oriented at each possible target location.

2.7 Obstacle-avoidance

The obstacle-avoidance task was used to dissociate the initial hand direction from the target direction. In contrast to the center-out task, the starting location was always in the center of the workspace. During the pre-movement delay period, a 3-sided box appeared surrounding the center, limiting the initial portion of the movement trajectory to the direction of the opening in the obstacle (fig. 2.2b). Five relative orientations of the obstacle opening and target direction were used - $\pm 90^{o}$, $\pm 135^{o}$, and 0^{o}. In the 0^{o} condition the obstacle did not impede a direct reach. The sequence of events for each obstacle-avoidance trial is below:

1) Center appears at center of workspace
2) Hand and cursor move to center location (duration: subject dependent)
3) Cursor-center contact; color change indicates contact
4) Delay period 1: target and obstacle are invisible (duration: 500 ms)
5) Target appears pseudo-randomly in one of 8 directions from center
6) Delay period 2: target is visible, obstacle is invisible duration: 500 ms)
7) Obstacle appears pseudo-randomly in one of 5 relative orientations
8) Delay period 3: target and obstacle are visible (duration: 500-1300 ms, random uniform distribution)
9) Center disappears: go cue
10) Hand and cursor move to target location, avoiding contact with virtual obstacle (duration: subject dependent)
11) Cursor-target contact; color change indicates contact
12) Hold period (duration: 500 ms)
13) Cursor freezes; color change indicates successful trial; reward delivered.
14) Reward and feedback period (duration: 500 ms)
15) Intertrial interval (duration: 600 ms [success] or 1100 ms [error])

Catch trials - trials with no obstacle - were interspersed throughout the obstacle-avoidance task. On these trials the go cue was given immediately following delay period 2, at the time when the obstacle would normally appear.

2.8 Blocked task design and pseudo-randomization of conditions

The two tasks were performed in interleaved blocks of movements. Each block consisted of one successful trial of each reach condition – 40 conditions in center-out (5 centers x 8 targets), and 48 in obstacle-avoidance (8 targets x 5 obstacles + 8 catch trials, 1 to each target). Within a block, the specific movement condition for each trial was selected randomly from the pool of non-completed configurations. Upon successful completion of a trial, that condition was removed from the pool. After a block of movements was completed, a new block began. The desired behavioral session consisted of 5 blocks of each task. Although both subjects were highly trained on the tasks and very proficient at completing all conditions, the block order made a subjective difference in how cooperative and motivated they were during behavioral sessions. For example, on some days beginning the session with a block of obstacle-avoidance trials was not a problem. On others, however, during the first block the monkeys would make a high rate of errors by contacting the virtual barrier, and often became visibly frustrated and stopped working. Once they were allowed to do a block of easier center-out trials, they resumed working and subsequent blocks of the obstacle task were no issue. Similarly, at the end of a session the monkeys were more likely to complete blocks of center-out than blocks of obstacle-avoidance - they were more willing to do the easy task than the difficult one when they were partially sated with water. For this reason, the block order was adjusted from session to session to most effectively keep the subjects engaged in the tasks.

2.9 Training procedure

Training monkeys to perform complex reaching movements, particularly given the lack of physical objects to interact with (i.e. a purely virtual workspace), was not a trivial process. Using manual control of the reward system, a closed-circuit video camera, and the real-time view of the infrared marker position provided via the control programs, the training regimen was a highly interactive process. To begin, the monkeys were rewarded simply for sitting calmly within the rig. The subjects soon began to made small, exploratory reaches into the space in front of them. Since the monkeys could not see their hands, these movements were typically tentative, and were rewarded to encourage the behavior. The solenoid valve in the reward system made an audible clicking noise upon activation, which the subjects quickly learned to associate with the delivery of drops of water. This immediate, audible cue was particularly helpful at early stages of training, because even if the subjects were not directly facing the reward tube when they made a hand movement and were rewarded, they would hear the click and quickly adjust to receive their water.

The next step was to associate subjects' hand movements with motion of the cursor on the screen. Hand position could be tracked only when the infrared marker was in view of the cameras, requiring that the back of the hand be oriented to the side. Thus, when the marker came into view, a cursor would flash on the screen, and a reward was delivered. When the hand was pronated such that the marker faced upwards and was out of view, the screen went blank and no rewards were given. Once the subjects learned to watch the screen and keep the cursor visible, small movements that kept the marker in view were rewarded with water.

Eventually, a second sphere was added to the visual scene – a "target" for reaching. To condition the monkeys to move the cursor to "touch" the target, initially both spheres were large

enough that small, exploratory movements would frequently cause them to touch. When this happened, the spheres would change colors and the cursor would stop moving, and a reward was given. Over a period of days, the radii of the spheres were gradually reduced, requiring longer and more purposeful movements. After visual feedback and reward, the target sphere was randomly moved to a new position on the screen, and the monkey could make another reaching movement. If at any time the infrared marker went out of view of the cameras, the screen was blanked and a short delay initiated before the task could be resumed. This encouraged the subjects to keep the cursor in view of the cameras at all times.

The concept of a "hold time" was then introduced. The color change and water were given after progressively longer periods of continuous contact between the two spheres, rather than immediately upon contact. To provide a visual cue that the spheres were touching, the cursor changed to a lighter shade of blue when it was in contact to the target. This color change was distinct from the "reward" visual feedback, in which the cursor and target both turned green.

Once the monkeys were reliably moving the cursor to the target and holding there, it was straightforward to introduce "center-out" movements. Essentially, instead of a reward occurring after holding at every target, the initial target (now termed the "center") would disappear, and a peripheral target would appear (now called "target"). Rewards were delivered after the cursor was held at this peripheral site. At this point, the center and target spheres were no longer placed randomly throughout the workspace; instead, a set of predefined locations were used. During this stage of training, the center was fixed at the location where the elbow was ~90 degrees of flexion and the hand was in line with the shoulder. From this position, targets in all directions were easily reachable. Surrounding this point, a target at one of eight possible locations (spaced 45 degrees apart on a circle in the frontal plane) was randomly displayed on each trial. This

stage of training is similar to the tasks used in many previous electrophysiological studies of primary motor cortex (Georgopoulos et al., 1982; Moran and Schwartz, 1999).

To allow the study of pre-movement planning-related activity in PMd, subjects were trained to wait during an instructed delay period during which the target of the upcoming reach was known, but movement initiation was withheld until a "go" cue was given. Rather than the center disappearing and target appearing simultaneously, the center sphere briefly remained on the screen, so that 3 spheres were visible at once. The disappearance of the center was used as the go cue – if subjects left the center before then, the screen went blank and there was a short delay before the task restarted again. Instructed delay duration was gradually increased over time, beginning at 50 ms and eventually lasting over 2 s. Subjects readily adapted to using the disappearance of the center sphere as a go cue. Delays up to 500 ms were achieved in a period of days. Longer delays required further training because subjects often became agitated, likely due to the slow pace of the task, and quit working for long stretches of time.

The final, and most difficult, stage of training was to teach subjects to avoid virtual obstacles. A number of strategies were tried. The simplest involved placing a visual object (a rectangle) between the center and target, and aborting the trial if the cursor touched that object. This training technique did not succeed, as the monkey repeatedly made direct, ballistic-type directly through the obstacle, even though that meant he was not allowed to complete the task and obtain a reward. After a short time doing this, he would quit working. A variation of this basic strategy was positioning the object so the natural variation in his hand trajectories would sometimes allow him to avoid touching the obstacle (the desired outcome). However, although he would continue working at this task, he never learned that he could purposely avoid contact with the obstacle.

Ultimately, a successful strategy termed the "tar pit" was developed. Rather than abort a trial immediately upon cursor-obstacle contact, the cursor would appear to stick to the surface of the obstacle (even though there was no physical object impeding the hand). The obstacle would change color, indicating that an error had been made, but a (reduced) reward was still available – this provided motivation to continue attending to the task and attempting to complete the trial. While "stuck" to the obstacle, the cursor would slide slowly along the surface toward the hand position. In this way the hand movement still had an effect on the cursor position, but the cursor movement was limited by the obstacle. If either the hand motion or the cursor sliding along the obstacle freed the cursor from the surface, the cursor would drift across the screen toward the hand. Once the cursor was coincident with the hand, the usual relationship between hand position and cursor position was restored, and the trial could be completed normally. With these rules in place, subjects could observe that the cursor was not capable of translating through obstacles, and must move around the edge. Contacting the obstacle led to reduced reward volume and reduced cursor speed, resulting in lengthier trials and reduced reward frequency, which provided a disincentive to continue the original behavior of moving directly to the target and correcting if necessary if an error was made.

2.10 Surgical methods and implanted hardware

Once subjects were trained in both tasks and could reliably complete two full behavioral sessions per day, they were surgically implanted with acute recording chambers. All surgical procedures were approved by the Animal Care and Use Committee at Washington University in St Louis and carried out under the supervision of Department of Comparative Medicine veterinary staff. The animals were sedated with ketamine, intubated, and anesthetized with isoflurane. A stereotaxic frame was used to target the craniotomy site to PMd, and to immobilize

the head during surgery. The incision site was shaved and scrubbed with povidone-iodine solution, and a sterile field was created. Surgical preparation of the instruments and animals, and anesthesia services, were provided by Donna Reedy. Surgeries were performed by Thomas Pearce and Dr. Daniel Moran, Ph.D.

A midline scalp incision was made from approximately 1 cm anterior to the occipital ridge to 1 cm posterior to the orbital ridge. The skin was retracted and a bone scraper was used to detach the insertion of the temporalis from the calvarium. 14-16 1/8 in. holes were drilled by hand, and surgical-grade stainless steel screws were inserted, serving as an anchor for the acrylic head cap. The craniotomy site was located stereotactically at 19 mm anterior (interaural), 14 mm lateral. A trephine (O.D. = 19 mm) was used for the craniotomy and the resulting bone plug was gently detached from the intact underlying dura. A stainless steel recording chamber (19 mm O.D., 16 mm I.D.) was fit into the craniotomy. Two-part dental acrylic was mixed, placed onto the surface of the skull around the implanted hardware, and allowed to set. Layers were progressively added to encapsulate the skull screws and secure the recording chamber to the skull. Three stainless steel posts were embedded into the acrylic and were used to immobilize the head during recording sessions. Once construction of the acrylic head cap was completed, the interior of the recording chamber was flushed to remove any debris, filled with ~1 ml of bacteriostatic saline, and sealed with a sterile cap. The skin edges were brought over the edges of the acrylic, and 1-2 sutures drew the skin securely against the head cap.

2.11 Head cap and chamber maintenance

Subjects recovered in their home cages for 5 days to allow the acrylic head cap to fully cure before being immobilized by the implanted hardware ("head-fixed"). Head cap maintenance, performed by Donna Reedy, involved weekly hair removal and cleaning of the skin

edges. During the electrophysiological data collection period, the recording chamber was opened and cleaned with chlorhexidine solution and bacteriostatic saline 5-6 times per week. Following cleaning, the chamber was sealed with a chemically sterilized chamber cap. To delay the thickening of the dura within the recording chamber and allow continued penetration by glass/tungsten electrodes, the anti-cancer thymidine analog 5-fluorouracil (5-FU) was utilized. 2-3 times per week, 0.3 ml of an aqueous solution of 5-FU (50mg/ml) was injected into the chamber after the cleaning procedure and allowed to sit for 5 minutes. The 5-FU was then removed and the chamber was rinsed with sterile saline, and the regular chamber maintenance procedure resumed.

2.12 Acute neural recording procedure

Prior to the first recording session each day, the Thomas drive was prepared for the electrode insertion process. This procedure began with immersing the drive head in a beaker of distilled water within a sonication bath for ~5 minutes. This helped release any debris from the guide tubes, and freed any electrodes that remained in the drive from the previous session. If additional electrodes were desired, they were loaded into empty guide tubes and connected to the headstage and the motors. All electrodes were advanced until the tips were protruding approximately 2 cm past the end of the guide tubes, and the liquid surrounding the electrodes and tubes was wicked away with Kimwipes. 1-2 drops of mineral oil were applied to the electrodes and allowed to wick into the guide tubes. This helped minimize electrodes sticking and breaking within the guide tubes. Electrodes were then retracted until the tips were ~0.5 mm recessed into the drive head.

The monkey and electrode drive were loaded into the recording rig. The headstage was connected to the preamplifiers and a power supply, and ground cables were attached to the

headstage, rig, chamber, and Optotrak strober. The insertion angle of the drive was matched to that of the recording chamber, and the drive was advanced until the chamfered edge of the drive-head was securely seated onto the matching surface of the chamber. Electrodes were advanced one at a time, with the individual motors controlled by software from Thomas Recording. The insertion process was monitored using an impedance meter and a custom-written TDT interface. Voltage traces were visualized on a computer monitor, and also routed to an audio amplifier and played over a speaker system. The initial stage of penetration involved advancing all electrodes past the dura, but not all the way to cortical tissue. A characteristic slow rise and sharp fall in impedance indicated penetration of the dura. Once all electrodes were beyond this barrier, the second stage - advancing into cortical tissue - began. Electrodes were individually advanced until spiking activity could be seen and heard (ideally on every channel). Since the recordings were not immediately stable after penetrations were made, data acquisition was delayed for approximately 90 to allow for settling of the tissue around the electrodes. As a result, by the time recordings were made some channels had one or more cleanly-discernable units, while others had none or too many to distinguish. Online isolation of units was not attempted, and within a behavioral session, the electrodes were not moved. Data were collected from 2-3 behavioral sessions per day. After one session was completed, each electrode was advanced at least 0.25-0.30 mm, so the same neuron would not be duplicated within the data set. The system was again allowed to settle for approximately one hour before the next behavioral session was started.

At the end of the recording sessions, the electrodes were retracted to their initial starting depths, with the tips recessed into the guide tubes. The drive was backed out of the chamber and disconnected from the rig. The drive head was immersed in a beaker of Tergazyme enzymatic

cleanser and underwent ~10 minutes of sonication. During the first sonication cycle, the electrodes were gradually advanced out of the guide tubes. After sonication, the drive head was removed from the detergent and immersed in distilled water for storage until preparations for next recording session were begun.

2.13 Preprocessing of neural data

Neural recordings were imported into MATLAB for further processing and analysis. Each channel of spike data consisted of a time series of extracellular voltage that was bandpass-filtered between 0.3-5 kHz in the DSPs and sampled at ~24.4 kHz. The time series lasted the entire duration of the behavioral session: typically ~45 min. The entire signal was analyzed using WaveCLUS, a MATLAB-based offline spike sorter (Quiroga et al., 2004). The sorting algorithm first determined positive and negative voltage thresholds from the standard deviation of the signal. Snippets of data surrounding threshold-crossing events were extracted as potential spike waveforms. WaveCLUS has options to use wavelet coefficients or principal coefficients as the basis for clustering; here, wavelet coefficients were used. Super-paramagnetic cluster analysis was then performed. The main parameter that can be adjusted for supervised sorting is the "temperature" – at low temperatures, a single cluster is found, and at high temperatures each spike is placed into its own class. At intermediate values, groups of similar waveforms emerge. Manual supervision of the clustering was done for each channel of data, and was based on a combination of visualization of cluster separation in the each of the 10 dimensions of wavelet coefficients, and inspection of the interspike interval histogram for adherence to physiological refractory period limits (i.e. few if any interspike intervals should be shorter than 3 ms). Clusters were subjectively graded for isolation quality and signal-to-noise ratio, and rejected if either measure was poor enough that the sorting was questionable. "Spikes" that visually appeared to

be artifactual in origin were rejected, as were all clusters that failed to exceed a minimum spike count of 600 in the entire session, since cluster quality was difficult to assess with few events. Finally, the spike times for each cluster were saved to a database.

2.14 Preprocessing of kinematic data

Raw 3D hand positions were filtered and differentiated using Woltring's algorithm (Woltring, 1986) with a low-pass cutoff frequency of 10 Hz, resulting in smoothed position and velocity estimates. Movement initiation time for each trial was calculated as follows: the maximum hand speed between the go cue and the beginning of the target hold time was determined. 15% of the peak speed was set as the threshold for movement onset. Threshold crossings (in the low-to-high direction) were determined via interpolation, and the first such occurrence in a window beginning 200 ms before the "go" cue was taken as the onset of movement. The common technique of working backwards from the time of peak speed was not appropriate for this data set, as a minority of obstacle-avoidance movements were double-peaked with the minimum between peaks falling below the 15% threshold, and these movements would be inappropriately considered to start a significant distance into the reach trajectory.

3 Single unit analyses

3.1 Introduction

How does the brain control reaching movements? Many stages of processing are required to go from visually identifying targets to generating muscle activities. Somewhere along the way, movements that would lead to undesired outcomes must be rejected and replaced by alternative motor plans. This chapter examines the activity of individual PMd neurons as monkeys plan direct reaches and curved obstacle-avoidance hand trajectories. Most neurons have weak but significant linear relationships to kinematic parameters of the upcoming movement, including the position of the hand, the initial direction of movement, and the direction of the target. Many carry information about more than one of these parameters. The preferred hand position and movement direction tend to be spatially congruent in neurons that are modulated by both. A different, unexpected pattern is seen in neurons that tune simultaneously to target and initial movement direction: the preferred directions (PDs) for these task features are spatially anti-correlated. These cells may play a role in combining target information with other spatial cues to generate more complex reaching movements.

3.2 Methods

3.2.1 Firing rate estimation

Identifying and quantifying patterns of neuronal activity is a major goal in neuroscience. Neurons transmit information by firing action potentials (also called spikes) – brief fluctuations of trans-membrane electrical potential that propagate rapidly down the axon and lead to the release of neurotransmitters at synapses with downstream cells. Spikes are by nature all-or-nothing binary events, so information must be carried either by the precise timing or the

frequency of the events. The latter is termed "rate coding," and decades of experimentation have shown that many individual neurons in motor cortical areas have a relationship between firing rate and movement (see (Shadmehr and Wise, 2005) for a review). To calculate the firing rate of a neuron, a finite number of discrete events must be used to estimate an underlying frequency of action potential discharge. A simplistic way to do this is to count the number of spikes in a given time window and divide by the duration of the window (Dayan and Abbott, 2005).

For the analyses in this chapter, firing rates were estimated by counting the spikes during certain time windows within the trial structure and dividing by the total time. The time windows are shown in figure 3.1. Each corresponds to a distinct epoch of the task. The first epoch begins 150 ms after the hand reaches the "center" position, 350 ms before the target onset. Neural activity during the first 150 ms of the delay is excluded in order to reduce potentially confounding effects of movement to, and initial stabilization at, the starting position. When the first epoch ends, 150 ms after target onset, another 500 ms epoch begins - during this epoch, the monkey is aware of the target location for each trial. During the obstacle-avoidance task, a third consecutive 500 ms delay-period epoch begins 150 ms after obstacle onset. The choice of 150 ms offsets from trial events was informed by the results of Weinrich, Wise and Mauritz (Weinrich et al., 1984). In that study, the median onset latency for visual- and set-related neurons in premotor cortex was found to be 140 and 145 ms, respectively, from the time of the visual stimulus. In addition to the three delay-period firing rates, two additional epochs were also considered - a variable-duration reaction-time epoch lasting from the go cue until movement onset, and a movement epoch consisting of a 400 ms window beginning at movement onset. Since the goal of this study is to determine how neural firing rates correlate with hand position, movement directions, and target direction, the analysis epochs were chosen such that visuospatial

information about the trial condition is consistent over the duration of each analysis period. Averaging a neuron's firing rate over relatively long time periods runs the risk of missing faster temporal dynamics that may be present in the underlying rate function. However, for the purposes of determining if task parameters influence neural firing rates, it is a commonly-used approach (Georgopoulos et al., 1982; Stevenson et al., 2011).

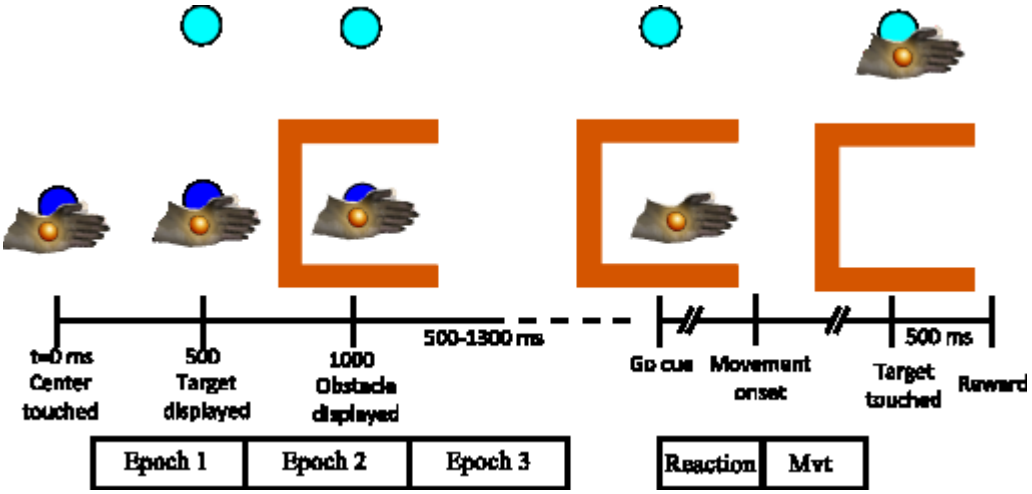

Figure 3.1: Task timeline and analysis epochs. Timeline is shown for the obstacle-avoidance task. In the center-out task, the final delay period begins at the target display (i.e. there is no obstacle delay period). Epochs 1-3 begin 150ms after the preceding trial events. The reaction time epoch lasts from the go cue until movement onset. The movement epoch begins at movement onset and lasts 400ms.

3.2.2 Cosine tuning functions

The firing rate response of motor and premotor cortical neurons can be described via "tuning curves" - functions that relate neural activity to various parameters. The classic description in the literature is one of broad tuning to movement direction, with maximal firing rate in the "preferred direction" (PD), minimal in the anti-preferred direction, and a smooth transition in between. This relationship can be fit with a cosine function and visualized by plotting spike rate as a function of angle.

Equation 2.1: $FR(\theta) = b_0 + d*\cos(\theta-\phi) = b_0 + b_1*\cos(\theta) + b_2*\sin(\theta)$

It should be noted that a cosine is not necessarily the best function to describe the activity of all motor cortical neurons. However, it a) has the advantage of being a simple least-squares linear regression model; b) is widely used in the literature making comparisons to previous studies possible; and c) does a reasonable job at describing the response properties of many neurons. If care is taken to limit the interpretation of results to those that do not depend on a cosine being an ideal fit to the stimulus-response relationship, the linear model can provide useful information about the way that neurons relate to spatial elements of movement.

In this chapter, multilinear least-squares regression models (cosine tuning) are fit to the neural firing rates during the different task epochs. Because raw firing rate data are heteroscedastic - the variance in firing rate is not independent of the value of the rate, but rather increases as the firing rate increases - the rate estimates have been square-root transformed to stabilize the variance and allow better statistical testing of the regression model (Reina et al., 2001). Statistically significant correlations between firing rates and various parameters were

determined using the F-test ($\alpha = 0.05$) on the residuals of the least-squares model fit. While this is not the only method that has been used in the literature to assess task-related activity in motor and premotor neurons, the proportion of significantly modulated cells found by a number of different statistical analyses is in broad agreement (Schwartz et al., 1988; Moran and Schwartz, 1999; Aflalo and Graziano, 2006; Kaufman et al., 2010).

3.2.3 Circular probability density functions

Distributions of angular differences between vectors are visualized using smoothed estimates of the underlying probability density function. A kernel density estimation routine adapted for circular data was downloaded from the MATLAB file exchange (http://www.mathworks.com/matlabcentral/fileexchange/32614). Kernel sigma was automatically calculated using the 'msni' method (minimum standard deviation interquartile range, improved). The likelihood that a peak in the probability density function could have occurred by chance is assessed by comparing the resultant vector length for the sample against the null hypothesis that no true relationship exists between angular features. Under this H_0, an infinite population of angular differences would have a completely flat distribution and resultant vector length of 0. With finite N, non-zero resultant vectors will occur even without a true bias in the sample. The distribution of resultant vector lengths obtained by chance is additionally dependent on the magnitude of N. Therefore, hypothesis testing of directional correlations in each population of N neurons was done using a distribution calculated from N randomly-generated angles.

3.3 Results

3.3.1 Tuning to position and direction during direct reaches

The center-out-with-position task is designed to evaluate neural tuning to a) static hand position and b) direction of target/movement. Firing rates were regressed against the center (starting) position to determine the preferred position gradient for each neuron. During this first epoch the target direction is hidden from the subject, so planned direction should have no influence on firing during this time. Figure 3.2 shows positional tuning in example neurons. Spike raster plots in the x-y plane are organized by center location and the mean firing rate for each panel is plotted in the z-dimension. The regression plane shows the best-fit plane that predicts firing rate as a function of hand position.

During the second delay period, information about the direction of the upcoming reach is available to the monkeys. The preferred direction for each neuron was found by regressing firing rates against the target direction, and the statistical significance of the fit was evaluated. Figure 3.3 illustrates the regression plane and equivalent 2D view of the cosine tuning curve for reaches in eight directions. This type of directional tuning is similar to that found in traditional center-out reaching experiments. One difference is that firing rates in the same target direction but from different initial positions were considered equivalently for the purposes of determining the overall directional tuning of each neuron. As in the case of many prior studies, neural tuning during this task cannot be interpreted as distinctly target- or movement-related, because the two directions are very highly correlated.

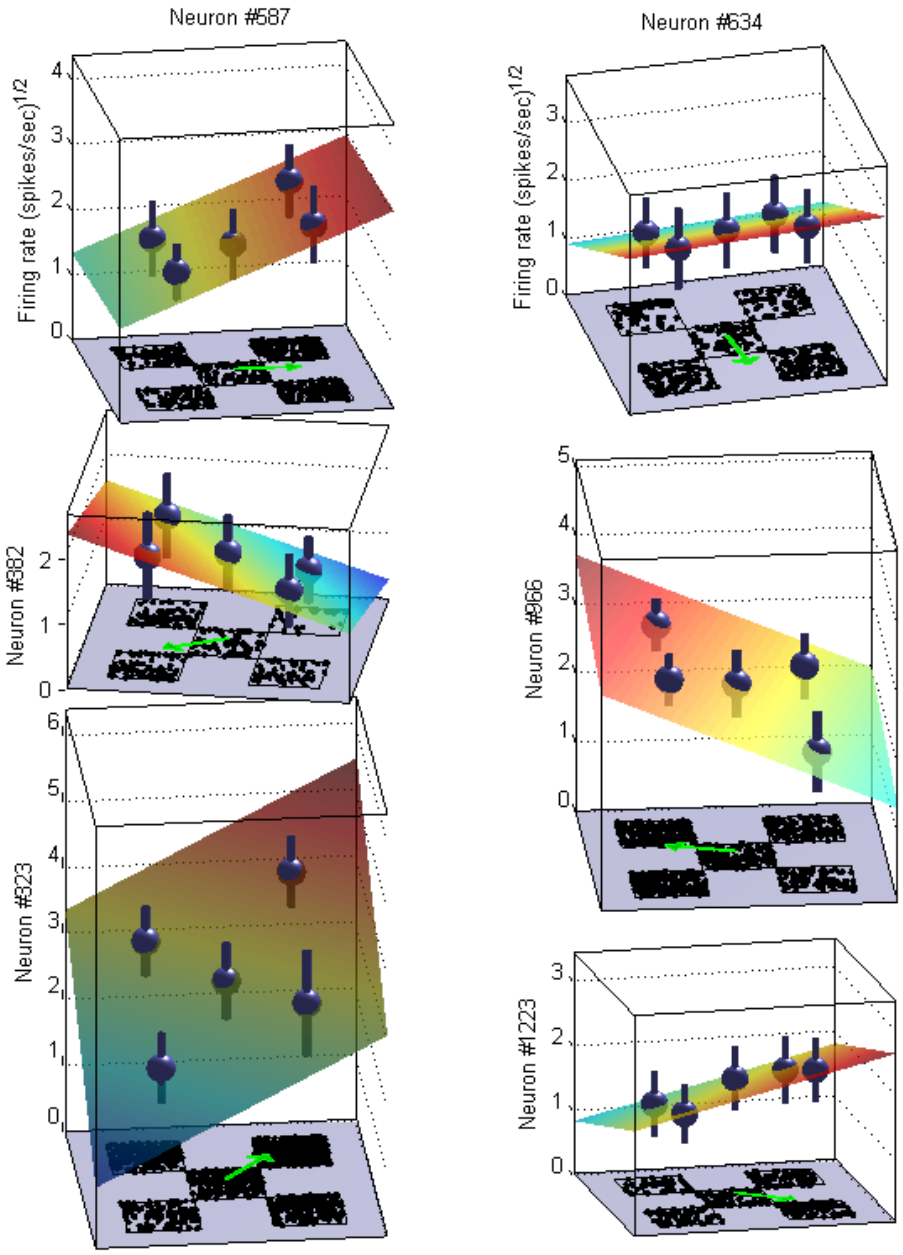

Figure 3.2: Position tuning, raster plots and regression planes. Left column: Exemplar neurons from Monkey H. Right column: Monkey G. Each panel of the raster plot corresponds to a center position. Time is along the horizonal axis, trials are on the vertical axis. Mean rate and standard deviation, and the best-fit plane, are shown on the z-axis. Green arrows: Position gradient (PG).

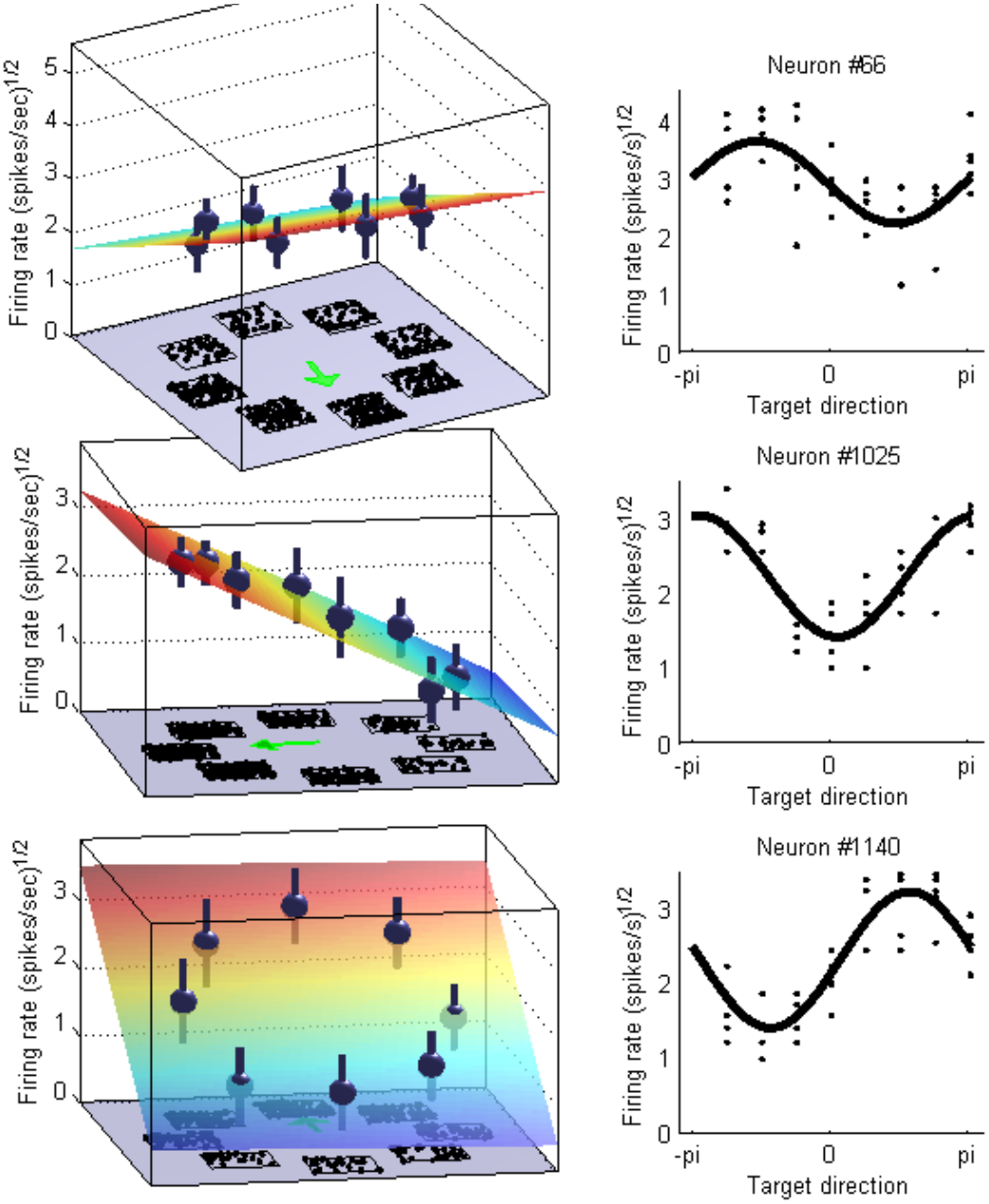

Figure 3.3: Tuning to instructed direction during delay 2 of the center-out task. Three exemplar neurons are shown, one from monkey H (top row) and two from monkey G. Rasters and regression planes are as in fig. 3.2. Right column: The equivalent cosine tuning curve for each neuron. Each individual point is the mean rate of five repetitions of each condition (combination of center position and target direction).

3.3.2 Distinguishing movement- and target-direction tuning

The purpose of the obstacle-avoidance task is to spatially decorrelate the direction of initial movement from that of the final target. In tasks with a single, fixed relationship between the two parameters, it is impossible to determine if a tuning curve during the preparatory period truly relates to either one, regardless of the angular distance between them - the tuning curve to one will simply be phase-shifted relative to the other. The neural relationship to each can be determined only when the relative angle between directional parameters is varied. Delay period 3 of the obstacle-avoidance task provides this dissociation: movements are planned in many directions to targets in many directions, with no consistent relationship between initial movement and final target across trials. This allows tuning curves for movement and target direction to be fit to the firing rate data independently (fig 3.4).

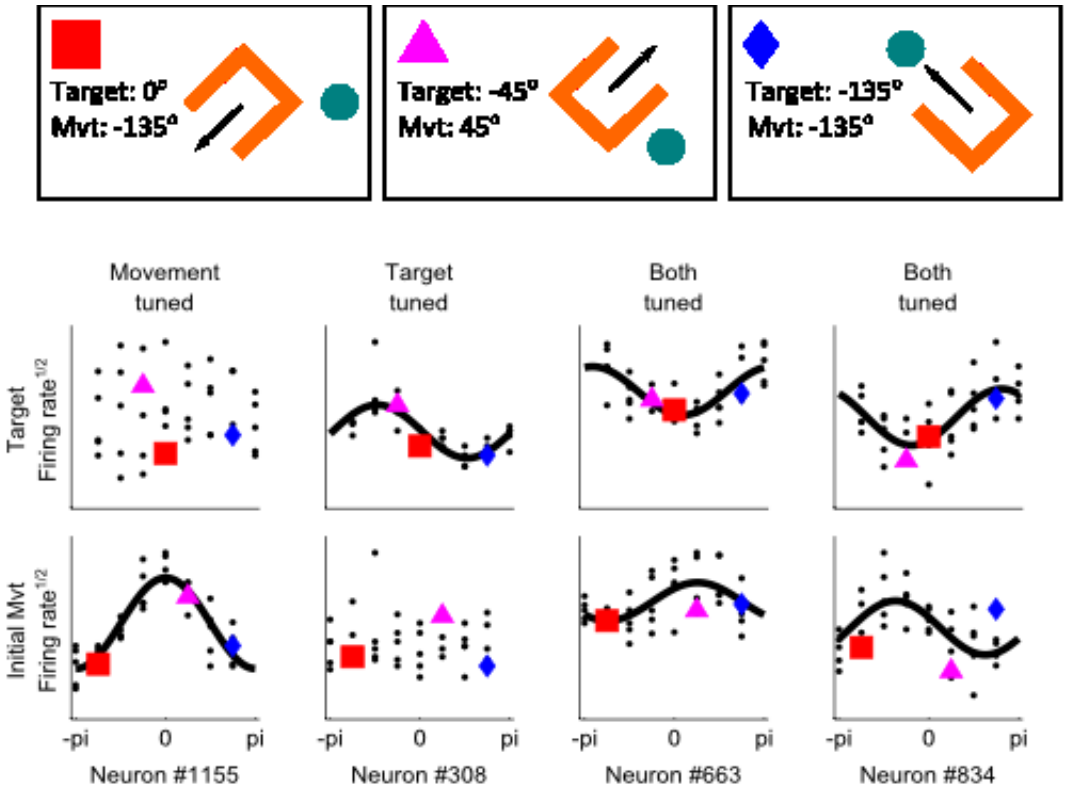

Figure 3.4: Delay-period tuning to initial movement direction, final target direction, or both. All firing rates are measured during epoch 3, when both the target and obstacle are displayed. Cosine tuning curves are shown for statistically significant fits. Three conditions are highlighted via colored symbols to illustrate that the same firing rates can be aligned by different parameters. Aligning the trials by different parameters generates tuning curves to each parameter independently.

3.3.3 Proportions of modulated neurons in the population

The previous sections provide examples of neurons that have a significant linear relationship between firing rate and hand position, target direction, and initial movement direction. How common is it to find neurons tuned in this manner? First, we have to figure out which neurons to consider. Most reports in the literature are restricted to high-firing neurons. Various thresholds are used to exclude low-firing cells. Typically, only those neurons with mean firing rates of 3, 5, or 10 spikes/s are included (e.g. (Batista et al., 2007)). There are a couple of reasons for this. First, traditional single-unit recording experiments involve placing the electrode tip as close as possible to an individual neuron so that spike detection and isolation can be done on-line while the recording is in progress. In order to maximize the yield of usable neurons, units with low firing rates are bypassed in favor of higher-firing cells. This process can also introduce a selection bias for neurons that respond during the particular task of interest, especially if a screening task is used to initially isolate the cell. Second, a low firing rate means that spike events are infrequent, so estimating the underlying rate function in a finite window is more difficult - the signal to noise ratio is low.

The data set for this thesis contains neurons that were recorded with minimal selection bias and sorted off-line. Thus, neurons with a wide range of mean firing rates are available for analysis. The exact proportion of neurons that "tune" to the different parameters depends on the criteria for including some units and excluding others. Figures 3.5-3.7 shows the proportion of tuned units as a function of mean firing rate. As neurons with lower and lower firing are examined, the total proportion decreases substantially but is not eliminated altogether. This finding agrees with a report from Paninski et al. (2004) that very low firing neurons in M1 contain kinematic information (Paninski et al., 2004). Interestingly, the relative proportions of

units tuned to different parameters over different time periods remains relatively fixed. This suggests that the lower number of tuned neurons may be due to decreased sensitivity of the linear regression when the rate estimates are noisier. Simulations of artificial neurons with known tuning properties have previously been used to assess confidence in estimating preferred direction with varying numbers of spikes (Stevenson et al., 2011). In that study it was found, unsurprisingly, that the confidence interval of the regression model is highly dependent on the spike rate of the neuron.

Overall, the majority of neurons in the data set have a statistically significant relationship with at least one, and often multiple, spatial parameters of the task. The number of tuned units during planning is slightly lower than during peri-movement time epochs. Although canonical descriptions of premotor cortex emphasize the role of these areas in movement planning, their continuing involvement during movement execution should not be ignored. This is unsurprising - many reaching movements are not purely ballistic, feed-forward processes, but are instead subject to feedback about the ongoing action and can be corrected, altered, or canceled online. In addition, even feed-forward processes must be monitored for errors and adapted to novel conditions. While these behavioral qualities do not guarantee that any particular brain region participates in this process, the neural data suggest that planning and execution phases of reaches engage PMd circuits in a similar fashion.

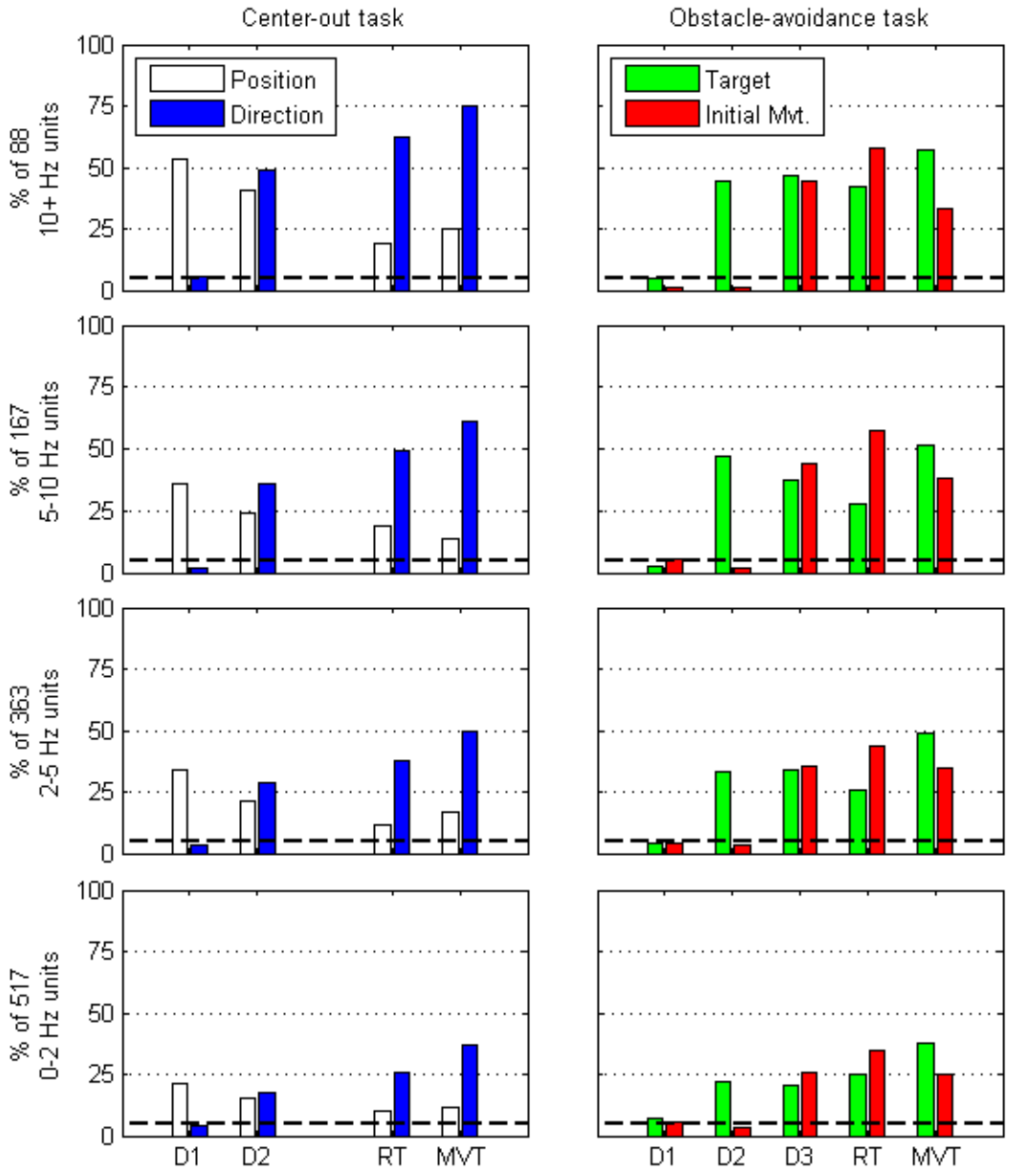

Figure 3.5: Proportion of units with significant cosine-tuning relationships to task parameters ($p<0.05$). Top to bottom: As mean firing rate decreases, fewer neurons are significantly modulated, but the overall pattern remains consistent. D1: Delay period 1, pre-target. D2: Delay 2, post-target (pre-obstacle, in the obstacle-avoidance task). D3: Delay 3, post-obstacle (obstacle-avoidance task only). RT: Reaction time. MVT: First 400ms following movement onset. Dashed lines: 5% chance level.

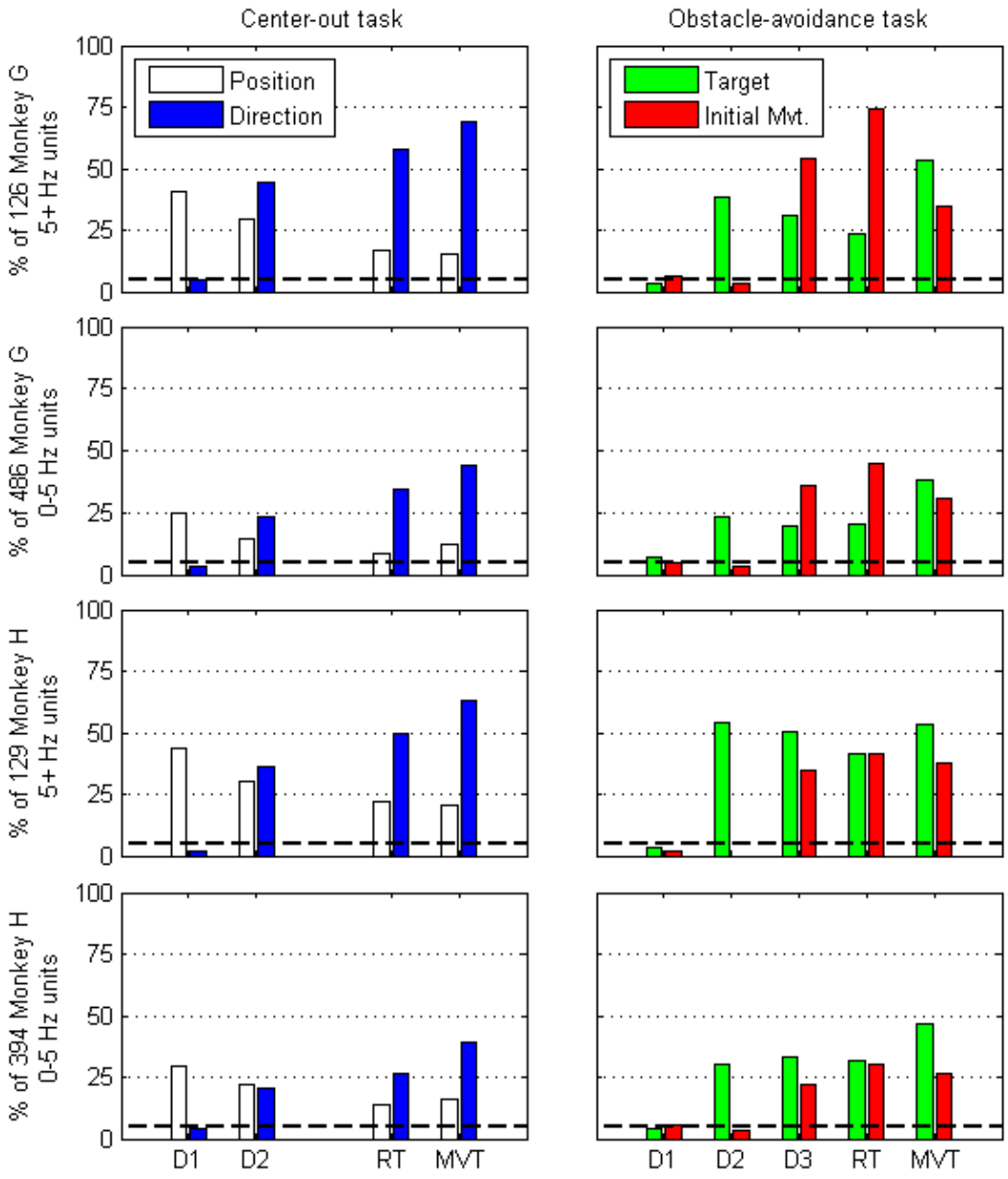

Figure 3.6: Comparison of proportion of tuned units by monkey. The top 4 panels are neurons from monkey G; the bottom 4 are monkey H. Within each block of 4, the top row is high-firing units (minimum of 5 spikes/sec on average), and the bottom row is low-firing (<5 spikes/sec). Monkey G has a greater proportion of units tuned for initial movement, and fewer for final target direction (D3 and RT). The overall pattern and proportions of tuned neurons over the course of the task are similar between the two monkeys.

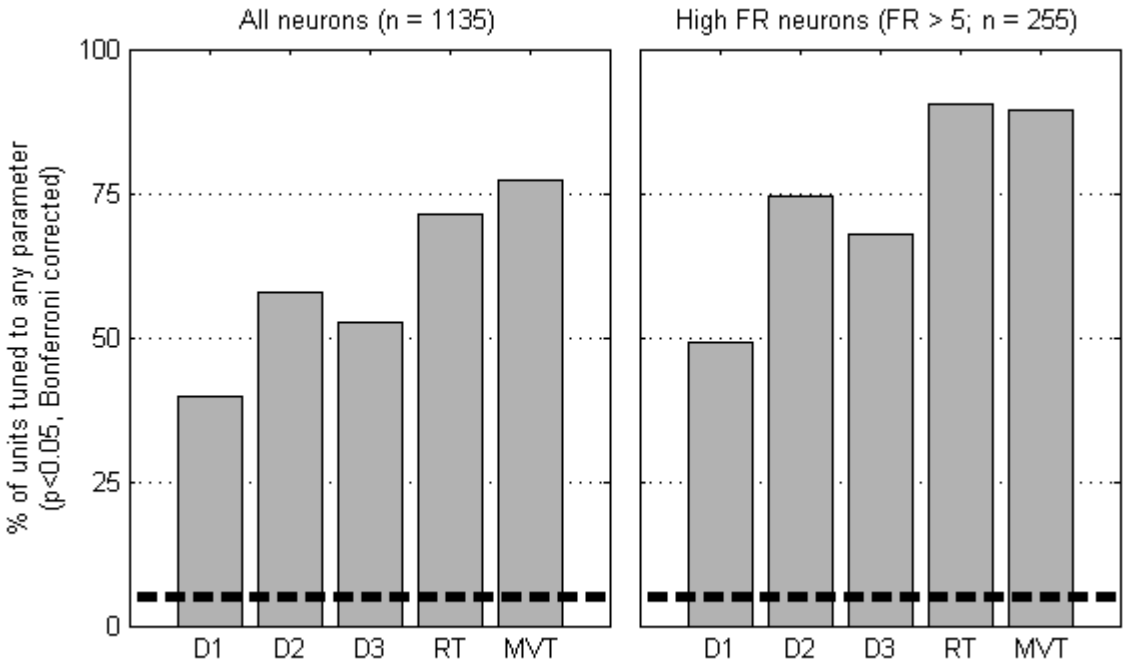

Figure 3.7: Proportion of units tuned to any parameter. Significance is defined as Bonferroni-corrected $p<0.05$.

3.3.4 Neurons are modulated by many parameters

Two related metrics are commonly reported for studies of neuronal tuning - R^2 (percentage of variance explained) and p-value (probability that the observed relationship is due to chance). The relationship between the two depends on the degrees of freedom in the regression model - fewer observations require more variance-explained to be considered a statistically-significant fit. Which metric is emphasized often depends on the aims of the study. Those wishing to argue that a particular parameter (e.g. movement direction) is represented in the firing of a population of neurons emphasize how many units achieve significance. Using the same data set, the low proportion of variance explained can be used to argue that the tuning model is very incomplete. Though they tend to be placed in opposition, these interpretations are not contradictory, and both are widely-reported descriptors of neuronal function (Crammond and Kalaska, 1994; Aflalo and Graziano, 2006; Churchland et al., 2010).

The data from the two reaching tasks studied here support the idea that individual PMd neurons have relationships with many kinematic parameters of movement, during both the planning and execution of reaching. Trial-averaging all conditions that are similar in one parameter can substantially increase the goodness of a cosine fit. Intuitively this makes sense - the contributions of any other parameters that influence firing rate is reduced by taking the mean, leaving only the parameter of interest unexplained (fig 3.8, left panel). This holds if the other sources of variance are equally distributed across the conditions being evaluated; if the effects of the other parameters are not counterbalanced across conditions, they will influence the shape of the observed response of the mean firing rates. Conversely, if other sources of variance are not reduced by averaging, the R^2 value of the regression model may drop substantially. This may in part be due to increased noise, since determining accurate rate estimates require repeated

observations. On the other hand, it can also reflect a true relationship between a neuron's rate and additional factors (fig 3.8, right panel).

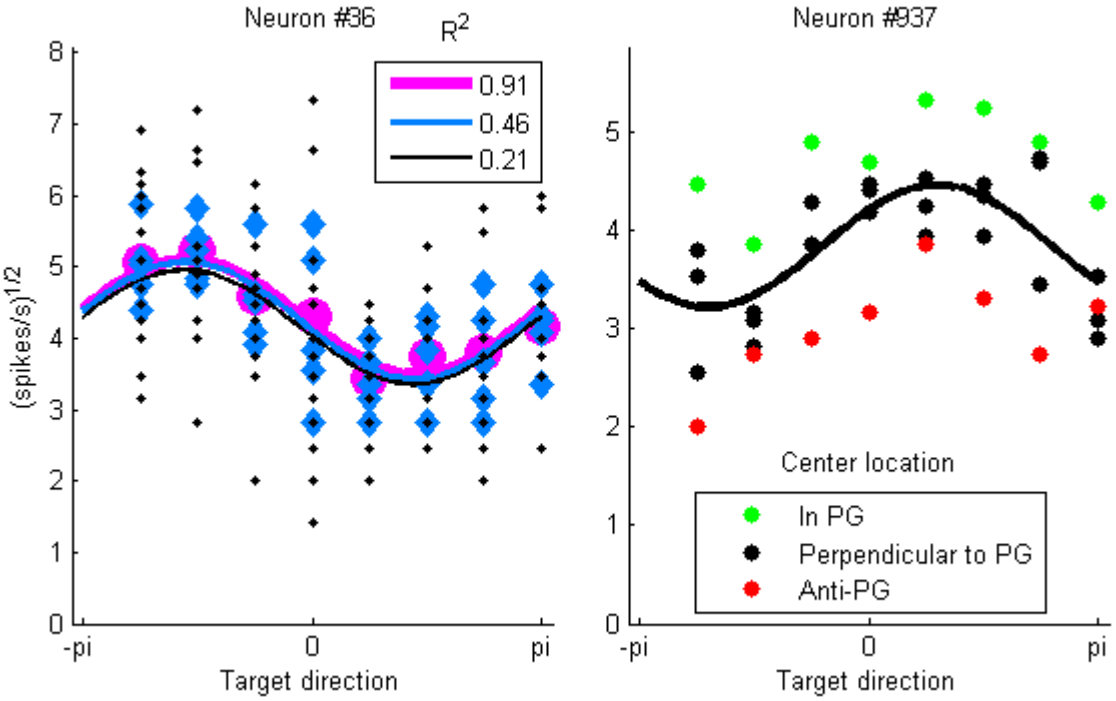

Figure 3.8: Variance-explained increases as trials are averaged. Left: Cosine tuning curves fit to instructed reach direction during delay 2 of center-out for a single neuron. Trials are unaveraged (black); averaged across repetitions of a single condition (center-target combination, blue); or averaged across all trials in each direction regardless of center location (magenta). A similar tuning curve is found in all cases, but the R2 value changes dramatically. Right: For this neuron much of the variance not explained by target direction is related to the starting position of the hand. Trials with the hand held in the PG have higher firing rates, while those in the opposite location have lower rates.

3.3.5 Stability of the tuned population prior to movement onset

As we have seen, many neurons tune to more than one spatial parameter, and the proportion of neurons tuned to any parameter can change over time. In the case of position tuning, the number of significantly-tuned units decreases from delay 1 to delay 2. At a minimum, the difference can be accounted for by a subset of units that lose significance in delay 2. At the other extreme, *all* originally tuned units could lose significance and be replaced by a new population. In the recorded population of neurons, 60% (205/341) of delay 1 tuned neurons were no longer significantly modulated by position in delay 2, and 96 became significant for the first time during that epoch. During the center-out task, neurons could be position-tuned during three pre-movement epochs, and direction tuned during two. Similarly, in the obstacle-avoidance task, units could be modulated by target direction during three pre-movement epochs and initial movement direction during two epochs. The proportions of units that were significantly modulated with each temporal pattern are shown in fig. 3.9.

For neurons that are significantly modulated by a given factor during multiple epochs, how stable is the preferred direction vector? Figure 3.10 shows circular kernel density estimates of the difference in PD between different epochs. All the distributions are centered at zero, indicating that individual neuronal PD is stable over the time period prior to movement onset. When neurons tune to a given parameter in one epoch but fail to meet a significance threshold in an adjacent time window, the distributions remain non-uniform (fig. 3.11). A reasonable hypothesis for this finding is that many neurons have an underlying linear relationship to the parameter during both epochs, but due to other factors such as noise or additional modulation, the regression analysis fails to find a statistically significant fit.

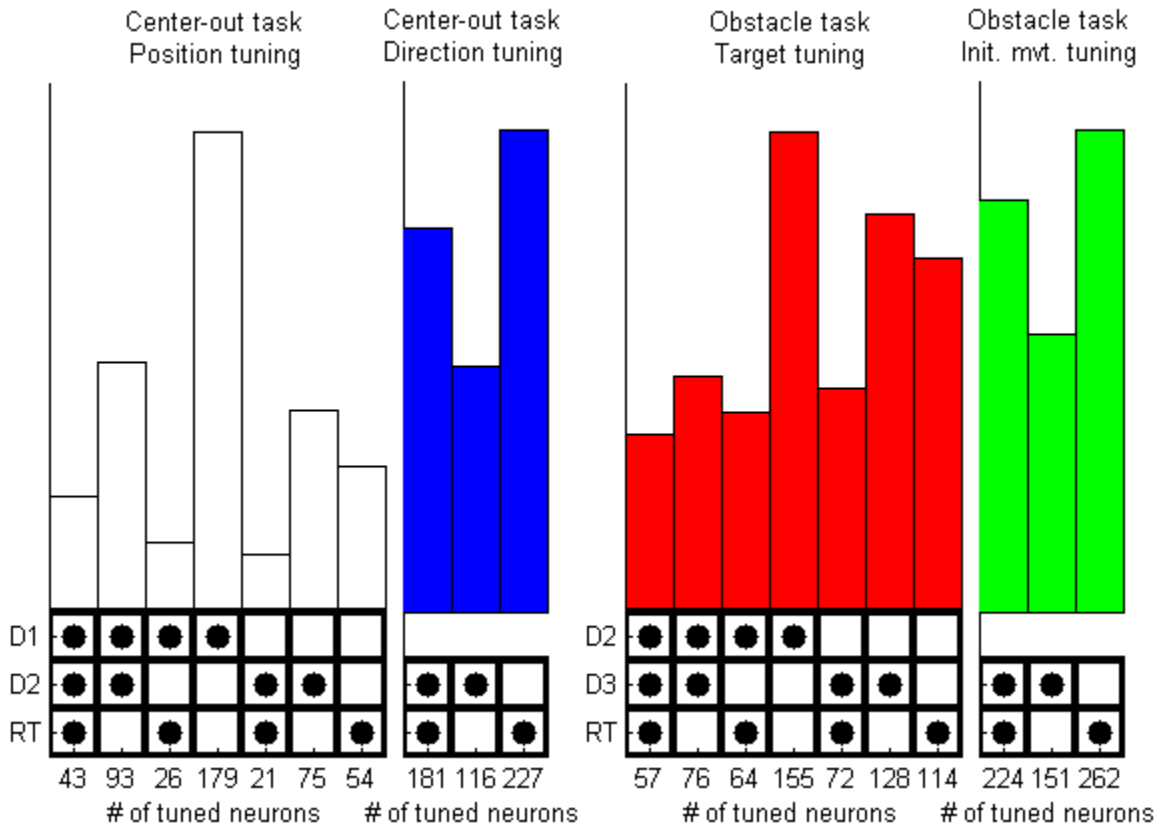

Figure 3.9: Tuning to the same parameter during different epochs. Many neurons in the data set tune to any given parameter during more than one task epoch. Many others do not. The number of tuned cells is shown for each possible combination of pre-movement epochs. Note that the bars are normalized within each panel - between-panel comparisons should be made using the absolute cell count, found on the x-axis.

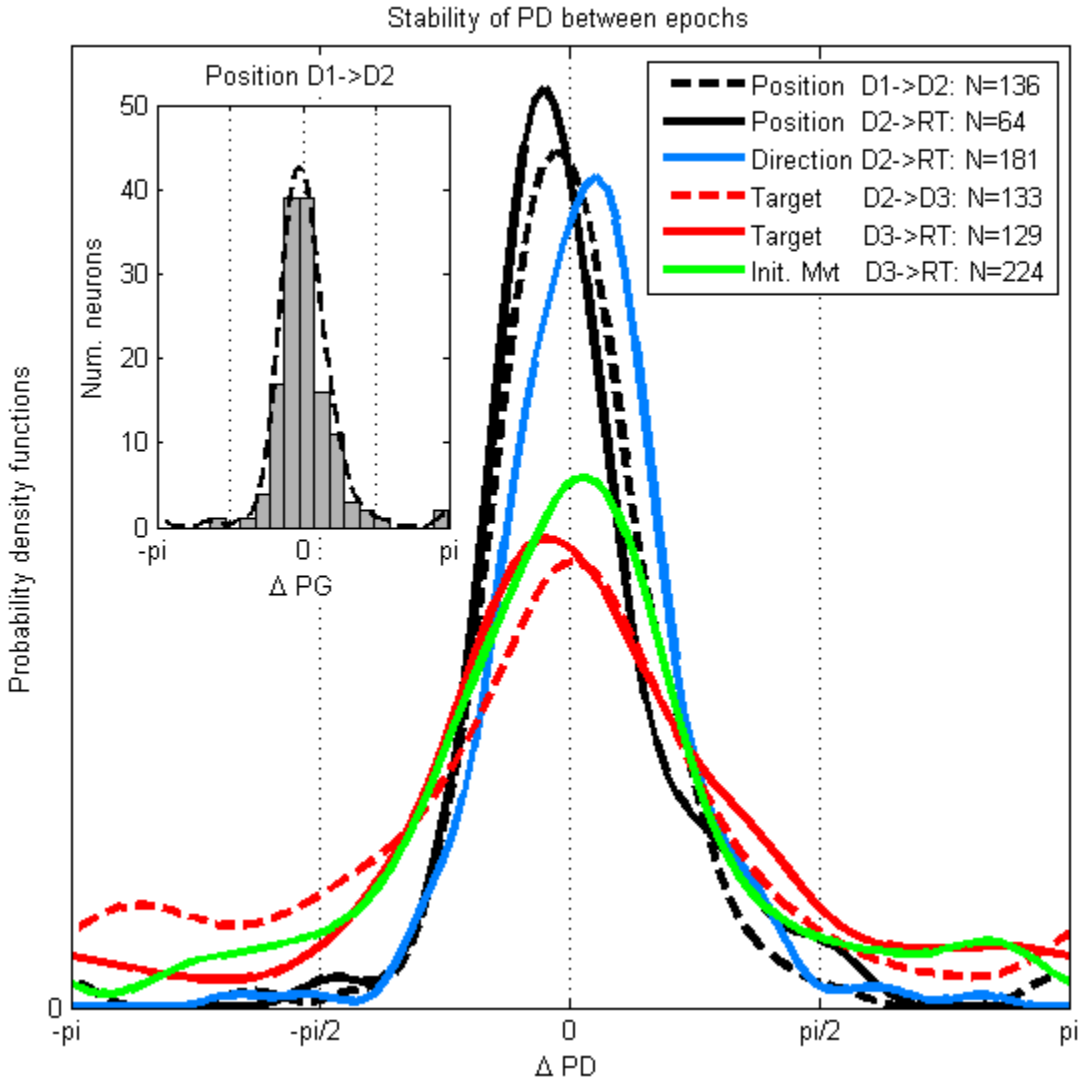

Figure 3.10: Distributions of angles between PDs. For each neuron with significant tuning to a given parameter in adjacent epochs, the angle between the two PDs was calculated. The distribution of these angles is plotted for each parameter-timespan. Between these time windows, the direction of maximal tuning does not rotate on average. All distributions: $p<0.001$. Inset: Histogram and scaled PDF showing congruence between the two visualization techniques.

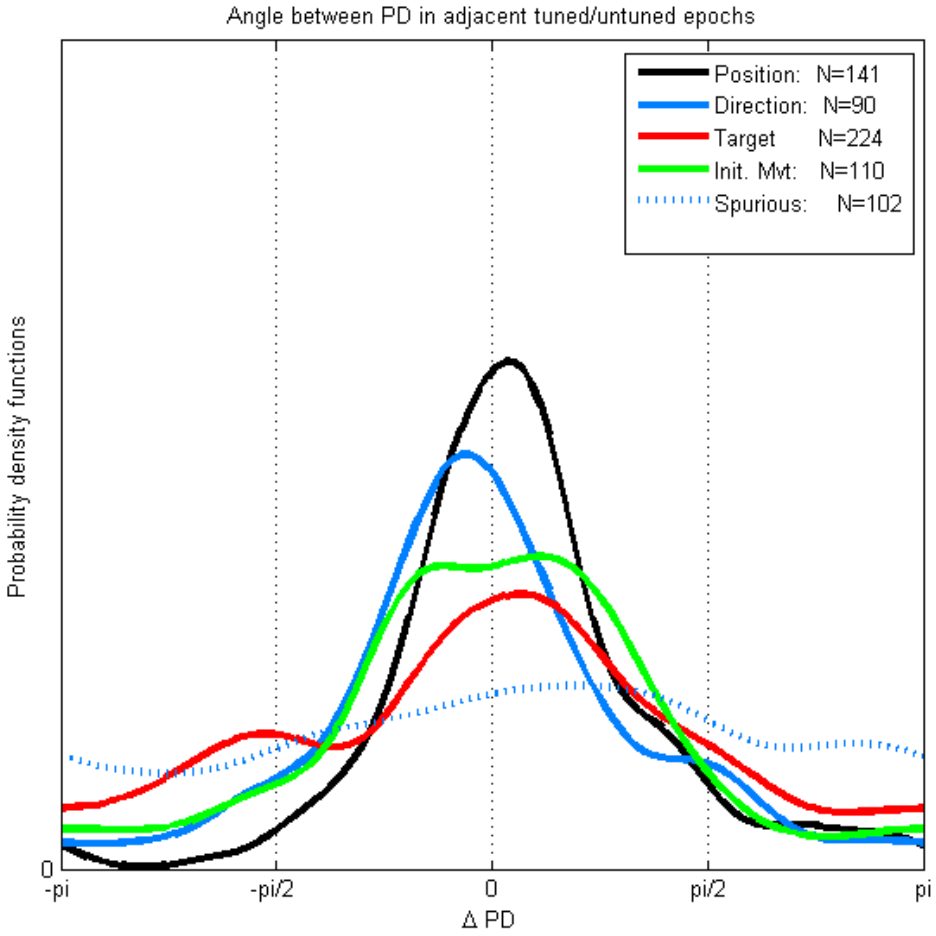

Figure 3.11: Due to noisy signal, many neurons that exhibit statistically-significant tuning in one epoch fail to meet significance in one or more adjacent time epochs. Nonetheless, a "non-significant PD" can be computed and compared to the statistically-significant PD. For time epochs when the relevant information is available to the animal (solid lines), these non-significant tuning curves correlate well with the significant tuning curves ($p<0.001$). Before information is available, the correlation is greatly diminished, as expected (dotted line). Vertical scale is the same as fig. 3.10.

3.3.6 Relationship between preferred position and direction vectors

When neurons are significantly modulated by both hand position and instructed direction, is there a spatial relationship between the two? As an example, if the PG and PD were spatially congruent across the population, neurons with a positional preference for hand positions to the right would also prefer instructed targets to be located to the right. Alternatively, the difference in PG and PD might tend to cluster at some other (non-zero) angle - perhaps a PG to the right predicts a PD downward or leftward - or the two spatial preferences may be unrelated, with a uniform distribution of angle between the vectors. The data suggest that during the both the instructed delay period and the reaction time, there is a tendency for the PD and PG to point in similar directions (fig 3.12), though the distribution of angles is broader between these parameters than it is across time epochs for each parameter individually (fig 3.10).

To test for interactions between position and direction in units significantly modulated by both, linear regressions against instructed direction were performed separately for start positions in the preferred vs. anti-preferred position. Likewise, regressions against hand position were performed for trials with the target in the preferred/anti-preferred direction of movement. The type of interaction can be determined by examining the regression coefficients (b_0, b_1, b_2 from eq. 1). An additive relationship is characterized by a change in b_0, shifting the curve up or down; conversely, a change in the vector magnitude $|b_1\ b_2|$ indicates a multiplicative interaction that scales the amplitude of the tuning curve. As seen in figures 3.13 and 3.14, across the population of PMd neurons, the interaction is best described as additive. This is in agreement with a similar analysis done for M1 neurons during 3D reaching, where Wang et al. observed an additive interaction between position and velocity tuning (Wang et al., 2007).

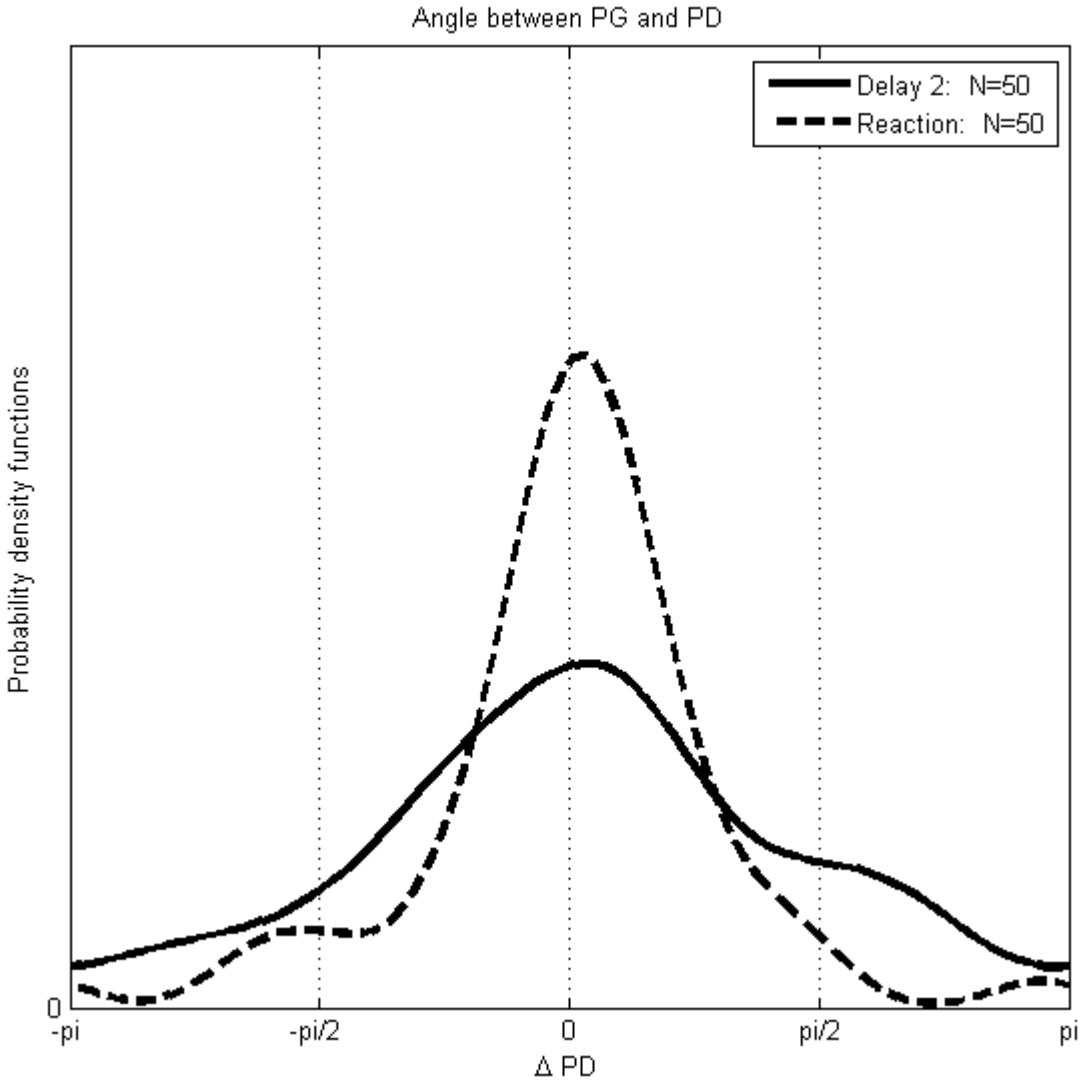

Figure 3.12: Preferred directions and position gradients are spatially correlated. The distribution of angles between PG and PD indicates that individual neurons' positional and directional tuning functions tend to have similar spatial orientations. All distributions: $p<0.001$.

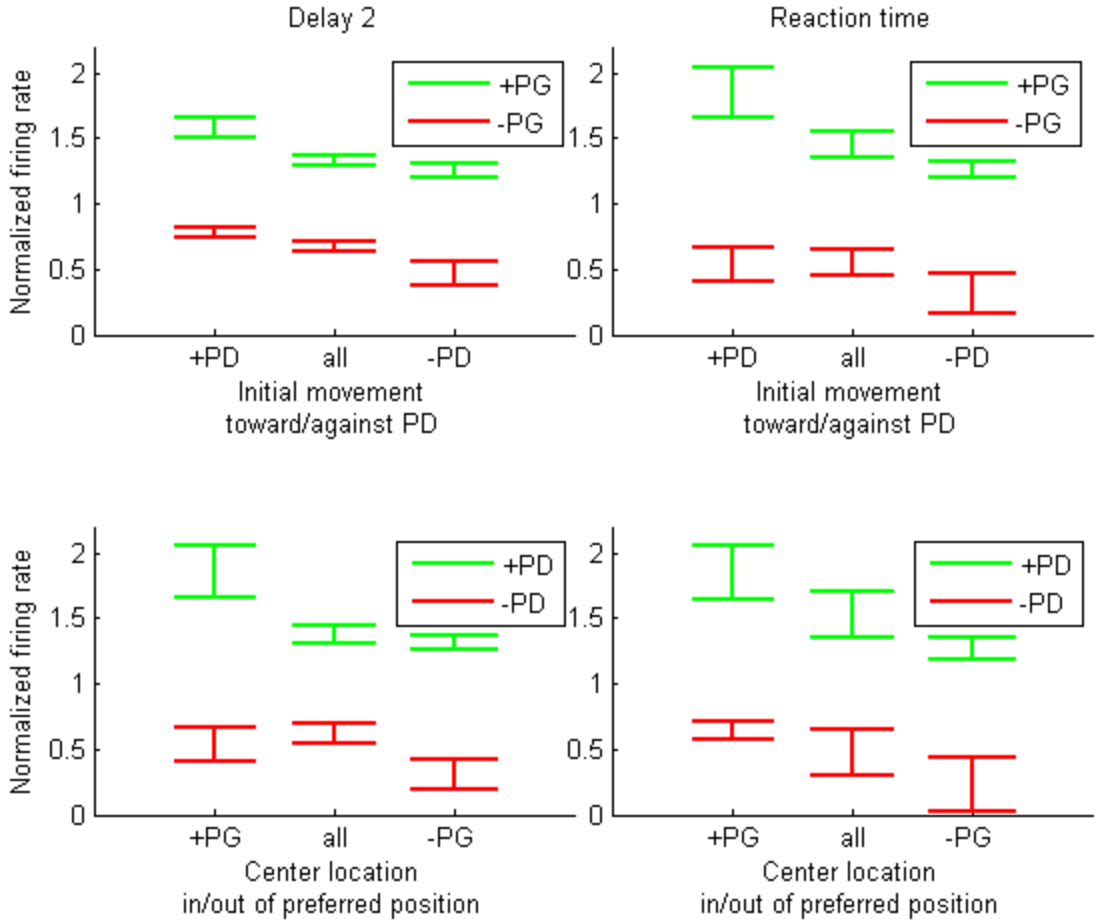

Figure 3.13: Interaction between position and direction. Top row: Trials towards/away from the preferred direction were considered separately and regressed against hand position. Bottom row: Trials with the hand held in/out of the preferred spatial location were regressed separately against the instructed direction. For comparison, the center column of each plot is the regression model from all trials. Overall, the interaction shifts the curve up or down but has only a modest impact on the amplitude of the tuning function. Each data point is mean +/ SEM.

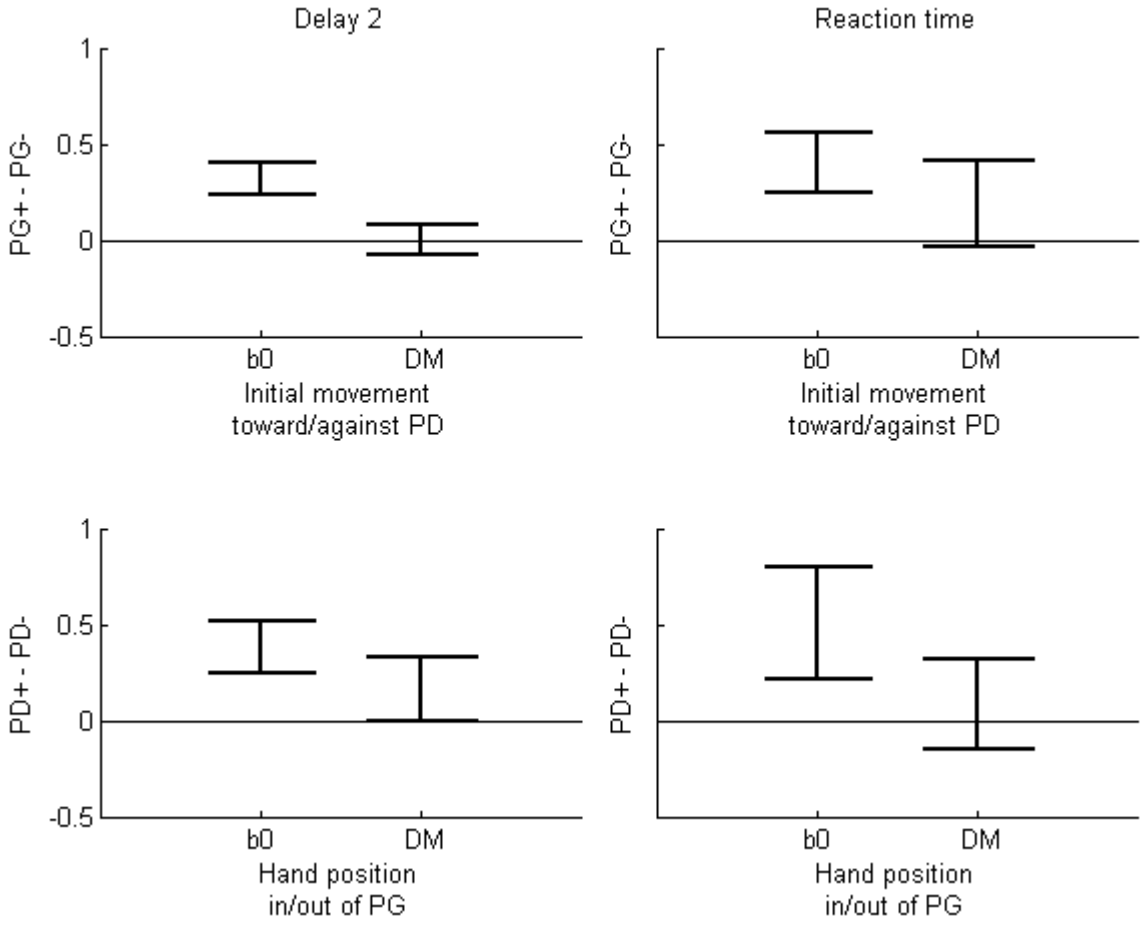

Figure 3.14: Interaction between direction and position tuning. Regressions were performed for trials in the preferred/antipreferred configuration. The differences in normalized baseline rate and depth of modulation are compared. 95% confidence intervals about the means are plotted.

3.3.7 Preferred directions are consistent across tasks

Although neurons do not necessarily tune significantly during all time periods with relevant information (fig 3.9), for those that do, the PD is stable across epochs (fig. 3.10). A related question is whether a PD measured in one task setting correlates with the same neuron's PD in another task. Unlike the basic center-out task, all reaches in the obstacle-avoidance paradigm begin from a single center location, so a comparison of static hand position tuning between the two is impossible. An across-task comparison can be made, however, with directional tuning. The extra obstacle delay period plus the addition of a separate directional parameter during that epoch provides three opportunities for neural tuning: target direction during delays 2 and 3, and initial movement direction (delay 3 only). For all neurons significantly tuned to i) one of these time-parameter combinations, and ii) instructed direction during center-out delay 2, the angle between the two PDs was compared (fig. 3.15). Reaction-time PDs were similarly evaluated (fig. 3.16). A clear trend can be seen - tuning measured during direct reaching is more correlated with the tuning to initial movement, rather than target, during indirect reaching.

An interesting observation is that the PDFs for the ΔPDs between center-out direction and target-tuning models appear qualitatively different than most of the other PDFs thus far (red curves, figs 3.15 and 3.16). In particular, the D2-target curve looks almost like the average of the D3-target and initial-movement curves; the target-tuning PDF during reaction time also shares this shape. To investigate further, the data were re-analyzed without combining the data across subjects. The results of this analysis reveal a clear difference - during delay 2, the distribution of target-PDs from monkey H is similar to the distribution of later movement-PDs. In contrast, target-PDs from monkey G do not correlate with the center-out PD, while the

movement-PDs do. During delay 3, target-PDs do not correlate with the center-out PDs in either monkey (fig 3.17, black curves). This delay-period difference in monkeys is explored in greater detail at the population level in chapter 4. It does not extend to the reaction time (fig. 3.18).

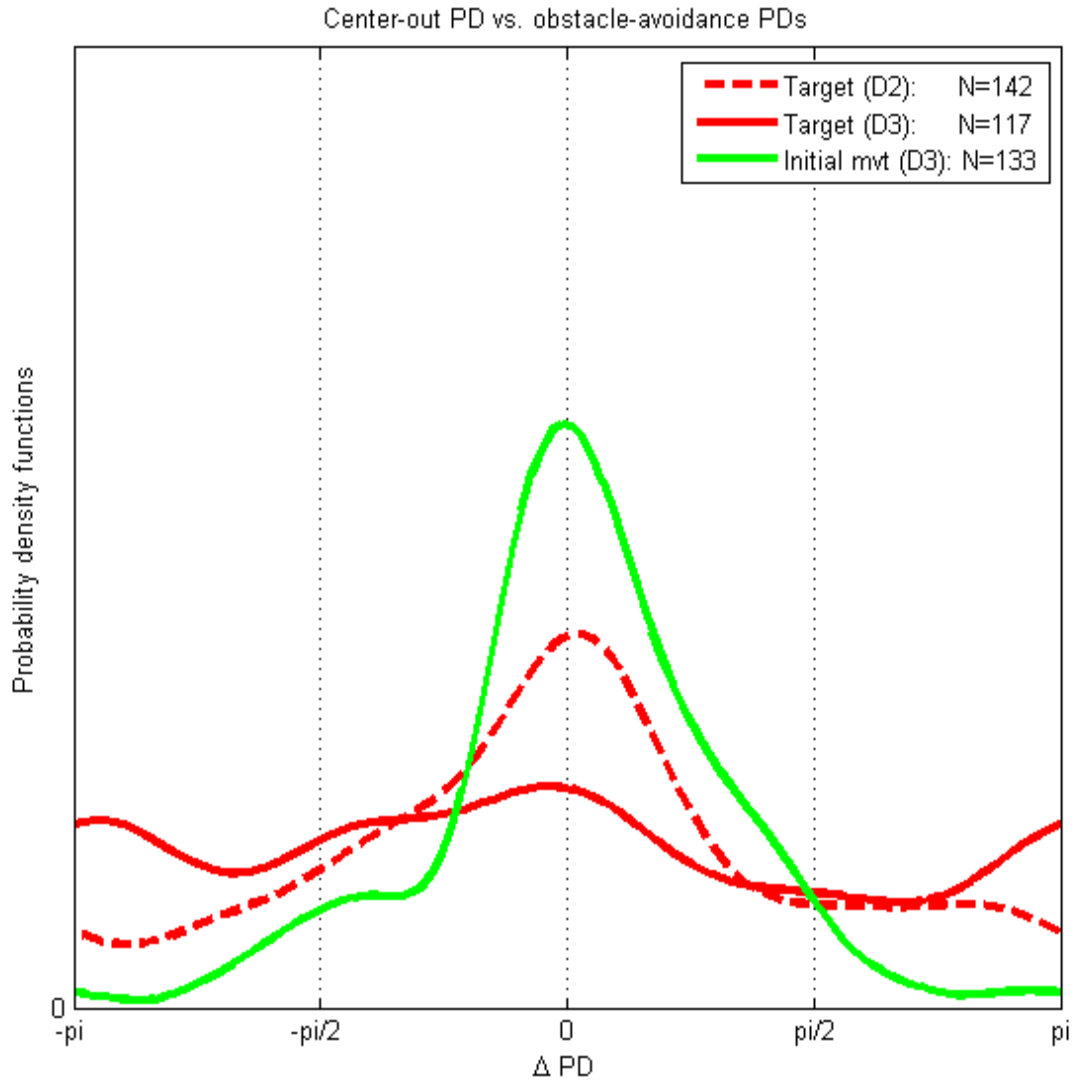

Figure 3.15: Correlation of center-out instructed direction PD and PDs from the obstacle-avoidance task during the delay periods. Center-out PD correlates strongly with initial movement PD ($p<0.001$); to a lesser extent (i.e. a lower peak in the PDF) with the target PD during delay 2 ($p<0.001$); and does not correlate with the target PD during delay 3 ($p>0.05$).

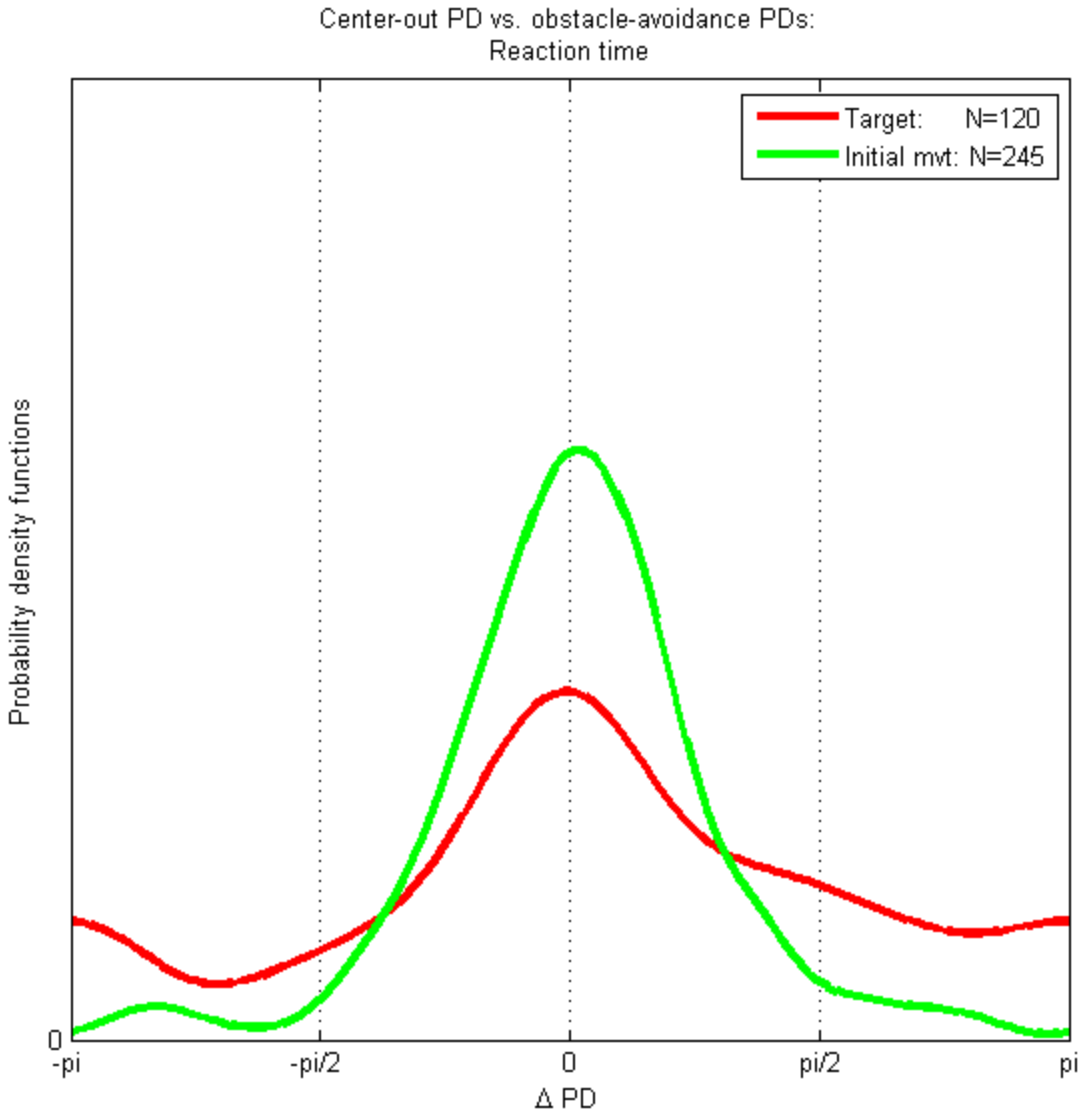

Figure 3.16: Reaction-time correlation between center-out PD and obstacle-avoidance PDs. As in fig. 3.15, the correlation is stronger between center-out and initial-movement PD than with the target PD. All distributions: $p<0.001$.

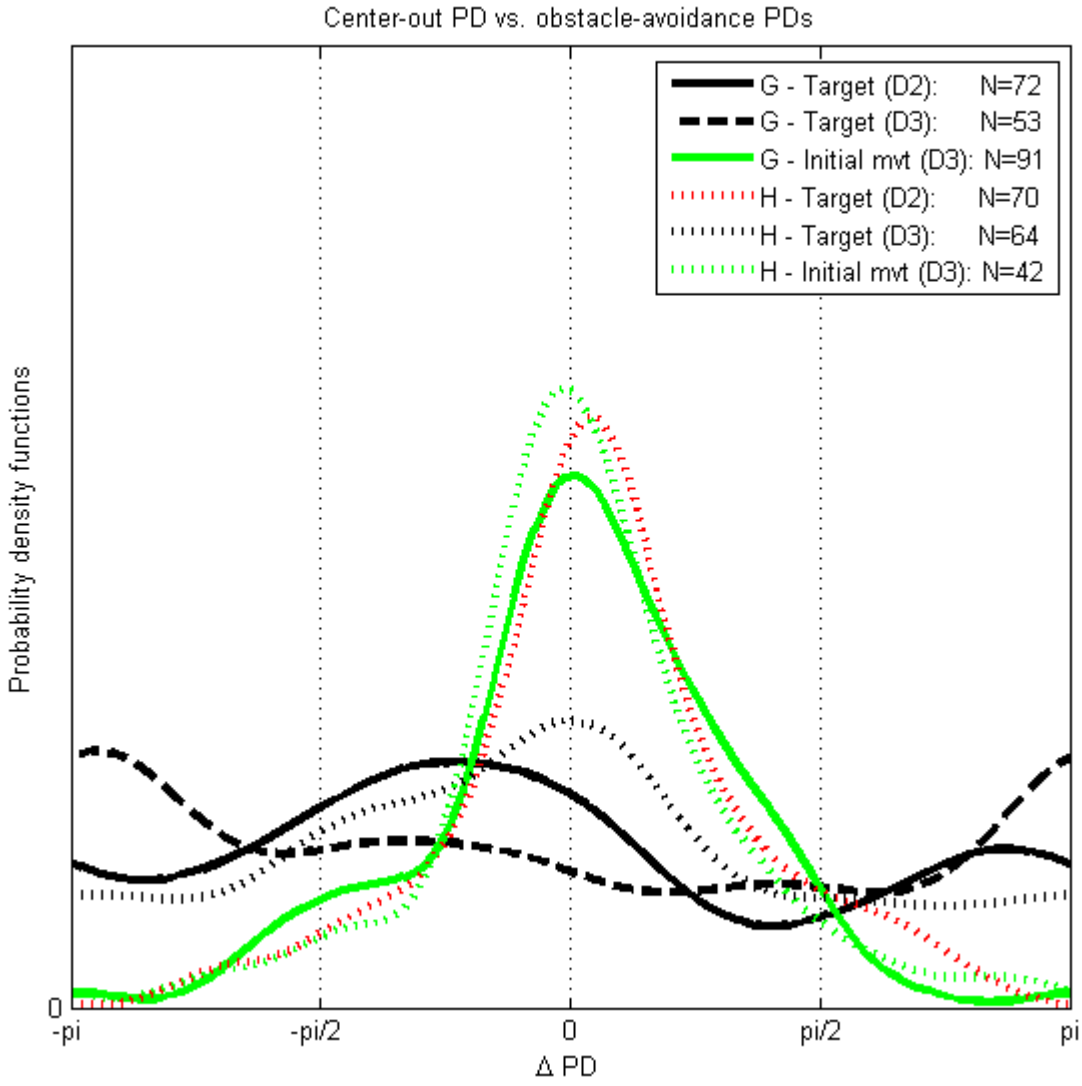

Figure 3.17: Delay-period correlation between center-out and obstacle-avoidance tuning curves, by subject. Same as fig. 3.15, with individual subjects separated. For monkey H, target-tuned PDs during delay period 2 behave equivalently to movement-tuned PDs during delay 3. This is not the case for monkey G. In both animals, target-PDs in delay 3 are not correlated with center-out tuning. Red and green curves are significant at a $p<0.001$.

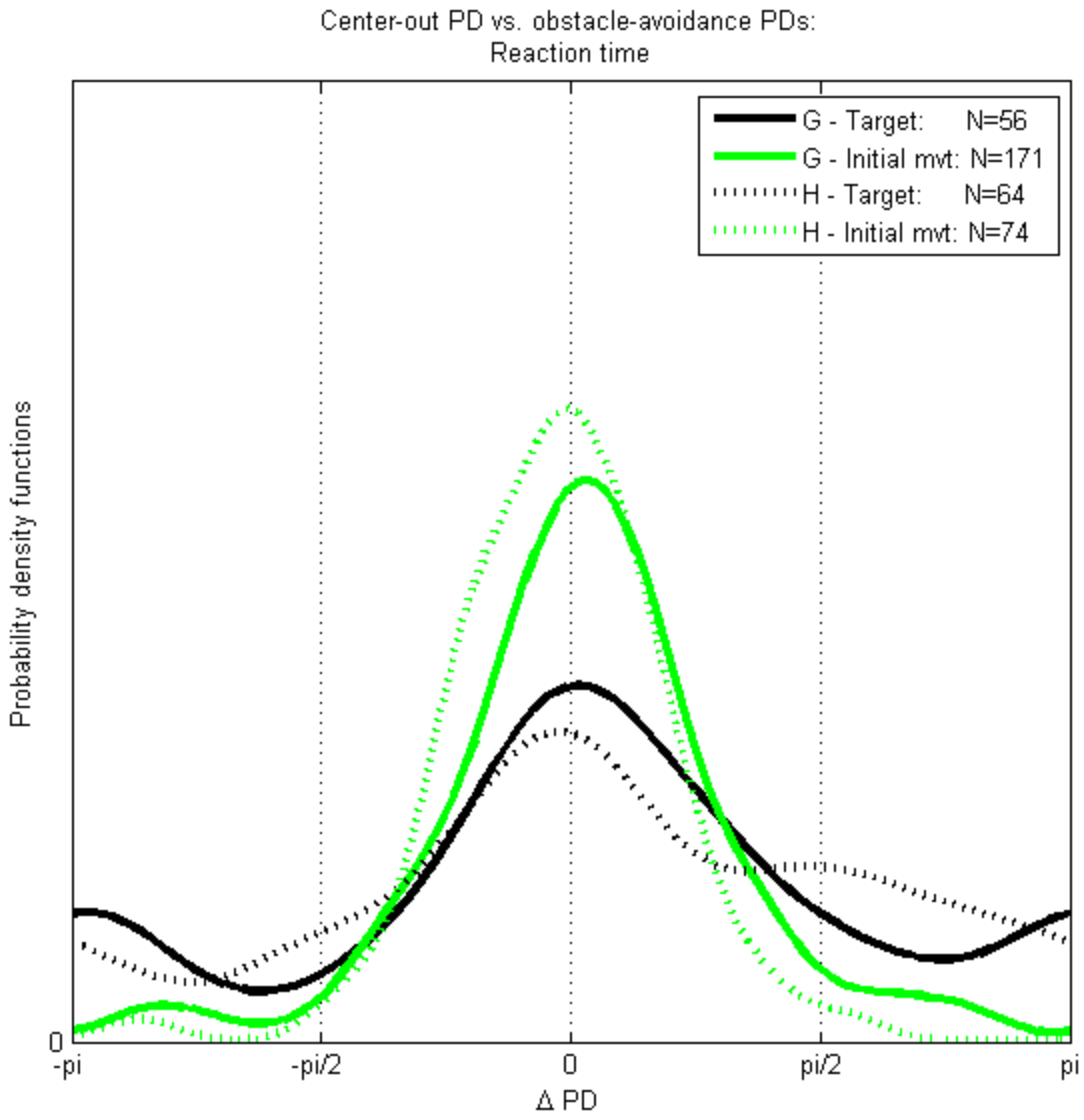

Figure 3.18: Reaction time correlation between center-out and obstacle-avoidance tuning curves. Same as fig. 3.16, separated by subject. During this epoch the monkeys do not show strong differences. All distributions: $p<0.001$.

3.3.8 Neurons tuned to initial movement and final target directions

During the epoch when the target and initial movement direction are both known to the animals, PMd neurons have significant linear relationships to both parameters. In fact, a subpopulation of neurons tunes to both parameters at the same time - two examples of this are shown in figure 3.4. In both exemplars, the tuning curves to initial movement and final target are roughly 180 degrees out of phase. Extending the analysis to all dual-tuned neurons, we find that anti-correlation of the PDs to the two parameters is a general feature of this subpopulation of neurons (fig 3.19). This result was not expected. Neurons that are modulated simultaneously by hand position and instructed direction tend to have similar spatial orientations of the two vectors, both in PMd (fig. 3.12) and in M1 (Wang et al., 2007). Similarly, in M1 cells that were modulated both by hand direction and final posture, preferred directions tended to move the arm toward the preferred posture (Aflalo and Graziano, 2006). Since the current finding is not congruent with these other results, a number of analyses were performed to rule out trivial explanations for the negative correlation between target and initial movement PDs.

First, we address the possibility that these units are not actually single neurons, but pairs of nearby cells each tuned to a single parameter. At first glance this seems possible, since neurons were not isolated online - more than one unit was frequently present on a single electrode, and putative individual units were determined later using offline spike sorting. Perhaps these dual-tuned units are actually pairs or groups of cells lumped together by poor spike sorting. To reduce the likelihood that this could account for the findings, the analysis was repeated on only those units with the largest amplitude spikes and most cleanly distinguishable clusters. Figure 3.19 (green curves) shows that this strict inclusion criterion does not alter the results. In addition, the proportion of tuned neurons is virtually identical between the most

exclusive subset and the population as a whole: 9.8% (D3) and 12.2% (RT) of the smaller population vs. 9.7% and 11.3% of the whole population.

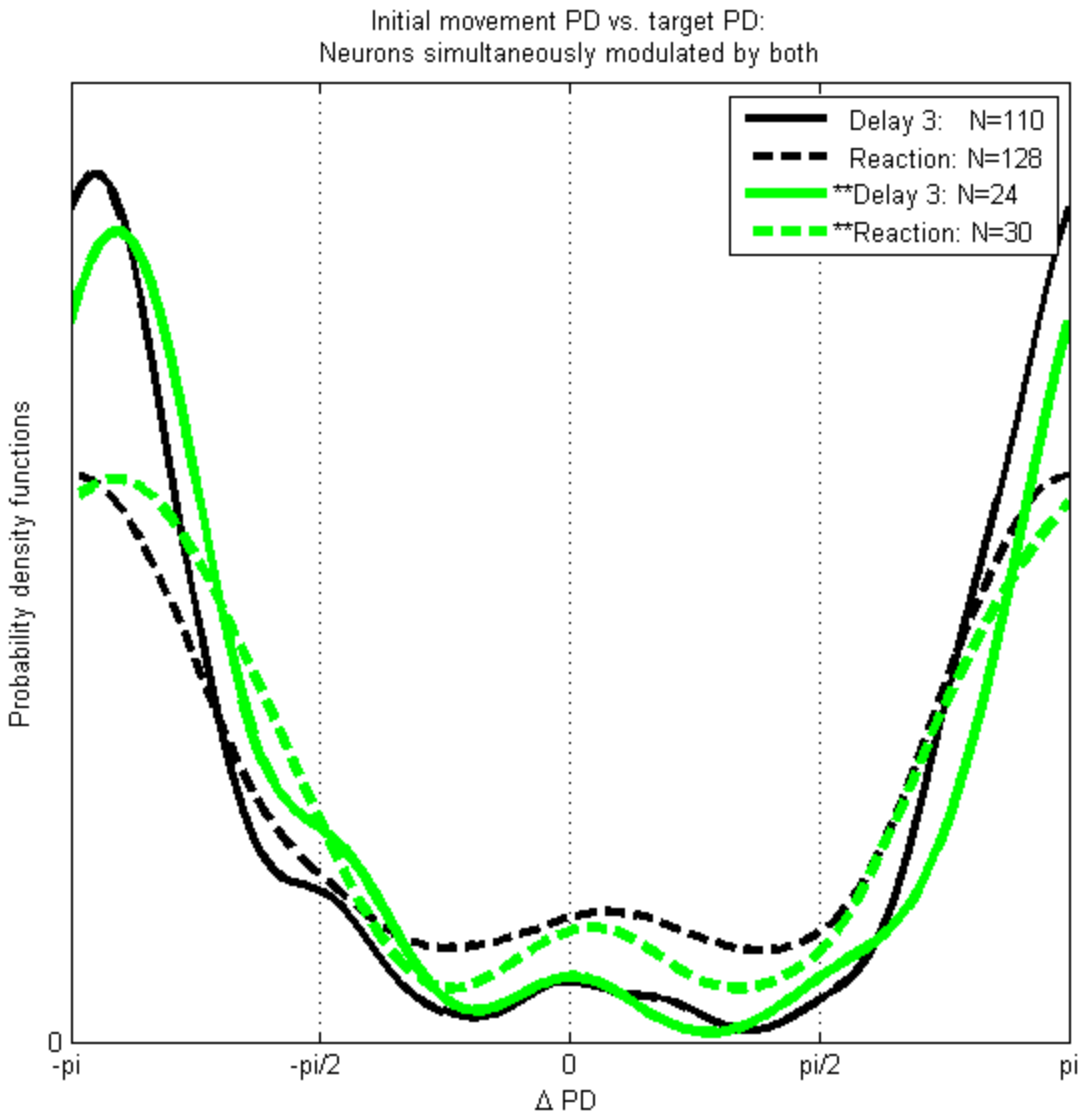

Figure 3.19: Anti-correlation between preferred movement and preferred final target direction. In neurons that are independently directionally modulated by both parameters, the PD vectors point in opposite directions. **Green curves are constructed from units with the largest spike amplitudes and cleanest isolations. All distributions: $p<0.001$.

A second potential confound is that the kinematics of the task may be at fault - the target direction and movement direction could be anti-correlated across conditions, even though the task was designed to decorrelate them. In this case, neurons that truly correlate with one parameter would spuriously appear to correlate with the other, with an opposing directional preference. Two findings argue against this explanation. First, many neurons that tune very strongly to either initial movement or final target direction do not tune significantly to the other (and many that tune to both do so only weakly). Second, the number of neurons modulated by initial movement direction during delay 2 (before the obstacle is displayed) is no greater than that expected purely by chance (fig 3.5). This would not be the case if the task was not adequately separating the parameters. As an example, firing rates during center-out-with-position can be regressed against relative target position or absolute target position. Prior to target onset, the only task variable is center position. Since the center positions and relative target directions are not correlated, only a chance number of cells show significance to the target. However, the absolute positions of the targets *do* correlate with center position. Thus, when neural firing rates are regressed against target position instead of direction, a significant number of cells appear tuned to the target before it has even appeared (fig 3.20). The same effect does not occur with initial direction tuning in delay 2, indicating that the conditions were adequately balanced.

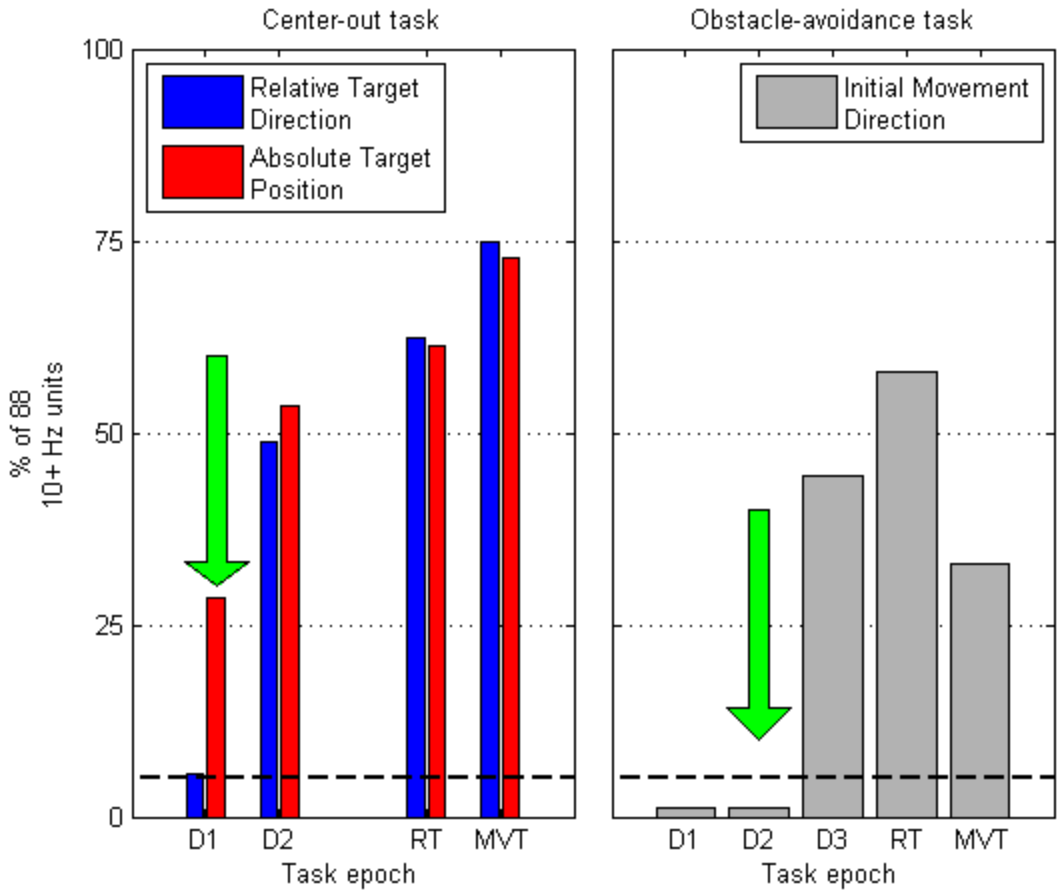

Figure 3.20: Example of the unobserved variable bias effect. In delay 1 of the center-out task the target has not been displayed, but some neurons tune significantly to the target position. This is because absolute target position is correlated with the starting position due to the task design. In contrast, only a chance number of neurons show significant effects of initial movement direction prior to obstacle onset (right). This indicates that the conditions are well-balanced and the initial movement direction is not correlated with target direction. Dashed line: p=0.05.

A third possibility is that these neurons may respond selectively to indirect hand trajectories. If direct trials fail to modulate the firing rate, for a given target the initial movement direction during all obstacle conditions is, on average, directly *away* from the target. A neuron tuned only for movement direction would thus appear tuned for the opposing target when all obstacle conditions are used in a regression analysis. The hypothesis that this anticorrelation is responsible for the appearance of opposite PDs to the two parameters can be tested by taking advantage of the task structure. The full set of trials can be subdivided by the relative orientation of target and obstacle: 0^o, $\pm 90^o$, and $\pm 135^o$. For each subset, firing rate can be regressed against both parameters. Hypothetical neurons with single-parameter tuning plus selectivity for indirect trials would be unmodulated on 0^o trials; modulated by either initial direction or target direction (but not both) on 90^o trials; and during 135^o trials would appear to be modulated by both with a negative correlation of the PDs. The 90^o condition is perhaps the most critical: all the trajectories are indirect, but the average initial direction is not correlated (positively or negatively) with the target. If the hypothesis is correct, this should abolish the appearance of simultaneous tuning; at the minimum it would eliminate the negative correlation between PDs.

The neural data do not agree with the predictions made above. Figure 3.21 shows tuning curves for exemplar neurons. A variety of properties can be seen in these examples. Direct trials may or may not be modulated, and can have higher or lower firing rates than indirect trials. The dominant feature, however, is that regressions on 90^o and 135^o trials find similar PDs, and the angular difference in PDs to the two parameters are anti-correlated, as in the full data set. The 90^o-trial analysis does not abolish the unimodal peak at 180^o (fig. 3.22, left). This result is incompatible with the explanation that the negative correlation is due solely to a single parameter.

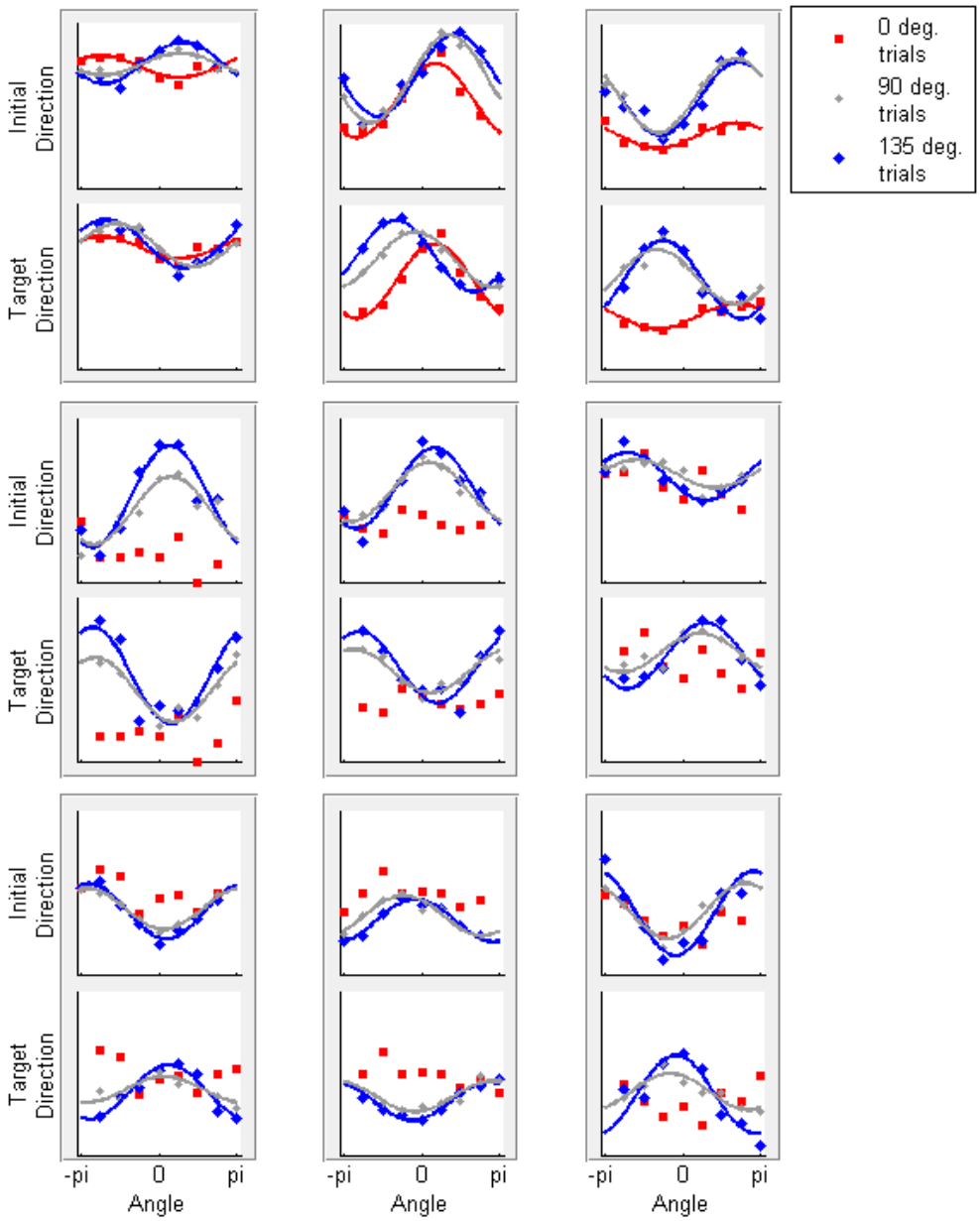

Figure 3.21: Exemplars of anticorrelated target and movement PDs with tuning curves fit independently for 0°, 90 ° and 135 ° trials. Each panel is a single neuron. The top plot in each panel is aligned by the direction of the obstacle opening; the bottom panel is aligned by target direction. Tuning curves are shown only when $p<0.05$. Note that for 0 ° trials the target and initial movement directions are the same, so by definition the red points and curves are the same in both panels.

A final possible explanation is that these neurons are modulated only by hand direction, but with a longer lead time - perhaps they respond to the direction the hand will be moving as it approaches the target, rather than the initial direction. During obstacle-avoiding paths, as the trajectory proceeds, hand direction becomes strongly correlated with the final target direction, and anti-correlated with the initial movement direction. This hypothetical cell would prefer direct reaches in the direction of the preferred target, since those reaches would be in the preferred approach-direction. Again, the data do not support this hypothesis. The preferred direction during direct center-out reaching correlates strongly with the initial movement PD, not the target PD - the opposite of the predicted pattern (fig 3.22, right). After ruling out these potential alternative explanations, it appears that the phenomenon of dual-tuned neurons with anti-correlated movement/target PDs is likely a true feature of the neural population in PMd. Like the interaction between position and direction tuning, the interaction between movement and target in this population is best described as additive (figs. 3.23, 3.24).

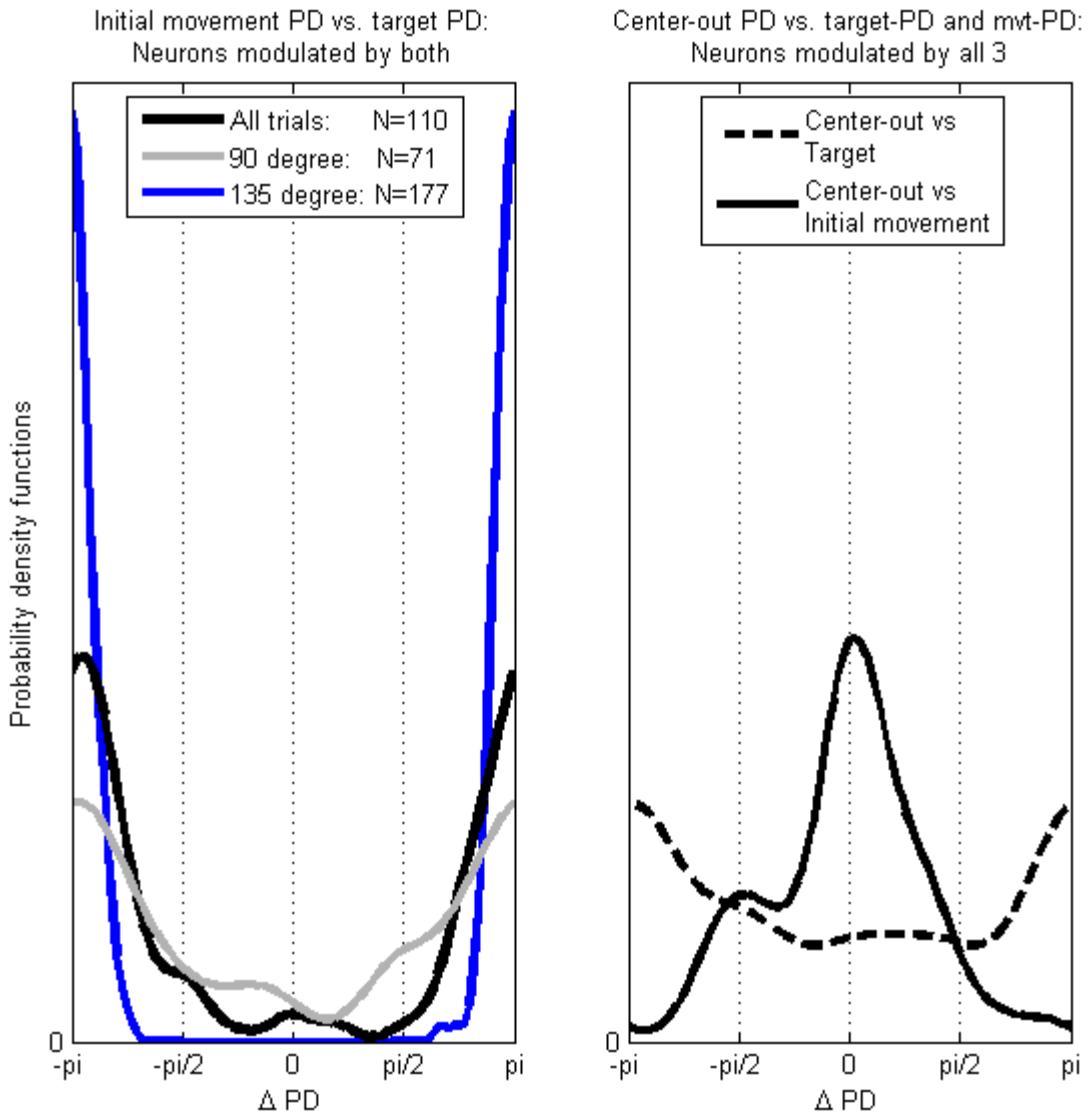

Figure 3.22: Features of dual-tuned neurons. Left: Neuronal responses to initial movement direction and target direction negatively correlate even when the regression analysis is limited to +/-90-degree conditions. It is likely that the extremely strong peak for +/-135-degree trials (blue curve) is a result of the trajectories on those conditions starting out, on average, exactly opposite the target direction. Right: In these neurons, the center-out PD is positively correlated with the initial movement PD, not the target PD.

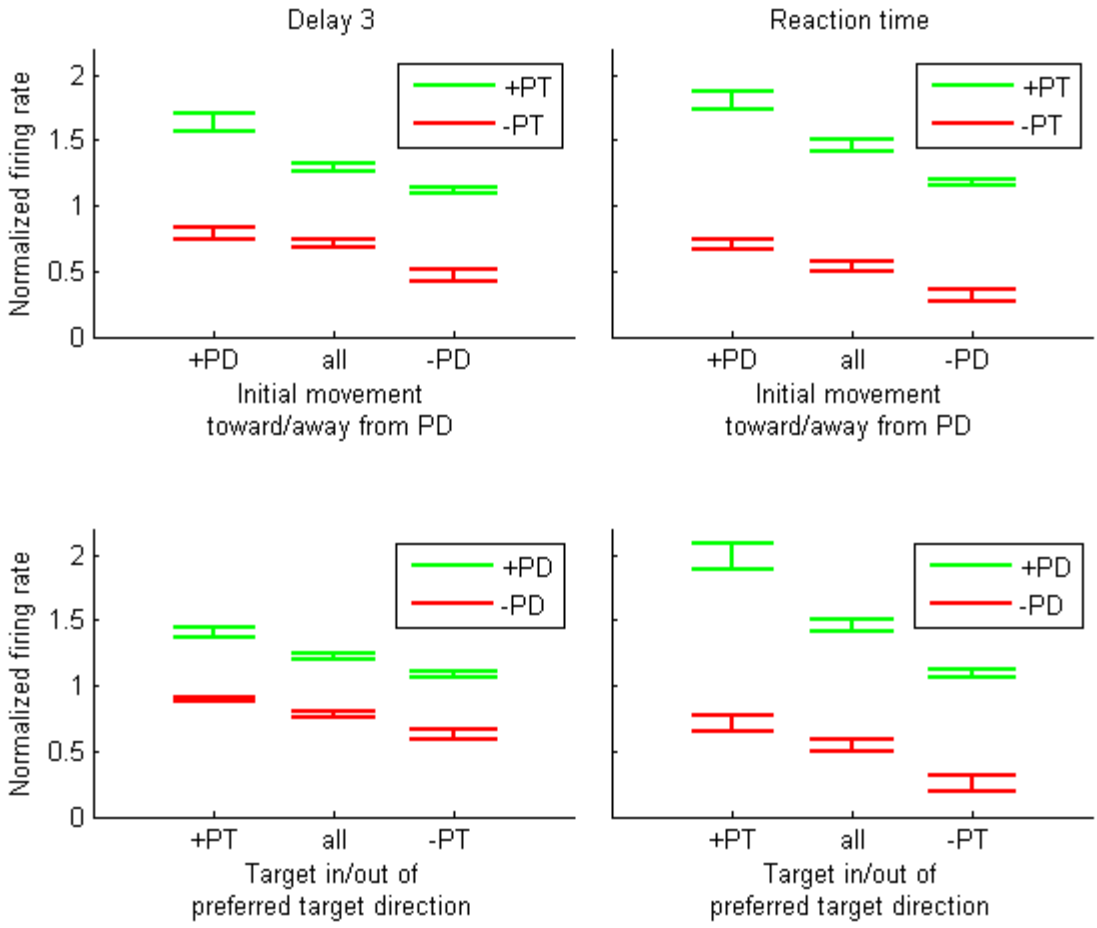

Figure 3.23: Interaction between target and initial movement directions. Top row: Trials towards/away from the preferred movement direction were considered separately and regressed against hand position. Bottom row: Trials with the target located in/out of the preferred target direction were regressed separately against the direction of initial movement. For comparison, the center column of each plot is the regression model from all trials. Overall, the interaction shifts the curve up or down but has only a modest impact on the amplitude of the tuning function. Error bars are mean +/- SEM.

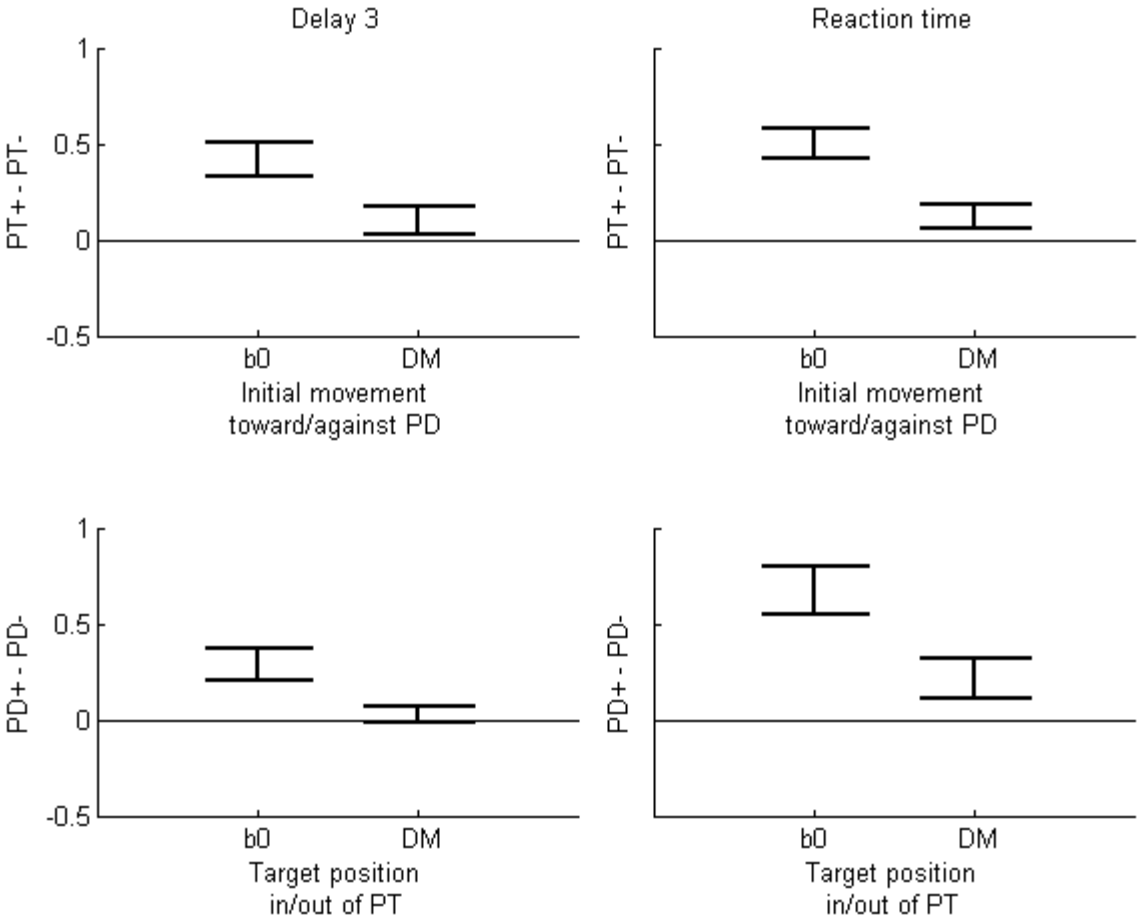

Figure 3.24: Interaction between initial movement direction and target tuning. Regressions were performed for trials in the preferred/antipreferred configuration. The differences in normalized baseline rate and depth of modulation are compared. Means and 95% confidence intervals are plotted.

Given the distinctive properties and low proportion of these neurons, it is possible that these are a distinct cell type – inhibitory interneurons, perhaps. A number of recent studies have utilized the shape of extracellularly-recorded waveforms to classify neurons as putatively excitatory or inhibitory, although the differences in response properties of the classes are generally small (Mitchell et al., 2007; Kaufman et al., 2010; Song and McPeek, 2010). Figure 3.25 shows the average waveforms (normalized by peak amplitude) and penetration locations of dual-tuned neurons, and of neurons tuned either for target or movement direction but not both. Consistent with other reports, the wave shapes generally fell into two general categories. These categories were well-represented across all three functional groups of cells, however, and there was no distinctive spatial clustering within the chamber.

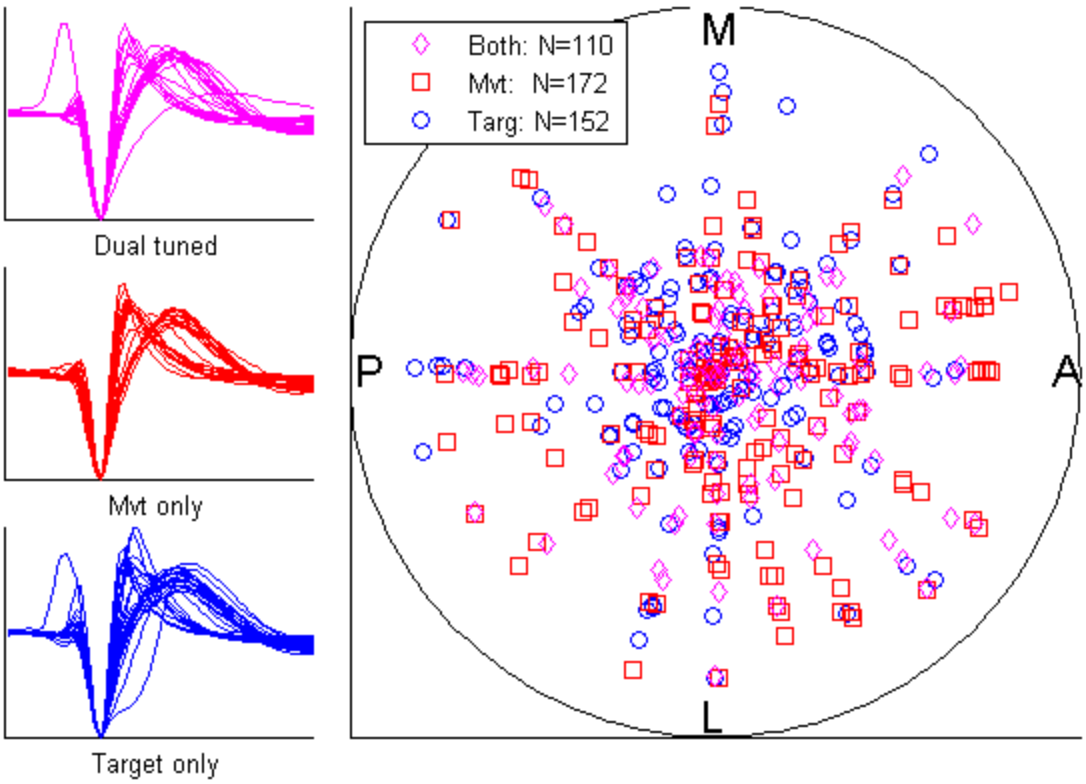

Figure 3.25: There is no evidence for anatomical differences in neurons modulated by target and movement direction at the same time, compared to either target or movement alone. Left: Extracellular waveforms of neurons tuned to both or only a single parameter. Waveform amplitudes have been normalized by the negative peak. Right: Penetration location within the recording chamber for the same classes of neurons. Significantly tuned cells were included at a threshold of $p < 0.05$. To be considered as tuned to only one parameter, a p-value threshold of $p > 0.2$ for the other parameter was used. True positions have been jittered slightly to show multiple neurons from a single penetration site.

3.4 Discussion

The experiments that comprise this thesis were designed with the primary goal of clarifying the effects of two directional parameters - target location and hand movement direction - on the activity of dorsal premotor neurons during movement planning. Outside the realm of common laboratory reaching tasks, the distinction can be quite critical. Voluntary reaching movements require the ability to consciously influence when to move, where to end up, and how to get there. In naturalistic environments, it is not uncommon for reaching movements to occur in the presence of non-target objects in the peripersonal space. To avoid injuring the limb or disturbing the environment, or a host of other reasons, it is often desirable to avoid contact with these obstacles. This requires computation of a hand trajectory based both on the location of the final goal and on other spatial constraints along the path. These types of movements are prominent in the primate behavioral repertoire, but not often studied in the context of primate neurophysiology.

Dorsal premotor cortex, long implicated in playing a role in planning visually-guided reaches, is a good candidate area to contain neural substrates supporting this behavior. The evidence from the current experiments supports the hypothesis that PMd neurons carry information about both the endpoint and initial movement plan. The majority of recorded neurons show broad tuning to a variety of spatial movement and task parameters. Although the relationship between any single parameter and neural firing rate is generally modest, simple linear regression models provide significant fits and allow (partial) quantification of the response properties of the neurons. For neurons with significant tuning functions, it was found that the orientation of the preferred direction was generally stable for the duration of the pre-movement period, including both the instructed delay and the reaction time (fig. 3.10). This was true even

of neurons that did not maintain a statistically-significant level of tuning at all times (fig. 3.11). Preferred directions were also found to be strongly correlated between different tasks: directional tuning during a simple center-out task corresponds closely with tuning curves for initial movement direction during a more complex reaching task. Although this result indicates that directionally-modulated PMd spiking reflects the planned hand movement direction, it by no means accounts for the full range of neuronal responses. Target direction also modulates a sizable proportion of PMd neurons, many of which are insensitive to the direction of initial movement.

3.4.1 A possible explanation for dual-tuned, anti-correlated neurons

The most interesting, and unexpected, finding of this chapter is a population of neurons that, during the same epoch within the task, are modulated by both the target direction and the initial hand direction. These dual-tuned cells consistently have oppositely-oriented preferred direction vectors to the two parameters. It is not immediately obvious why this should be the case. The response properties of many cortical neurons depend on multiple features of a stimulus; examples include direction and orientation of visual bars (Albright, 1984), optic flow and vestibular signals of heading (Gu et al., 2006; Yang et al., 2011), gaze angle and arm position in parietal cortex (Chang et al., 2009), and many others. Often the preferred stimuli are congruent, as with position and velocity tuning in PMd (fig. 3.12) or uncorrelated (like the hypothetical eye-related tuning discussed above). Strong negative correlations are less common, and cells with this feature are often considered to play specific computational roles in multisensory integration (Yang et al., 2011) or sensorimotor transformation processes (Chang et al., 2009). The neurons in question are a fairly modest proportion (~10%) of the recorded population of cells, and in simple reaching experiments appear similar to a larger set of

directionally-tuned neurons. Small numbers of cells with non-canonical and difficult-to-observe properties are not likely to be widely reported in the literature (e.g. (Shen and Alexander, 1997) note the presence of complex responses but go no further than showing a single example neuron). Nonetheless, a careful reading of prior work reveals potentially congruent observations from a number of previous studies in PMd.

A subset of PMd neurons described in the mid-1990s (Crammond and Kalaska, 1994) are interpretable as additional examples of the phenomenon of oppositely-oriented preferred target and movement vectors. In a direct-delay/reversal-delay task, monkeys were presented with a spatial cue in one of two locations. The color of the cue indicated that a reach should be made either toward or away from the cue location. Late in the delay period virtually all neurons were modulated by the reach direction, and an interaction with the cue was present in roughly 1/3 of the cells. In the two example neurons shown in that report, delay period firing before movement in the PD was enhanced by a reversal cue in the anti-preferred movement direction, compared to a directly cued reach. A number of task differences limit the ability to compare of neuronal responses in that report and the current one: for one, only the preferred and anti-preferred directions were used, making it impossible to determine whether the observed interaction was due to cue location or, as the authors suggest, stimulus-response compatibility. Another difference is that unlike the obstacle-avoidance task, in reversal-delay reaching the hand does not ultimately go to the instructed target location. However, neurons with dual-tuned, anti-correlated PDs would be expected to respond to that task in the same manner, under the following interpretive framework: Some neurons with movement direction preferences (as measured during direct reaching) are also recruited in order to help suppress direct movements to targets in the anti-preferred movement direction. In these cells, "target tuning" is not indicating that the hand

will end up there eventually; rather, the neurons fire strongly because the hand *should not* move in that direction initially. The preferences to move in one direction, and to *not* move in the opposite direction, have an additive influence on the overall firing rate (fig. 3.24).

This theory is, of course, speculative at this point. However, it does help make sense of a number of reports in the literature. Kurata and Hoffman injected PMd with muscimol (a $GABA_A$ agonist) during a task where monkeys made wrist movements toward one of two illuminated targets depending on a spatial or non-spatial color cue (Kurata and Hoffman, 1994). The pharmacological manipulation caused monkeys to make directional errors, always in a single direction for a given injection site. In addition, the direction of the erroneous movements was typically toward the preferred direction measured at the injection site. This result is consistent with the idea of directionally-tuned suppression of movements to incorrect target locations; muscimol may have inappropriately *enhanced* suppression of the target in the anti-preferred direction. The injections did not lead to errors when the correct target was cued directly (spatially, rather than by color).

In a different study, Sawaguchi et al. injected PMd with bicuculline, a GABA antagonist (Sawaguchi et al., 1996). At some injection sites, the monkeys made inappropriate (pre-cue) reaching movements that were consistently spatially oriented for each injection site. These were not random reaches; they were the same movements as the monkeys were performing in the task, just at the wrong time. Each inappropriate movement was associated with a burst of neuronal activity at the injection site. The authors suggest that GABAergic action in PMd plays a role in suppressing the initiation of trained reaching actions. Similarly, Moll and Kuypers noted that following lesions of a large swath of premotor cortex, including PMd, monkeys were unable to reach around transparent plexiglass barriers between their hands and a visible food target.

Rather, they repeatedly attempted to move their hands directly toward the food, in spite of the presence of the barrier (Moll and Kuypers, 1977).

Perhaps the strongest congruent evidence in the literature is a recent study from Gail et al. (Gail et al., 2009). Examining reaches toward and away from a target in the PD of neurons in PMd and PRR, they report that while PRR neurons preferred reaches toward a visual target, cells in PMd were on average enhanced by reaching toward inferred targets (opposite from the cue). The authors interpret this as evidence for "gain modulation [as] the computational mechanism underlying the integration of spatial and contextual information for flexible, rule-driven stimulus-response mapping, and thereby forms an important basis of goal-directed behavior." As with the neurons from Crammond and Kalaska (Crammond and Kalaska, 1994), this is exactly the pattern of activity that dual-tuned, anti-correlated neurons would be expected to have, particularly if the experiment was limited to testing only the preferred and anti-preferred directions.

Combining the current observations with previous reports, a picture of PMd emerges in which the suppression of practiced but (circumstantially) inappropriate movements is a critical feature. This interpretation may extend to virtually all types of nonstandard sensory mappings, or tasks with arbitrary and conditional relationships between sensory input and motor output. The current finding extends the previous ones in two important ways: first, it proposes that a common mechanism in PMd underlies both arbitrary stimulus-response mappings and a more inherent ability to make reaches in the presence of environmental obstacles – although the virtual reality obstacle-avoidance task is hardly natural, in the physical world this task poses little problem for monkeys. Second, it characterizes these neurons as having a very particular set of properties, which could play a useful role in computational models of motor planning. It should

be noted that although these neurons were not distinctive in terms of extracellular waveform shape (fig. 3.25), that finding does not preclude inhibition as a potentially important role for cells with these properties.

3.4.2 Individual differences between monkeys

These experiments provide an illustration of an underappreciated difficulty in determining the relationships between neural activity and behavior – monkeys can choose to perform a task differently, leading to different neuronal responses. The temporal structure of the two tasks is such that during delay 2, the same visual information is available - the hand is held at a central location, and a target appears somewhere in the periphery. In both tasks, and in both monkeys, a substantial proportion of neurons are cosine-tuned by the direction of the target during this delay period (figs. 3.5, 3.6). Going further, in both monkeys many of the same neurons were significantly modulated in both tasks. Despite this fact, a dramatic difference was seen in the cross-task PD correlations: in monkey H the PDs were highly congruent, pointing in similar directions in both tasks, while in monkey G there appeared to be a random distribution of angular differences between the two. The likely explanation is that since the obstacle-avoidance task usually contains an extra delay period with more spatial information, monkey G planned his movements differently than in the simpler task, while monkey H planned similarly. This difference in planning strategy is quite apparent in population-level analyses (chapter 4). The "uncorrelated" neurons in monkey G are interesting in their own right, however. Many of the same cells that tuned to target direction in a simple task also tuned to target direction in a different task, though perhaps not for the same purpose - and the directional preferences of the two types of tuning appear to be unrelated. Although eye fixation was not enforced in these tasks, a limited amount of eye-tracker data was collected during some of monkey G's recording

sessions. On many of the trials during these sessions, G would briefly saccade from the center to the target and back during delay 2. Eye position effects have been previously noted in PMd (Boussaoud et al., 1998) - it is possible that the tuning seen during this time period is related to eye movement in some way. Whether or not this is the case, a significant proportion of neurons in monkey G were directionally tuned to *something* during delay 2 of the obstacle-avoidance task, and that tuning was not spatially correlated with tuning during direct reaching. Further interpretation with only the data collected during these experiments is not possible.

3.4.3 Position coding in PMd

Evidence in the literature of PMd neurons tuning to static hand position is mixed. In one of the original neurophysiological studies of premotor cortex, it was reported that there was no obvious relationship of firing rate to hand position: "Movement-related premotor cortical units were examined for relationships between the parameters of movement and neuronal activity. Premotor cortex neuronal activity did not bear any obvious relationship to maintained position of the limb or the target of the movement, that is, units did *not* show a characteristic pattern of activity for movements to a given target regardless of the starting position of the movement, nor did they show different steady-state levels of discharge for different maintained positions." (Weinrich et al., 1984). The opposite result was found in a 1991 study, where it was reported that nearly 90% of PMd neurons had siginficant positional relationships (Caminiti et al., 1991). Part way between these two seemingly contradictory results, in 1996 Crammond and Kalaska reported statistically significant but relatively weak effects of hand position in premotor neurons (Crammond and Kalaska, 1996). More recent studies have investigated positional effects not in isolation, but in the context of relative coding of position, target and eye (Pesaran et al., 2006, 2010), or in various extrinsic or intrinsic reference frame experiments (Batista et al., 2007).

The results in figures 3.2 and 3.6 illustrate the existence of statistically significant positional effects on the firing rates of PMd neurons. The highest number of cells showing positional tuning was found during the initial hold time, before a target direction was specified. This relationship was found in fewer neurons during the second delay period. It is possible that this decrease in the proportion of significantly tuned cells is a result of some neurons losing (or weakening) their positional representation - responding to hand position only prior to target instruction. An alternative explanation is that the presence of additional preparatory directional information during the second delay may make it harder to detect the contribution of position to the overall firing rate at a particular statistical threshold. Figure 3.11 provides some evidence that this may be a contributing factor - the preferred position gradient of sub-statistically-significant neurons is correlated to the PG from earlier or later epochs in which tuning achieves significance.

4 Population vector analyses

4.1 Introduction

The cosine tuning properties of PMd neurons during large windows of delay-period activity were examined in the previous chapter. In this chapter, those tuning functions are used as the basis for constructing population-level decoding models. The decoders are applied to smoothed estimates of instantaneous firing rates, and are used to predict kinematic features of the monkeys' behavior during the planning and execution phases of the obstacle-avoidance task. The kinematic encoding models determined from the center-out task transfer well to the neural data during obstacle-avoidance: a decoder built from preferred direction vectors during center-out preparatory activity predicts the initial direction of hand movement that is needed to escape the obstacle, and a position-gradient-based decoder predicted the hand path during movement with an approximately 200 ms neural lead time. The temporal evolution of the decoded initial movement plan suggests that the two monkeys utilized distinct planning strategies on the task, consistent with the observations from chapter 3 about differences in single-neuron tuning properties between the monkeys.

This chapter consists of a modified final author version of a published report (Pearce and Moran, 2012). For clarity and continuity in the current format, the figures from the main text and the supporting material have been merged and re-numbered according to the order they are referenced within the text. Footnotes referring to supporting material have been removed, as the information is available within the methods and materials located at the end of the chapter. Note: in this report, all neurons with fewer than 5 repetitions of any movement condition were

excluded. This is a stricter criterion than was used in chapter 3, so the size of the data set is correspondingly reduced.

4.2 Pearce and Moran (2012)

Humans and other primates are adept at reaching for visually-identified targets, an important element of the behavioral repertoire. The neural mechanisms supporting this have long been an active area of investigation. For reaching movements, the output of the motor system is a sequence of muscle activations which guide the hand appropriately through space to achieve the goal of the reach. Before movement initiation, sensory information and cognitive processes interact to form an initial movement plan. During this preparatory period, neural activity relating to the upcoming reach can be seen in a network of frontal and parietal cortical areas, including the premotor (PM) and primary motor (M1) cortices (Wise, 1985; Georgopoulos, Crutcher, et al., 1989; Kalaska and Crammond, 1992; Wise et al., 1997). Instructed-delay reaching tasks, an experimental paradigm in which a monkey is shown a target but must withhold movement until a 'go' cue is given, allow this preparatory neural activity to be probed. Electrophysiological (Crammond and Kalaska, 2000; Cisek and Kalaska, 2005; Churchland and Shenoy, 2007a), imaging (Kurata et al., 2000; Simon et al., 2002), and transcranial magnetic stimulation (Busan et al., 2009) studies highlight dorsal premotor cortex (PMd) as a critical area for planning reaching movements. However, the precise relationship between neural activity in PMd and reaching behavior remains unresolved. Many PMd neurons show a sensitivity of firing rate to direction, be it the direction of arm movement (Weinrich and Wise, 1982; Wise, 1985; Moran and Schwartz, 1999; Cisek and Kalaska, 2005), an effector in visual space (Ochiai et al., 2002), a target location (Shen and Alexander, 1997), visuospatial

attention (di Pellegrino and Wise, 1993; Lebedev and Wise, 2001), or other parameters. Unfortunately, virtually all of these factors correlate with each other under normal circumstances - the hand movement and visual movement are correlated, the target direction and movement direction are correlated, and so forth. Neural activity related to any of these parameters will thus also correlate with the others. The widely-used center-out task (Georgopoulos et al., 1982, 1986), in which a subject makes hand movements in all directions from a central starting point, is particularly susceptible to this limitation. To interrogate directional tuning properties in more detail, tasks designed to decorrelate certain aspects of the behavior, such as arm movement from visual cursor movement (Ochiai et al., 2002; Schwartz et al., 2004) or position from velocity (Wang et al., 2007), are commonly employed. We dissociated target direction from initial movement direction, allowing us to independently examine the effects of target and planned movement directions on preparatory neural activity.

To investigate the importance of target selection and motor planning in PMd and provide a framework for relating our findings to classic center-out based studies of motor cortical function, we adopted the following experimental approach: 1) train rhesus macaques to perform two reaching tasks, a standard center-out and a complex obstacle-avoidance paradigm; 2) record single-unit activity from PMd while the monkeys perform both tasks in a blocked design; 3) quantify the relationship between the firing of individual neurons and various parameters by fitting cosine tuning curves; 4) construct population decoding models from these tuning properties; 5) evaluate the performance of the models at predicting behavior by decoding the recorded neural responses.

The behavioral tasks consist of arm movements in free space within a virtual reality simulator, with hand position mapped onto a frontoparallel plane (fig. 4.1-4.2). Both tasks

involve a set of instructed delay periods with information revealed sequentially prior to a 'go' cue. The basic center-out task consists of direct reaching movements in eight directions from five different starting locations. Since the hand is held at different locations and the target is unknown during delay 1, the preferred position gradient for each neuron can be determined without interference from the formation of a movement plan. In the second delay period the target is revealed; during this time neuronal preferred direction can be determined analogous to prior studies. The obstacle-avoidance task begins with the same delay sequence but with a single, central starting position. During a third delay period, an obstacle is revealed which may or may not require the monkey to make an indirect hand trajectory to reach the target successfully. In both tasks, after a random length final delay, the sphere representing the start position is extinguished, indicating that the reach can begin. Successful movements (those that acquire the target while avoiding the obstacle, if necessary) are rewarded following a target hold period. Two monkeys performed the reaching tasks while acute intracortical recordings were taken from contralateral PMd. A total of 723 single units were recorded (monkey G, 343; monkey H, 380).

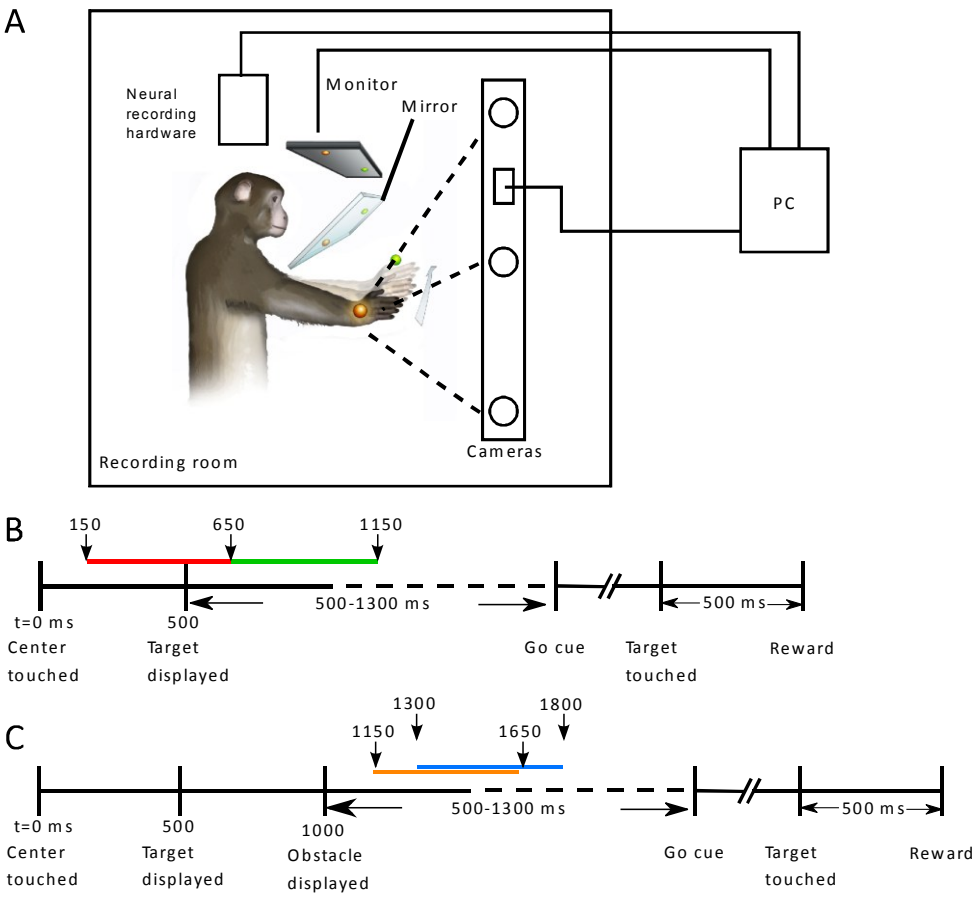

Figure 4.1: Experimental setup. A) The monkeys sat in a primate chair with the arm ipsilateral to the recording chamber restrained. An optoelectric marker was located on the dorsum of the hand contralateral to the chamber and used to track hand position. Movements were unconstrained and occurred in 3D space. B) Detailed timeline of a center-out trial. Position regressions were performed using the firing rate from 150 to 650ms after the initial position was reached (red line). Initial velocity regressions were performed during a window 150 to 650ms after the target onset (green line). C) Detailed timeline of an obstacle-avoidance trial. Initial velocity regressions were performed using the firing rate from 150-650ms after the obstacle was displayed (orange line). Target/goal direction regressions were performed using the firing rate from 300-800ms after the obstacle was shown (blue line).

Population vector (PV) analysis (Georgopoulos et al., 1986) was used to investigate the spatial and temporal aspects of the neuronal population representation of planned and executed movements. Position and velocity encoding of the hand are represented at the single neuron level within motor cortex (Wang et al., 2007). To evaluate contributions of these parameters in PMd, we calculated the preferred movement direction and position gradient of each neuron from delay-period activity in the center-out task. These tuning properties were then used to construct two PV decoders, one for position and another for velocity. The PV models were applied to the obstacle-avoidance data to decode time-resolved estimates of instantaneous firing rates during the planning and movement epochs. Taking advantage of the rotational symmetry of the task, we collapsed all trials (fig. 4.2C and fig. 4.3) down to the 5 relative orientations of target and obstacle (Fig. 4.2D-E), effectively increasing the repetitions of each movement. Figure 4.2E shows the neural prediction of hand path for each relative orientation, as decoded by the positional PV from movement-epoch activity. The neural population response preceded the actual hand movement by approximately 200 ms (fig. 4.2F-G). The velocity PV decoded from movement time activity yielded poor reconstructions (fig. 4.4) suggesting that PMd activity better represents hand position versus hand velocity during movement.

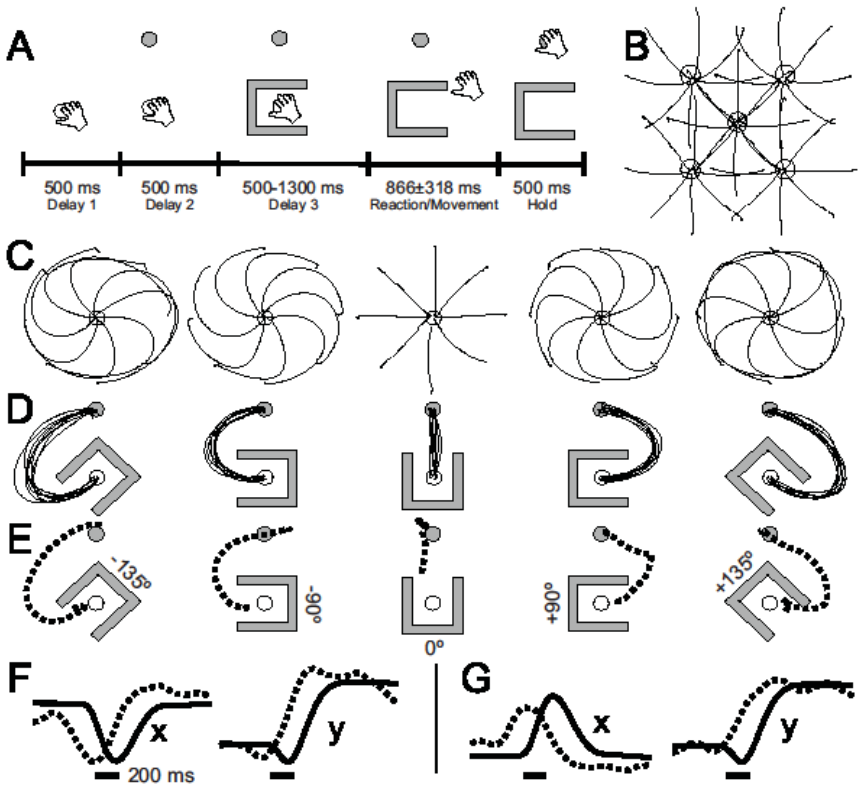

Figure 4.2: Kinematics and neural decoding of hand trajectory (monkey G). A) Single trial timeline for the obstacle-avoidance task. B) Mean hand trajectories for the 40 unique center-target combinations in the center-out task. C) Mean hand trajectories for the 40 unique target-obstacle combinations. For clarity the trajectories have been separated into panels according to orientation of the obstacle relative to the target direction. D) The trajectories from C, rotated such that the target direction is always straight up. E) Neural prediction of hand path for the conditions in D, decoded with the position-PV during the movement epoch. F) x- and y-components of hand position (solid line) and neural prediction (dashed line) for the -135° condition (D-E, left). Scale bar: 200ms. G) Same as F, for +135° condition (D-E, right).

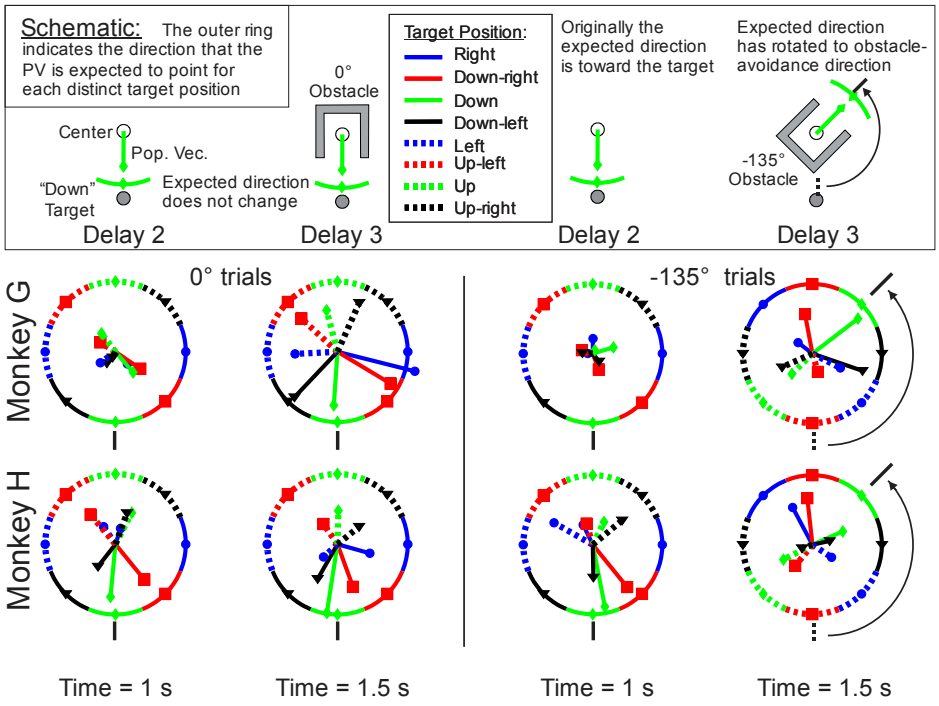

Figure 4.3: Population vector (PV) performance to individual targets for two relative obstacle orientations. The velocity-based PVs are decoded from neural activity for 5 repetitions to each of the 8 targets**.** Top: schematic illustration of a PV to a single target, for two obstacle conditions. The vector originates from the "center" circle, where the hand is located during the delay periods. The arc with matching color and line style indicates the direction the PV is expected to point based on the information available in each epoch. Bottom: PVs from monkeys G and H. Time = 1 s occurs at the end of delay 2, immediately prior to obstacle onset while time = 1.5 s occurs 500 ms after obstacle appearance. In both the 0° and -135° trials, monkey G waits for the obstacle information to appear before developing significant length in the population vectors. Monkey H, in contrast, develops significant populations pointing to the target at time = 1s. By time = 1.5s, monkey H has rotated these vectors to the appropriate obstacle exit direction.

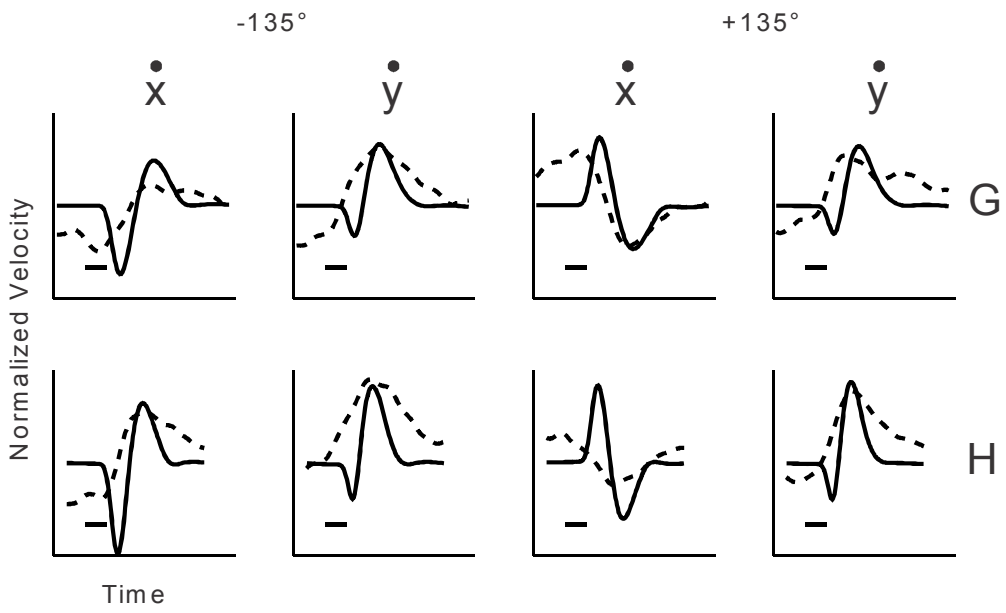

Figure 4.4: Decoding velocity during the movement period. *x* and *y* component velocities are shown for the ±135° conditions (the same conditions as in fig. 4.2 F-G for the position decoder) for monkey G (top) and monkey H (bottom). Solid lines are the average velocities of the recorded kinematics, while dashed lines are the PV-decoded velocity estimates. A relationship exists but is weaker than that seen for the decoded hand positions (fig. 4.21 E-G). Scale bars: 200ms.

During the preparatory period, the velocity-based PV predicts the initial direction of movement required to escape the obstacle. The temporal evolution of the neural activity suggests that the two monkeys likely adopted different strategies on the task. Figure 4.5 illustrates the behavior of the velocity-based PV for two trial conditions for each animal, as it changes over the course of the delay periods. The lengths and directions of the PV for all trial types are shown in figure 4.6. In monkey G, the length of the PV remained insignificant until the final delay period, and pointed in the direction of the upcoming hand movement soon after lengthening. The PV for monkey H, in contrast, achieved significant length and pointed toward the target during the second delay, when only the target was shown. When the obstacle was revealed, the vector changed to the new direction. In both monkeys, the velocity-based decoder (built from target-tuning properties in the center-out task) ultimately predicted the movement direction rather than the target direction, suggesting that directionally-tuned planning activity during a simple reaching task primarily represents the planned initial hand direction rather than the final spatial goal of the reach.

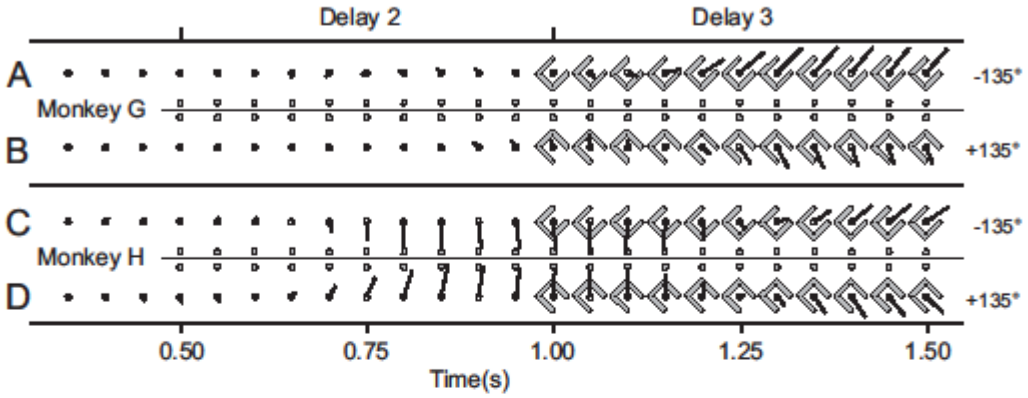

Figure 4.5: Decoding delay-period neural activity with the velocity-based PV. A-B) Monkey G, +/-135° trials. The PV remains insignificant until the obstacle is shown. C-D) Same as A-B, for monkey H. The PV initially reflects the target direction before switching to the initial hand direction.

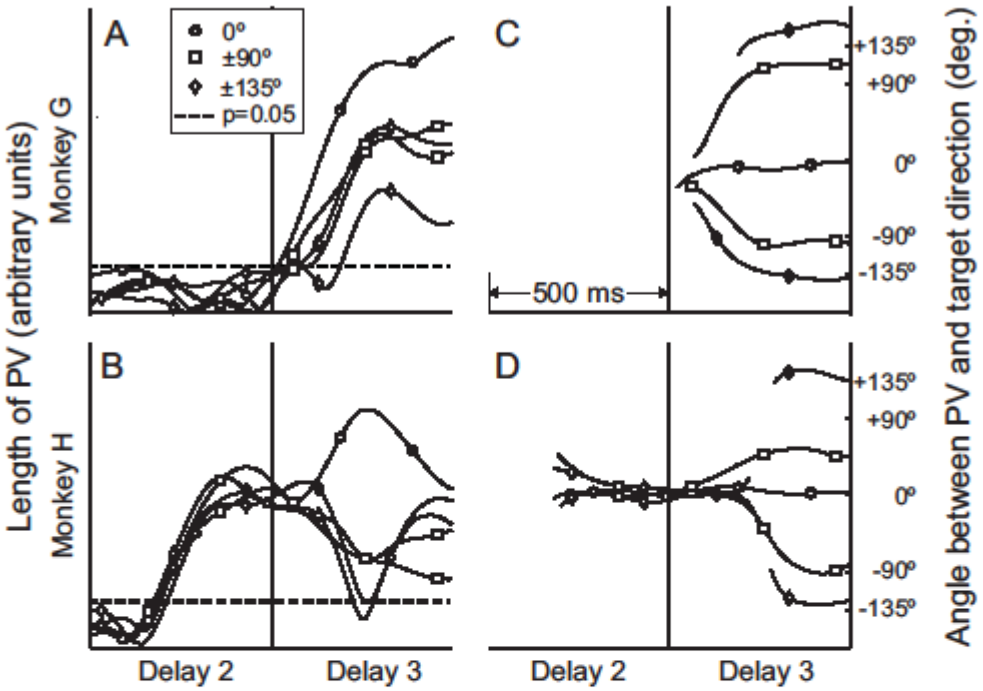

Figure 4.6: Planning strategies seen in the velocity-based PV response. A-B) PV length for each monkey during delay 2 and 3 for the 5 relative orientations of target and obstacle. Monkey H lengthens the PV immediately after target onset while monkey G does not. C-D) Angular difference between PV and center-target vector. Lines are hidden where the length of the PV is insignificant.

We next asked whether, in a more complex situation, a representation of the target might also be present in PMd. The obstacle-avoidance task fully decorrelates the target and initial movement directions, allowing us to perform regression analyses of the two parameters independently. Individual neurons can significantly tune to both target and movement directions simultaneously (fig. 4.7). This suggests that single cells in PMd participate in the population coding of a high-dimensional space which includes both the initial segment and ultimate goal of a movement. Some of the variance left unexplained by a particular tuning model can be accounted for by tuning to additional parameters, while some is truly noise (either intrinsic or due to sampling effects). Of the entire sample of recorded units, some tuned significantly to target direction, others to movement direction, some to both and some to neither. An insignificant proportion of units showed tuning before the relevant information was revealed, confirming that the directional parameters were successfully separated and were not anticipated by the monkey before the visual cues were given. Upon display of the target or obstacle, the directional information began to influence neural responses, with over 60% of all units tuning significantly to at least one parameter during the final delay. The diverse single neuron tuning properties in this study are reminiscent of the heterogeneity of neural responses reported previously in the spatial (Hocherman and Wise, 1991) and temporal (Churchland and Shenoy, 2007b) domains. It has been hypothesized that this heterogeneity allows the neural population to act as a basis set for encoding multiple movement parameters (Kalaska and Crammond, 1992; Churchland and Shenoy, 2007b). Our results support this view: the myriad ways that multiple spatial and temporal parameters are combined in the firing of single neurons leads to complex rate codes that can nonetheless be decoded in the context of the whole population. The combination of position, velocity and goal encoding is particularly relevant to computational

models of reach planning that utilize current state and target information to generate desired movement vectors (Shadmehr and Wise, 2005; Schaal et al., 2007).

The single neuron regression analyses suggest that target direction, in addition to initial movement direction, is present in the population code in PMd, at least in some circumstances. We tested this using PV models built from preferred target directions during the final delay of the obstacle-avoidance task, when the animals were aware of both the target and the necessary hand path. The results of this analysis confirm that by using a population model built from target tuning properties measured in the appropriate setting, target direction can be decoded independently of initial hand direction during the planning period (figs. 4.8, 4.9). This target representation appeared in the population code only when indirect movements were being planned: during delay period 3 of trials where an obstacle-avoiding, curved trajectory was needed, the PV lengthened and pointed toward the target. In contrast, when the obstacle did *not* interfere with a direct movement to the target, the PV was significantly shorter (fig. 4.9). Target encoding was also absent during delay 2, before the obstacle was displayed. During that period, the velocity-based PV analysis indicated that monkey G was not yet planning a movement, and monkey H was preparing a direct reach (figs. 4.5, 4.6). As neither monkey was planning an indirect trajectory at that time, the lack of a significant target-PV response is expected. A third result consistent with these findings is that the velocity-based decoder - built by regressing against target direction in the center-out task - predicts initial movement direction, not target direction, when applied to indirect movements. This suggests that the goal representation was significantly weaker than the movement representation during the center-out task. In this framework, target encoding would be expected to be minimal during that task, since all movements are unimpeded during center-out reaching. The finding that ultimate goal direction

is strongly represented in PMd for indirect relative to direct reaches suggests a potential role in shaping the reach beyond the initial segment of movement, similar to sequential reaching tasks (Catalan et al., 1998; Baldauf, 2011), but this hypothesis was not explicitly tested.

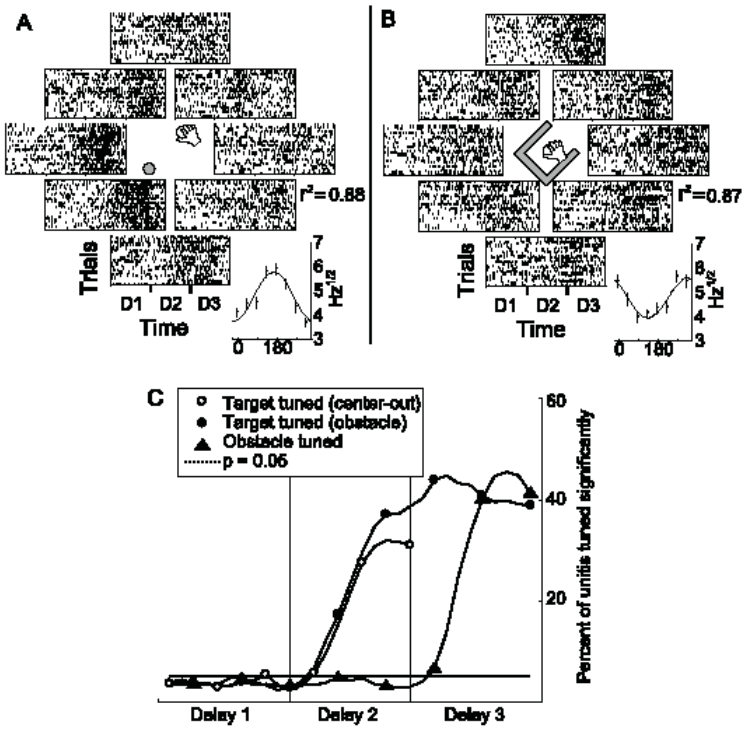

Figure 4.7: A single neuron simultaneously tuning to target and obstacle directions during the delay period. A) Spike rasters during delay periods 1-3 for a single neuron. Each row is a single trial, and the panel in which a row is located indicates the target direction for that trial. Inset: cosine fit to target direction during delay 3. This neuron prefers targets down and left. B) The data shown in A have been reorganized according to the direction of the obstacle opening for each trial. Inset: cosine fit to obstacle direction during delay 3. The same neuron that prefers targets down and left (from A) prefers obstacle openings pointing up and to the right. Two independent directional parameters are encoded simultaneously via noisy cosine tuning. C) Percentage of all recorded neurons significantly tuned ($p < 0.05$ for cosine fit) as a function of time. Tuning to each independent parameter occurs only after the information regarding that parameter is revealed to the monkeys.

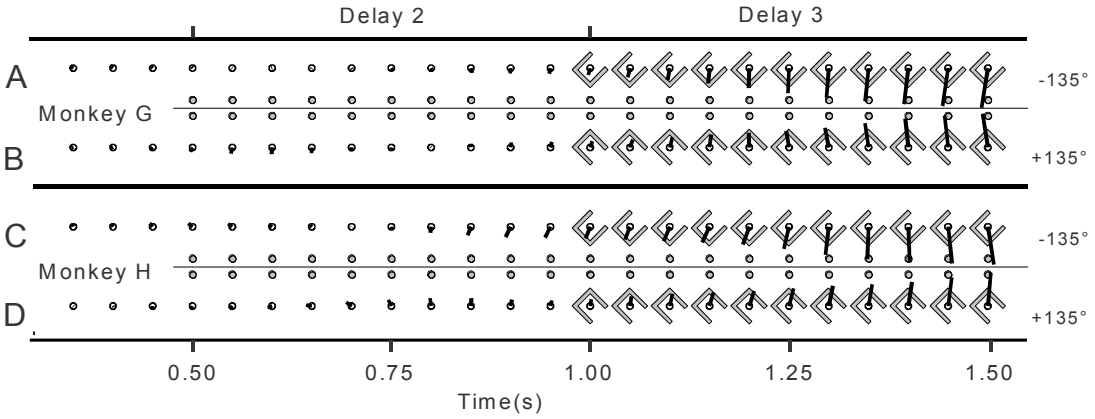

Figure 4.8: The target-based PV predicts target direction regardless of the initial movement direction. A-B) Monkey G, ±135° trials. Task visualization and decoded vector are shown every 50ms. C-D) Same as A-B, for monkey H.

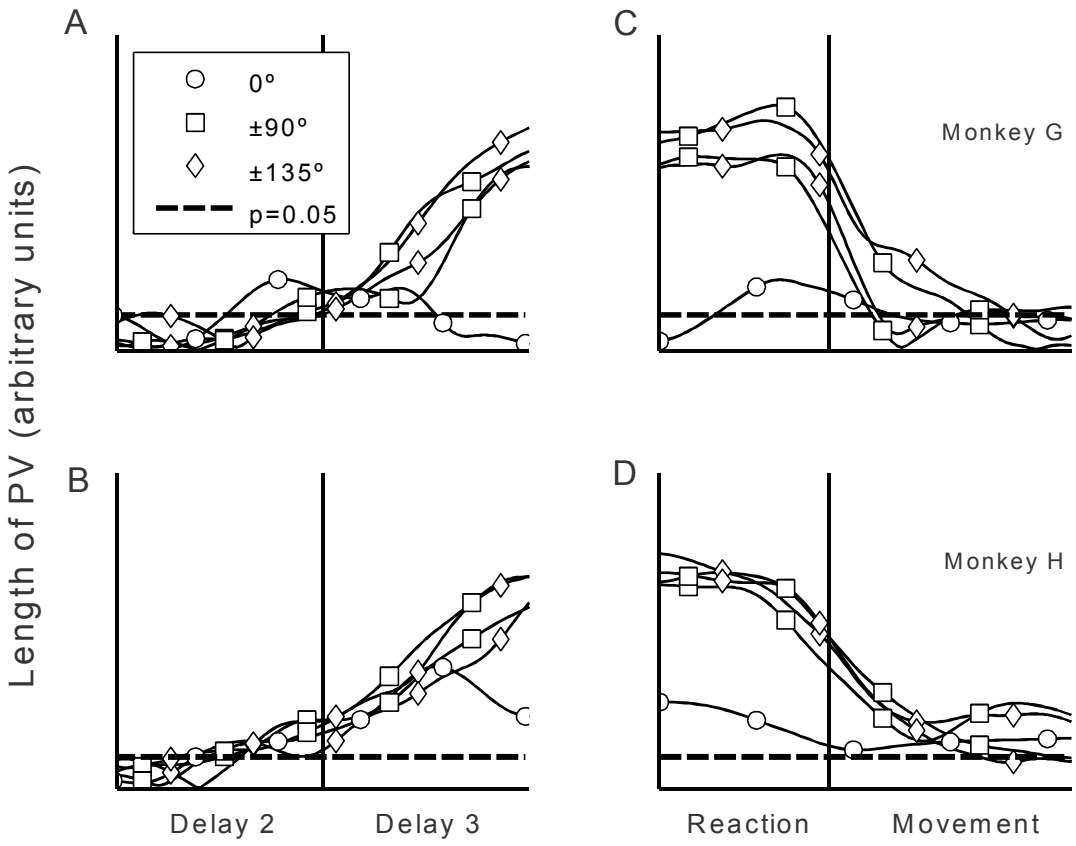

Figure 4.9: Length of the target-based PV as a function of time. A-B) PV length during the delay periods for monkeys G and H respectively. C-D) Same as A-B, during reaction and movement times. Note that the vector for the 0° condition is reduced in length compared to the other conditions, where the obstacle impedes a straight reach.

The population analyses reveal that the time course of preparatory neural activity in premotor cortex is subject to top-down modulation suggestive of distinct cognitive strategies. It appears that monkey G waited until all information was known before generating a movement plan, while monkey H planned to move directly to the target until the obstacle instructed him otherwise. In monkey H, the early planner, the direction decoding vector initially lengthened in the direction of the target. Once the obstacle was revealed, the population vector shortened and rotated to the required hand movement direction before lengthening again. In contrast, the PV from monkey G only achieved significant length during the final delay period, when the task was fully specified. As the vectors lengthened, they quickly stabilized in the direction of the initial movement required by the obstacle. This occurred sooner in monkey G than in monkey H (fig. 4.6 C, D).

Although the monkeys were trained similarly and performed identical tasks, the behavioral (Fig. 4.10) and neural lines of evidence indicate that the two animals utilized different approaches when planning obstacle-avoidance reaches. Why might one monkey have adopted a strategy requiring a change of plan? One explanation has to do with the task structure. On ⅙ of the trials the obstacle did not impede a straight movement (0° trials), and on another ⅙ of the trials the 'go' cue was given instead of an obstacle appearing (catch trials). Thus, ⅓ of the time an initial movement plan would in fact be valid, and on half of those trials it would be useful immediately. We tested for behavioral correlates of planning by examining the angular deviation of the take-off angle (hand direction relative to target direction at movement initiation) on 0° trials, when both monkeys' PVs were significant, versus catch trials, when only monkey H had a significant PV. For 0° trials, the difference in accuracy of the two monkeys was not statistically

significant. On catch trials however, monkey H, had a substantial accuracy advantage (fig. 4.10C).

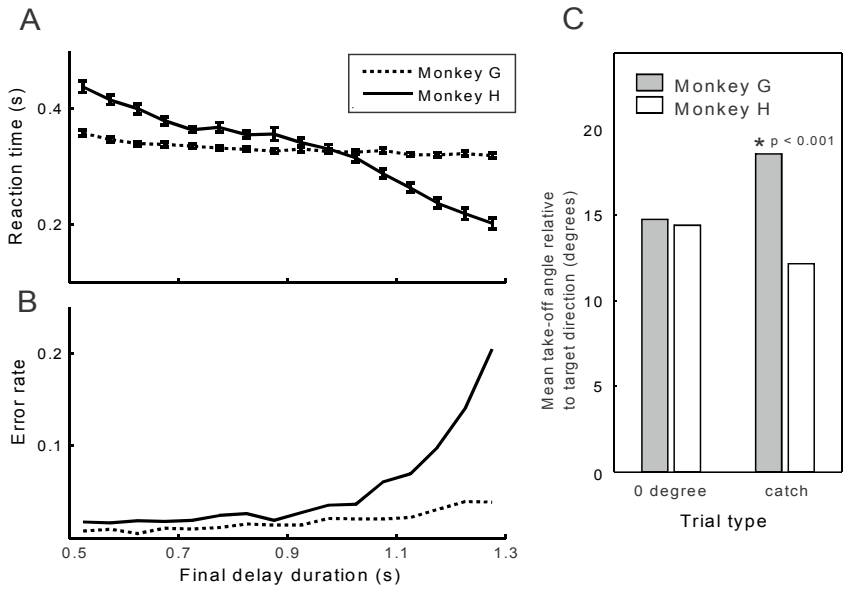

Figure 4.10: Behavioral evidence of different planning strategies on the obstacle-avoidance task. A) Reaction time (mean ± SEM) as a function of random delay length. Monkey G reacted with nearly the same response time for the shortest and longest delays, while monkey H appeared to be attempting to anticipate the occurrence of the "GO" cue. B) Error rate as a function of random delay length. Monkey H was substantially more likely to make reaction-time errors (moving before the "GO" cue) for the longest of the random delays. C) Mean angle at movement onset between the hand and target directions for two trial types. For direct (0°) trials, the obstacle was present but did not impede a straight path to the target. Catch-trials had no obstacle, and the "GO" cue was given 500ms after the target onset, at the time when the obstacle would usually be displayed. At that time, the velocity-based PV for monkey H was significant, while that for monkey G was not. Accuracy on catch-trials was significantly different ($p < 0.001$ using the parametric k-test, a test for equal concentration parameters of von Mises distributions, and the non-parametric Kuiper's test.

The work presented here makes a number of points about the role of PMd in the movement planning and execution process. First, information about multiple independent spatial parameters is often embedded in the firing rate of a single neuron (e.g. fig. 4.7A-B). The precise combination of parameters relevant to each cell is highly variable, leading to heterogeneity in the responses of individual neurons. Despite these spatially and temporally complex responses, a simple linear decoding scheme can meaningfully extract lower-dimensional information from the population as a whole. Second, the timing and strength of spatial information in the population code suggests that PMd activity is modulated both by task demands and by the particular planning strategy being used. The directional tuning observed in classic studies of center-out reaching is predictive of the initial hand movement direction, not the target direction, when those parameters are not separated. The time course with which population activity resolved to a significant directional prediction was consistent with two distinct approaches to the task, in which a tradeoff between planning speed and reach accuracy could be seen. A target representation, distinct from the initial movement representation, was also seen in the neural population. The strength of this representation was reduced for direct relative to indirect reaches, which suggests that relevant information can be selectively encoded as it is needed for the task. Finally, using position tuning properties in a population decoder provided a high-fidelity prediction of the hand trajectory during movement, consistent with prior reports of position coding in premotor areas (Fogassi et al., 1992; Pesaran et al., 2006). Although the velocity-based decoder strongly predicted the initial hand direction prior to movement initiation, it did not predict the hand velocity particularly well during execution of the movement. These findings contrast with population decoding in M1, which shows good prediction of velocity and relatively worse performance when estimating position (Wang et al., 2007).

4.3 Materials and Methods

4.3.1 Animal use

All experiments were carried out following the guidelines of the NIH and Washington University in St Louis Animal Care Committee.

4.3.2 Virtual reality workspace

Reaching tasks were carried out in a virtual reality setup (fig. 4.1A). The 3D position of the freely-moving, unconstrained hand was projected onto a 2D fronto-parallel plane and used to control a spherical cursor (radius = 7mm for monkey G; 8mm for monkey H). The workspace was centered such that the cursor was at (0,0) when the hand was in line with the shoulder, with an approximately 90° bend at the elbow. This configuration allowed the monkeys to reach comfortably to all targets while keeping the optoelectric marker in view of the camera system.

4.3.3 Center-out task

The center target (starting position) for each trial was at one of five possible positions: (0,0) or in one of the four quadrants in the planar workspace (fig. 2.2A). The *x* and *y* coordinates of these locations were ±40mm (monkey G; monkey H ±35mm). The eight peripheral targets were arranged every 45° around a circle of radius 60mm (monkey G; monkey H 50mm) centered on the starting position for the reach. Center and peripheral targets were 8mm in radius. Each block of movements consisted of 40 successful movements (5 centers x 8 targets), pseudorandomly ordered.

Each center-out trial began when the cursor first touched the randomly-chosen center target. A detailed timeline is shown in fig. 4.1B. After a fixed-length (500 ms) initial delay period, the

peripheral target was displayed, beginning a random-length second delay period (500-1300 ms, drawn from a uniform distribution). Following this random delay, the center target was extinguished, signaling the "go" cue. The monkey was given 5 seconds to complete the movement. Upon reaching the peripheral target, a 500 ms final hold period was started. A small liquid reward was delivered upon successful completion of each trial. Failure to hold at the center until the go cue and failure to reach the target in the allotted time were considered errors; those trials were excluded from the single-unit and population analyses in this study.

4.3.4 Obstacle-avoidance task

The center target was always located at (0,0) and peripheral targets were arranged every 45° on a circle of radius 80mm. The cursor, center and peripheral target dimensions were unchanged from the center-out task. The virtual obstacle consisted of a three-sided box surrounding the center target. The perpendicular distances from (0,0) to the bottom (opposite the opening) and sides of the box were 25mm and 24mm respectively. The direction from (0,0) to the middle of the open side was considered the obstacle direction. For each target direction, the obstacle could be in the same direction (0° condition, straight reach required), rotated ±90° or ±135° (Fig. 4.2E). 8 targets x 5 relative orientations of the obstacle = 40 conditions. In addition, catch-trials with no obstacle were performed. Each block of movements consisted of 48 successful movements (the 40 distinct obstacle conditions + 8 catch trials, one for each target), pseudorandomly ordered.

Each obstacle-avoidance trial began when the cursor first touched the center target. A detailed timeline is shown in fig. 4.1C. After a fixed-length (500 ms) initial delay period, the peripheral target was displayed, beginning a second fixed length delay period (also 500 ms), at the end of which either an obstacle was displayed (5/6 of total) or the "go" cue was given (catch-

trials, 1/6 of total). For non-catch-trials, a random-length third delay was then started (500-1300 ms, drawn from a uniform distribution). Following this random delay, the center target was extinguished, signaling the "go" cue. The monkey was given 5s to complete the movement. Upon reaching the peripheral target, a 500 ms final hold period was started. A small liquid reward was delivered upon successful completion of each trial. Failure to hold at the center until the go cue, contact between the cursor and the obstacle, and failure to reach the target in the allotted time were considered errors; those trials were excluded from the single-unit and population analyses in this study.

4.3.5 Neural data acquisition

Extracellular recordings were made using glass/tungsten microelectrodes, from a cylindrical chamber centered at 19mm anterior, 14mm lateral in interaural stereotactic coordinates. Electrodes were driven until spiking activity was seen, then left for the duration of a session. Multiple sessions at different cortical depths were performed daily. Recordings were bandpass-filtered (2.2-7700 Hz), pre-amplified, and digitally sampled at 24,414 Hz. On the digital signal processors (TDT, Alachua, Fl), the signal was filtered from 300-5000 Hz and streamed to disk. Single units were identified using a Matlab-based offline spike sorter (Quiroga et al., 2004). Units were not screened for task- or reach-related activity; rather, while the monkey was at rest, electrodes were driven until spiking activity was seen and not moved for the duration of the behavioral session. All units which remained stable for the duration of the session were included in the analysis, minimizing selection bias in the population of recorded neurons. Two recording sessions per penetration site were performed, with the electrodes advanced at least 0.25mm deeper between sessions.

4.3.6 Single unit tuning analysis

Two-dimensional multiple linear regressions were used to quantify cosine tuning properties.

R: firing rate estimate for each trial; $(\text{spikes/s})^{0.5}$

$P_{x,y}$: coordinates of the parameter of interest

b: regression coefficients

$R = b_1 * P_x + b_2 * P_y + b_3$

Single-bin regression analysis

Position regression (center-out task): $P_{x,y}$ are the coordinates of the initial hold position. R is the single-bin rate during the time window 150-650 ms after the center target was touched (Fig. 4.1B, red line).

Initial velocity/target regression (center-out task): $P_{x,y}$ are the coordinates of the peripheral target relative to the initial hold position. R is the single-bin rate during the time window 150-650 ms after the peripheral target was displayed (Fig. 4.1B, green line).

Initial velocity regression (obstacle-avoidance task): $P_{x,y}$ are the coordinates of the center of the obstacle opening. R is the single-bin rate during the time window 150-650 ms after the obstacle was displayed (Fig. 4.1C, orange line).

Target regression (obstacle-avoidance task): $P_{x,y}$ are the coordinates of the peripheral target. R is the single-bin rate during the time window 300-800 ms after the obstacle was displayed (Fig. 4.1C, blue line).

4.3.7 Temporally-resolved regression analysis

The same procedure was used as with the single-bin analysis, but smoothed estimates of the instantaneous firing rate were calculated by convolving the spike train with a Gaussian kernel (σ = 66 ms).

4.3.8 Square-root transform

In both single-bin and temporally-resolved regression analyses, the firing rates were square root transformed to stabilize variance so that parametric statistical tests of the significance of the cosine fit could be performed (Reina et al., 2001). We also performed regression analyses on the raw, untransformed firing rates, and confirmed that the distribution of preferred directions in the two cases was largely unaffected by the transform, and did not affect the interpretation of the findings in this study.

4.3.9 Population vector analysis

The PV models were built using the regression coefficients from single-bin analyses (see above). In an effort to avoid arbitrary decisions regarding inclusion criteria, all recorded units were used in the population decoders regardless of the significance of tuning. For this reason, we did not normalize the preferred direction/position vectors (i.e. the regression coefficients) to unit length. This provides higher weights (i.e. Euclidean length) to units with strong tuning, and lower weights to those with weak tuning or very low rate, which contribute noisier signal. The indirect optimal linear estimator method (Wang et al., 2007) was then used to compute population vectors as follows:

n: number of neurons in model

t: time points being decoded

E [t x 2]: estimate of a particular parameter (position, velocity, or target)

R [t x n]: z-score normalization of instantaneous firing rate estimates

B [n x 2]: encoding vectors (coefficients b_1, b_2 from single-unit regression analysis)

W [n x 2]: decoding vectors or weights;

M^{-1} is the matrix inverse of a matrix M

M^+ is pseudoinverse of a matrix

M' is the transpose of a matrix

Decoding vectors W are calculated from encoding vectors B:

$W = (B^+)' = B\,[(B'B)^{-1}]'$

Neural population estimates E are calculated from decoding vectors W and measured rates R:

$E\,[t \text{ x } 2] = R\,[t \text{ x } n]\; W\,[n \text{ x } 2]$

Models were tested by decoding the estimated instantaneous firing rate measured during the obstacle-avoidance task. The rate estimates for each neuron were z-score normalized across all successful trials. Two of the three models (position and target-direction regressions from the center-out task delay periods) were built from tuning during the center-out task, so testing on the obstacle-avoidance task was a completely independent data set. The third model was constructed from target-tuning regressions during the final delay period of the obstacle-avoidance task. Since the encoding and decoding were done from the same task, a leave-one-out cross-validation was used to avoid building and testing on the same data. In this method, each trial was considered independently; the regression coefficients used in the decoder were calculated from the remaining 199 trials. This procedure was repeated for all trials. The target-based PV analyses in this paper (figs. 4.8-4.9) were all calculated using leave-one-out regression models. We also performed the analyses without a cross-validation (including all 200 trials in the regression), and leaving out all trials of a particular target-obstacle condition (including 195 trials in the regression, and testing on the other 5). The results of these analyses were not significantly different than the leave-one-out results.

To determine the magnitude at which a PV should be considered significant, we utilized a bootstrap technique. The firing rates were randomly resampled and multiplied by the real decoding matrix W to create a distribution of PVs obtained when the relationship between firing rate and trial type was due to chance alone. The magnitudes were then sorted and the 95^{th} percentile was used as a p=0.05 significance threshold (Fig. 4.6 and fig. 4.9). As an illustration of the statistical properties of PV length, consider the initial period of each trial. Prior to the first display of the target on each trial, the magnitudes of the velocity and target PV decoders are small and the directions are unstable, which is to be expected, as no information about the upcoming movement is available to the subject. As visual information becomes available over the course of the trial, the PV lengthens and the direction stabilizes.

5 Viewing PMd through jPCA

5.1 Introduction

In the preceding chapters, neural activity in PMd was examined in a variety of reaching conditions, both at the level of individual neurons (chapter 3) and with a population vector algorithm (chapter 4). There, we saw that neurons had modestly sized but statistically significant relationships with kinematic features of hand movements, and that these relationships could be used in a linear decoder to predict the position, velocity, and target of the hand movement from the population of neurons. A different interpretation of motor cortical activity has recently been proposed that, instead of emphasizing kinematic encoding properties of neurons, treats population activity as a linear dynamical system (Churchland et al., 2012). In this framework, firing rates evolve over time in a systematic manner that can be described as intrinsically oscillatory, even when the hand is not making rhythmic or repeating patterns of movements. The authors find that across a diverse set of reaches of different directions, magnitudes, speeds, and curvatures a consistent pattern of rotation in neural state space emerges. A mathematical technique termed "jPCA" is used to project high-dimensional neural population data onto state-space planes that best capture these rotational dynamics. They found that simulating neural data based only on a kinematic encoding model was not sufficient to reproduce the dominant rotational features of the actual neural data set. In this chapter, the jPCA technique is applied to the neural data set of this thesis. Special thanks are due to Dr. John Cunningham for providing MATLAB code and guidance on using jPCA.

5.2 Methods

Spike times from each neuron on each trial were converted into a smoothed rate estimate by convolution with a Gaussian kernel with $\sigma = 66$ ms. (as in chapter 4). Trials were aligned by movement onset time, and all repetitions of each condition were averaged together. All neurons with activity for the duration of the recording session and minimum of 3 repetitions per condition were included (612 for monkey G and 523 for monkey H). A time window spanning 100 ms prior to until 300 ms after movement onset was used for most of the analyses (exceptions are noted). Data were mean-centered and soft-normalized as in Churchland et al. 2012. For all analyses, standard principal component analysis (PCA) was first performed to reduce the data to 8 principal components before applying the jPCA algorithm. Data for each monkey was analyzed separately.

Simulated data sets were generated based on kinematic encoding models. For each neuron, encoding vectors for three parameters – position, velocity and target direction - were calculated using linear regression during the delay periods. These vectors are from the same analysis, including the same time periods, used in chapter 4 to build the population vector decoders: Preferred position from delay 1 of center-out, preferred direction from delay 2 of center-out, and preferred target from delay 3 of obstacle-avoidance. For each condition, a mean trajectory was computed. At each point in time, the instantaneous hand position, velocity, and target-minus-hand vector were determined and the dot product with the corresponding encoding vector gave the expected firing rate based only on that parameter. This simulated rate was shifted in time to generate neural leads (kinematic lags). Finally, the activity level 100 ms before movement onset was extended back in time to the beginning of the simulation to provide "plan activity." Individual neurons could have small or large encoding vectors depending on the

regression model. To match the observation that the overall depth of modulation for each tuning model was similar across the population, the relative weightings for the kinematic variables (in units of meters and meters/s) were scaled so that a similar dynamic range of firing rates across conditions and neurons was generated for each. Thus, when multiple parameters were combined in a simulated data set, no single parameter dominated the overall responses. Different data sets were generated by including or excluding parameters from the model, and adjusting the kinematic lag relative to neural firing for each parameter individually. All simulations were based on neurons from monkey G.

5.3 Results

To begin, the basic jPCA algorithm was applied to the neural data from all obstacle-avoidance conditions (catch-trials were excluded because the trial structure was different than all other conditions). The projections into the top jPCA plane for both monkeys are shown in figure 5.1. As in Churchland et al. 2012, the dominant feature of these plots is a rotational pattern: from the initial point of each trajectory, the paths proceed to orbit the origin in a counterclockwise direction. That the rotations are counterclockwise is not particularly relevant, because the algorithm defines that to be the case. What is relevant is that the majority of the trajectories all behave in a consistent manner. Two major differences between these plots and those reported by Churchland are apparent: 1) The initial conditions are spread over the plane, rather than clustering along the axis of jPC 1; and 2) the overall amount of variance captured by these planes (~15%) is considerably lower than the top planes captured in the previous report (~28%). A number of factors may explain this discrepancy – for example, neurons in the previous study were recorded over many repetitions of each condition, and only trials with very stereotyped kinematics were utilized to calculate mean firing rates for each distinct condition. In

contrast, the obstacle-avoidance task consisted of only 5 repetitions of each condition per neuron, and did not mandate extremely stereotyped hand trajectories.

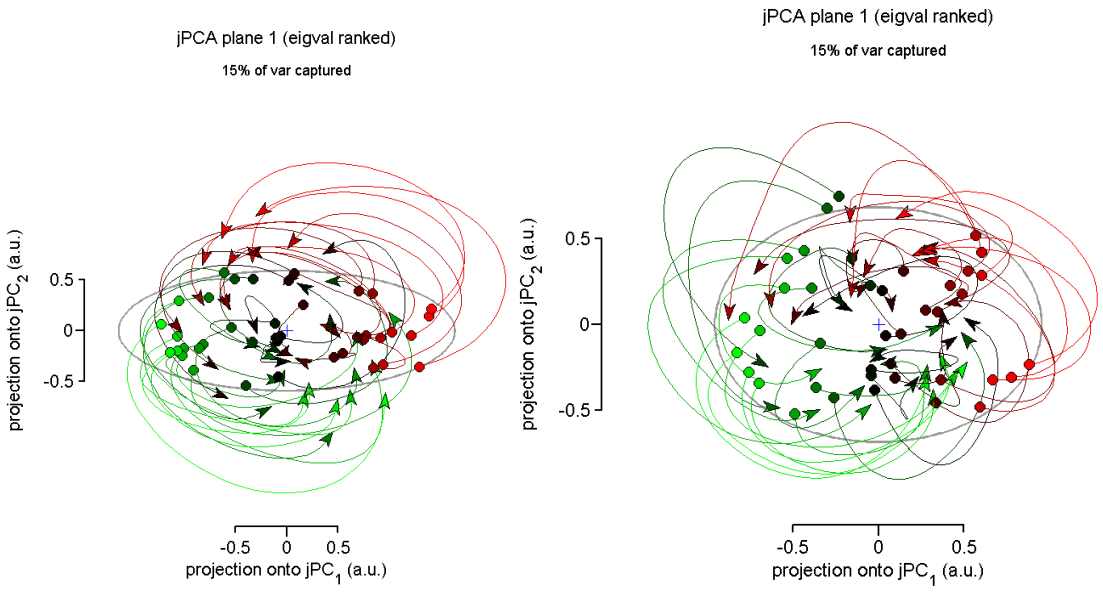

Figure 5.1: The top jPCA plane for all combinations of target and obstacle orientation. Left: Monkey G. Right: Monkey H. Strong counterclockwise rosette patterns are seen in both plots. Each trajectory corresponds to a single condition. As in Churchland et al. (2012), the colors are determined by the position on jPC_1 of the starting point of each trajectory (filled circle). Although rotation is a dominant feature in these plots, the percentage of overall variance explained by these planes (~15%) is low compared to Churchland et al. 2012

Another difference between the previous and current study is the proportion of conditions with highly curved hand paths. In Churchland et al. 2012, curved trajectories were present in some data sets (the maze task), but unlike in the obstacle-avoidance task they were not a preponderance of the total set of reaches, nor were they uniformly distributed in space or balanced clockwise vs. counterclockwise. Neural representations of hand kinematics in M1 and PMd are widely-observed phenomena (see chapters 1, 3, and 4), and jPCA specifically finds projections that capture rotational dynamics, making it likely that this analysis could be influenced by rotational structure in the hand movements. When clockwise or counterclockwise reaches are considered separately in jPCA, the state-space trajectories become very orderly and the variance captured in the top plane rises to nearly 30% on average (fig. 5.2). This increase is not simply due to fewer conditions being considered (16 vs. 40 originally): taking a subset of 16 conditions where half are clockwise and half counterclockwise reduces the effect substantially (fig. 5.2, right panels). Thus, while all the curved conditions are all rotational in state space, the top plane does not capture both directions equally.

As was noted in Churchland et al. 2012, looking beyond the first jPCA plane can be informative. In that study it was found that the second (and sometimes third) planes had rotations of different frequencies than the top plane. Here, we find that the first and second planes actually capture different types of reaches (fig. 5.3). Abandoning the red-green color scheme in favor of coding the different types of conditions with different colors, it is obvious that one plane contains neural trajectories from clockwise reaches while the other contains counterclockwise conditions. The variance explained for each subset in each plane confirms this.

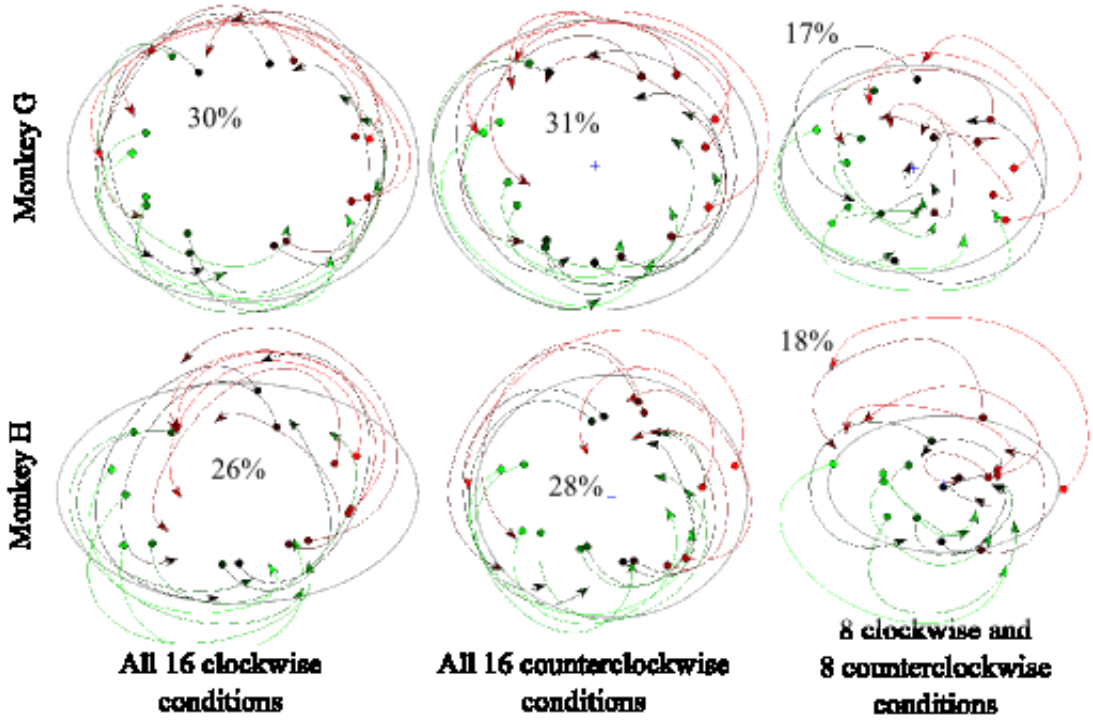

Figure 5.2: jPCA planes found using only a subset of conditions. Inset: The percentage of variance captured in each plane. When planes were found with only clockwise or only counterclockwise conditions (in the left 4 panels), the amount of variance captured increased substantially compared to using all conditions (fig. 5.1). Keeping the same number of conditions but mixing clockwise with counterclockwise reduced this effect (right panels).

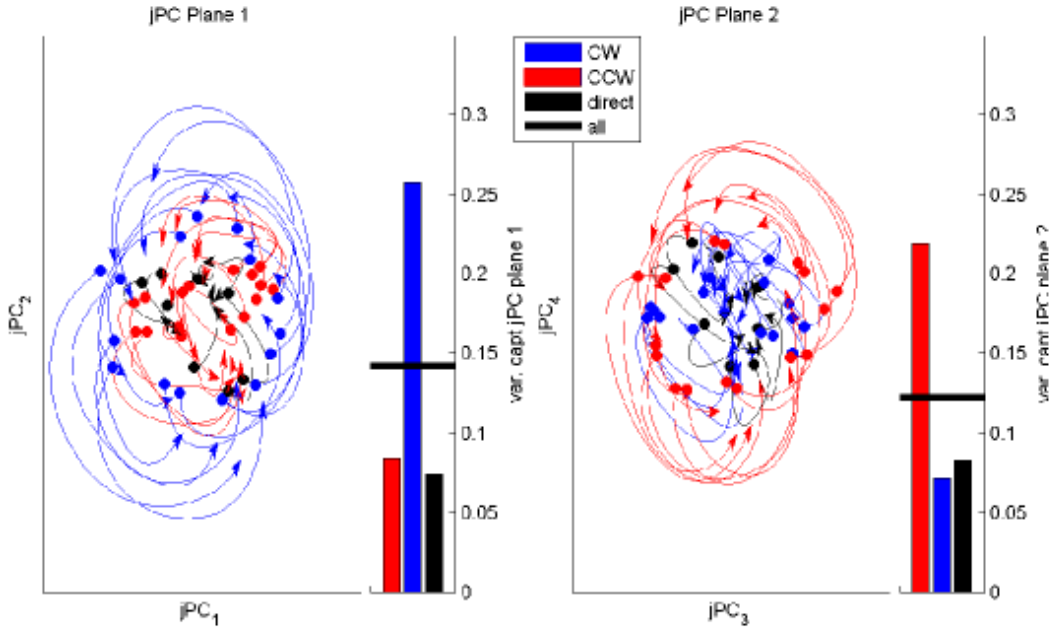

Figure 5.3: Top 2 jPCA planes, all conditions. Data are from monkey G. Instead of a red-green colormap, all clockwise conditions are colored blue, all counterclockwise conditions are red, and all direct reaches are black. Bar plots show the variance explained for each subset of conditions. The black horizontal line shows the overall variance explained. Plane 1 captures primarily clockwise hand movements; plane 2 counterclockwise.

In addition to different classes of hand trajectories falling in different jPCA planes, the state-space trajectories, like the reach paths, are distributed evenly in the plane. To check for further correspondence between neural space and physical space, the organization of trajectories within each plane was examined. The obstacle-avoidance task uses 8 distinct obstacle orientations to specify the initial direction of movement. For each obstacle orientation there are two clockwise and two counterclockwise conditions. Figure 5.4 shows the distribution of state-space trajectories in each plane as a function of the initial movement direction. Each segment of a green arrow links the state-space initial points that correspond to adjacent starting directions of the hand trajectories. The arrows proceed as in the schematic diagram. In extrinsic space, the direction of the arrow is clockwise. Clockwise hand paths thus rotate similarly to the green arrow, while counterclockwise proceed oppositely. This relationship holds true in neural space as well – blue trajectories rotate in the same direction as the green arrow, while red rotate opposite the arrow (fig. 5.4). Again, as was noted before, the direction that state-space trajectories rotate is arbitrary. That both the green and blue arrows are the reverse of the expected direction based on extrinsic space simply means the plane is being viewed from the "wrong" direction.

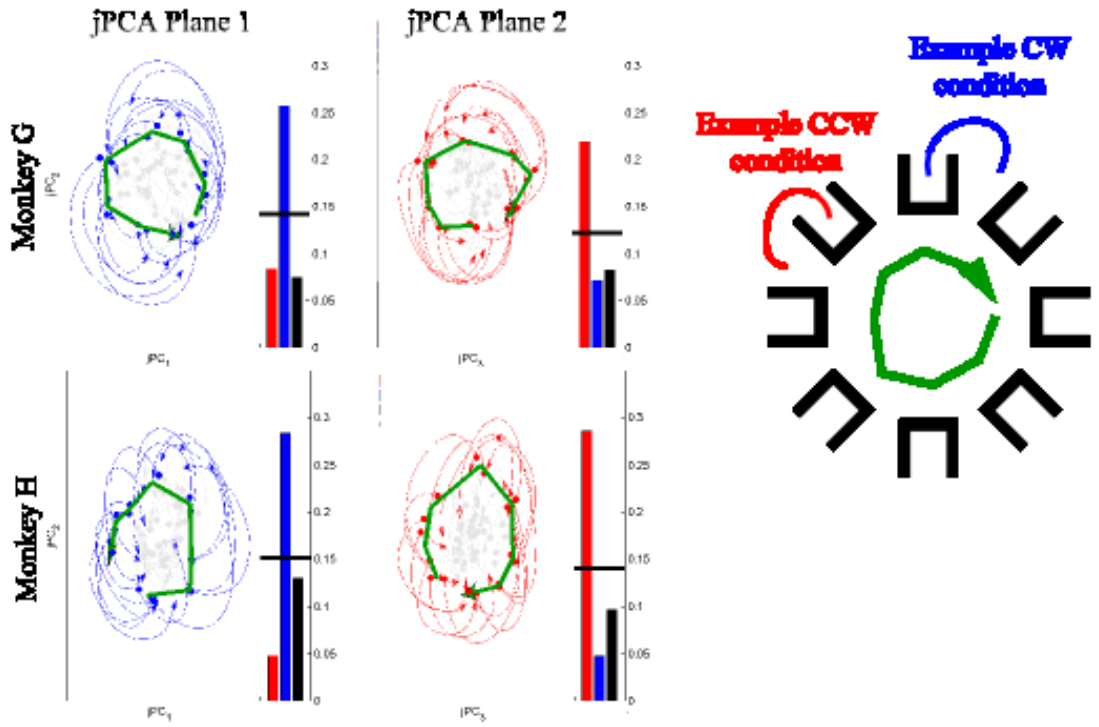

Figure 5.4: Trajectories in jPCA space match the direction of curvature of the hand in physical space. For each of the 8 starting directions (defined by the orientation of the obstacle – see schematic in the right panel) there are two clockwise and two counterclockwise conditions. The base of the green arrow in each plot begins at the average state-space starting point for the conditions where the initial hand movement was in the +x direction. The arrow proceeds as in the schematic. In plane 2, the green arrow is clockwise, congruent with physical space. The state-space trajectories rotate opposite the direction of the green arrow. In contrast, in plane 1 the blue arrows rotate the same direction as the green arrow, but both directions are opposite of expected. Viewing the plane from behind makes both features match the physical orientations of the hand paths.

Based on these analyses, it appears that kinematic features including direction of rotation and initial movement direction have a sizable impact on the neural state space. Can a cosine-tuning model of kinematic encoding reproduce these features? Figure 5.5 shows results from performing jPCA on simulated neural data. Simulations based on single parameters – position or velocity in isolation (panels A and B) – yielded poor reproductions of the key features of real data in jPCA space. The position + velocity single-lag (200 ms) model (panel C) appears to be rotational on first impression; however, the curved state-space trajectories are not rotating about the center of the plane, but are making loops in the periphery, a phenomenon not seen in the real data. When the position and velocity encoding models were allowed to have different lags – in particular, lags that the population vector analysis suggested would be appropriate (panel D; 200 ms for position, 120 ms for velocity) – the simulations became more realistic-looking in terms of rotational behavior (fig. 5.5 bottom). Upon adding target encoding (panel E), also with neurons leading the hand by 120 ms, the simulated state-space trajectories begin to appear quite similar to the true neural state-space (panel H). In fact, clockwise and counterclockwise conditions dominate planes 1 and 2, as they do in the real data (fig. 5.6; see fig. 5.3 for comparison). The combination of position and velocity encoding with different lags is sufficient to generate state-space rotations even for straight-line, center-out reaches (5.5F; compare to 5.5G. Center-out trajectories are based on a 300 ms window starting 100 ms prior to movement onset).

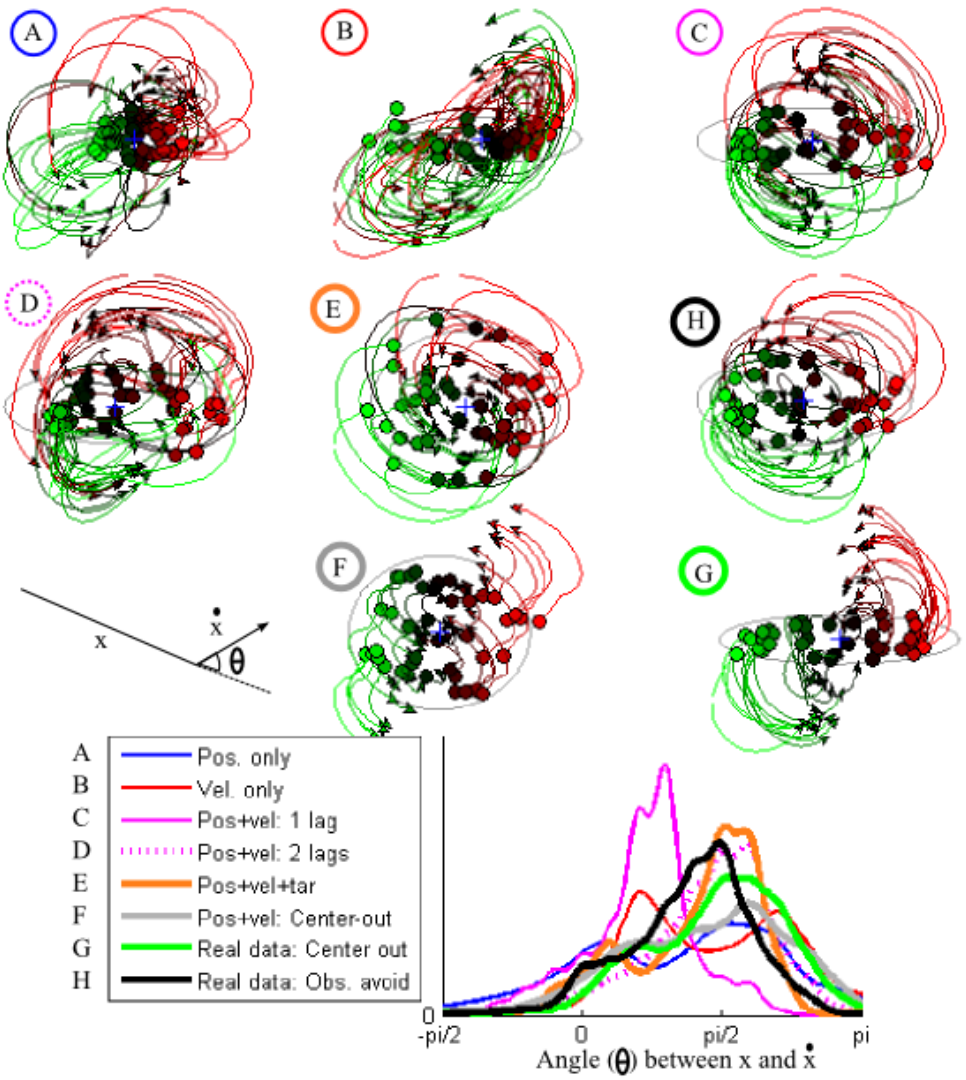

Figure 5.5: Simulations based on certain combinations of kinematic variable encoding have similar properties to real neural data. After Churchland et al. 2012. A-F) Encoding models based on different combinations of parameters and lags between neural activity and hand movement. G-H) Real neural data from the center-out and obstacle-avoidance tasks. All panels show the top jPCA plane. Bottom plot: Probability density functions for the angle between the neural state (x) and its derivative (dx/dt). See schematic above the legend.

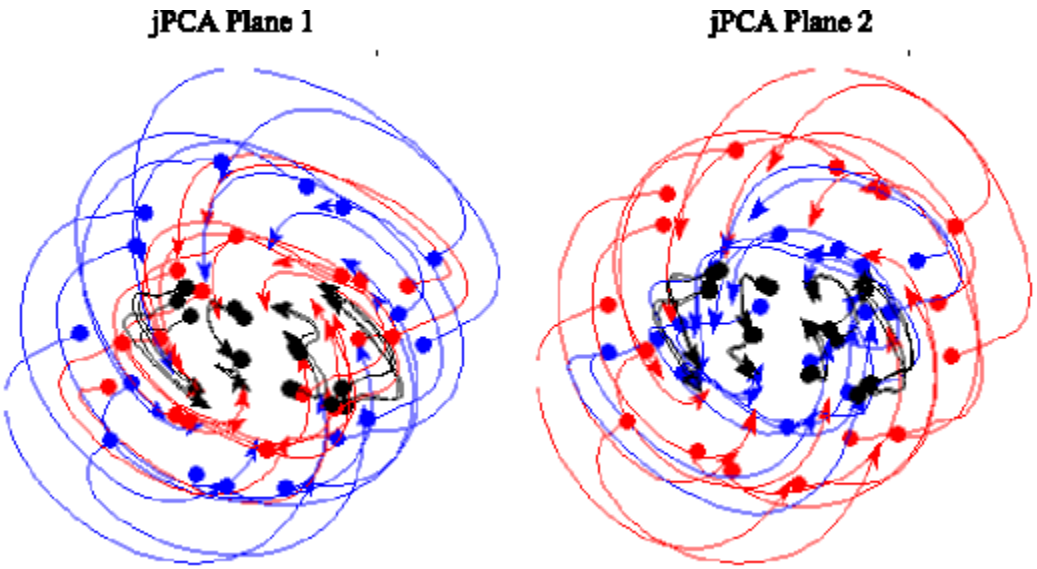

Figure 5.6: Clockwise and counterclockwise conditions of simulated neural data primarily lie in distinct planes. Like the real neural data (fig. 5.3), neural firing rates simulated from kinematic encoding of position (200 ms neural lead), velocity (120 ms) and target (120 ms) show a distinctive pattern in jPCA space. As in figures 5.3 and 5.4, blue trajectories correspond to clockwise hand paths while red are counterclockwise conditions.

The previous analyses were restricted to examining a window of neural activity surrounding the time of movement onset. However, many of these neurons have ongoing task-related activity beginning in the delay period and changing as information is revealed. Do firing rates at other times, such as temporally evolving delay period activities, behave similarly as a rotational dynamical system? Figure 5.6 looks at this question. First, jPCA was applied to the data in a sliding window. The resulting planes were tested by projecting data from other times (including the other task) and calculating the percentage of variance captured by the first 4 jPCs. The diagonal of the plot consists of times when the plane-finding and -testing time windows overlapped. Along the diagonal, two features are worth discussing. First, the algorithm is more successful at describing the neural activity during movement time compared to delay. Second, as the obstacle-avoidance delay period progresses from delay 1 to delay 2, the variance in firing rates explained by the model increases. This transition marks the first time that any distinguishing information about the trial condition becomes available, and is thus the first time that neural activity can begin to reflect the upcoming action. Looking off-diagonal, the jPCs that best capture this delay period process do not do well at explaining the variance during movement. The reverse is also true; planes that capture dynamics during movement do not predict delay period activity. Movement-time dynamics do transfer between tasks, though to a limited degree.

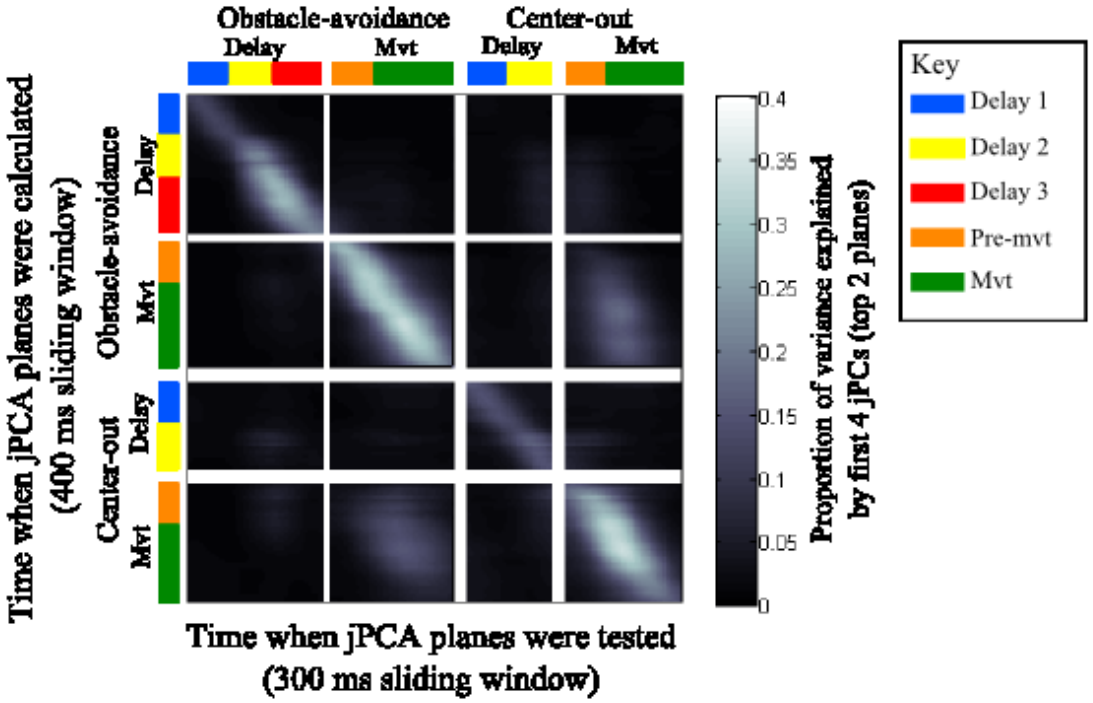

Figure 5.7: Testing how well jPCA planes found at one time explain neural dynamics at other times. Top row: A 400 ms window beginning 500 ms before target onset was used to fit a linear dynamical model. Each pixel in the row indicates the variance explained by projecting a 300 ms sliding window of data onto the top two jPCA planes. Subsequent rows: In each row, the plane-finding window was advanced 30 ms. Data from before, during, and after this window are tested. Planes were found from, and tested on, data from both tasks. Along the diagonal the plane-finding and projection testing occur at the same time within the task. Data in 'Delay' panels are aligned to target (and obstacle) onset events. Data are re-aligned to movement onset for 'Mvt' panels. The models from movement time in one task have some success explaining movement-time data from the other task. Models from movement time do not explain delay-period activity (or vice versa).

5.4 Discussion

The analyses and results presented here differ from those of Churchland et al. (2012) in a number of ways. The data collection and processing methods are also different in important ways, so direct comparisons between the sets of results are necessarily limited. For example, the obstacle-avoidance reach trajectories here are less stereotyped than the movements in that study. A wider smoothing kernel for neural data and fewer trials per condition, combined with less-stereotyped movements, would obscure higher-frequency dynamics in the firing rates of individual cells. Most of the data in the original study were recorded from primary motor cortex, while the data here are from PMd (or very rostral M1), which could influence how the population activity behaves in neural state space. However, in spite of these differences, the basic finding exists in both sets of results – there exist projections in state space in which rotational dynamics are a dominant feature around the time of movement. Does this result follow from cortex being an intrinsically dynamical system? Or is it that the firing rates of motor cortical neurons are representing kinematic features of a dynamically-moving limb?

The results presented in this chapter argue that neural state space, as identified by an algorithm naïve to the kinematics of individual conditions, corresponds closely to spatial features of the reach including the initial movement direction and the direction of curvature of the hand trajectory. State-space rotations for clockwise vs. counterclockwise hand movements tend to be found in distinct planes in the high-dimensional neural space. Both features – the rotational state-space trajectories and the distinct planes – can be replicated with simulated data based on kinematic encoding. For the simulation to succeed, multiple kinematic parameters (position, velocity, target-relative-to-hand) with different neural lead times must be included, and must contribute roughly equally to the overall variance in the firing rates.

Although these simulations can generate data that look similar in some regards to real neuronal responses, other features such as rotations in additional jPC planes are not reproduced. There is likely a combination of encoding and network dynamics at play, and neither should be disregarded. To truly get at these issues, simultaneous recordings from hundreds or thousands of neurons made with penetrating multichannel electrode arrays, optical methods, or other novel recording modalities will be needed. Faced with such vast quantities of data, dimensionality reduction techniques like the jPCA algorithm will be especially important.

6 Conclusions

The data and analyses presented in this thesis provide a picture of neural activity in dorsal premotor cortex from multiple perspectives, from the level of single cells up to the population response. PMd is widely held to be involved both in action selection and in learning arbitrary rules that specify appropriate responses (Murray et al., 2000; Pastor-Bernier et al., 2012). Indirect reaching is an interesting scenario in which the location of the goal is important, but is not the only factor that determines the hand trajectory. Such movements are a common primate behavior, and lesion data suggest that premotor areas are involved in generating the appropriate hand trajectories (Moll and Kuypers, 1977). The experiments in this thesis were motivated by a desire to resolve ambiguity about whether directionally-tuned preparatory neuronal activity is principally related to the direction of planned hand movement, or alternatively reflects the spatial goal of the movement. Although this is a fairly straightforward question, previous studies have not provided clearly interpretable results. By thoroughly describing neuronal activity during the planning and execution of indirect reaching behavior, this study helps to advance the larger goal of characterizing how the cortical circuitry may function to generate consciously-specified movements.

The clearest distinction between neural representations of movement vs. goal direction comes from the population vector analysis in chapter 4. A decoding model was constructed from individual neurons' cosine tuning properties, determined by regressing firing rates against instructed direction during the preparatory periods of the center-out task. This model is therefore predictive for whatever parameter the neurons are representing during direct, straight-line reaching. The decoder was then applied to neural data recorded during the obstacle-avoidance task. By the end of the delay period, the population vector predicted the direction of hand

movement rather than the direction of the final target. Interestingly, the way that these population vector responses evolved over the course of the instructed delay periods was clearly different in the two monkeys. The lengths and directions of the vectors, combined with the timing and spatial orientation of the task, suggest that monkey H was planning an initial direct movement and changed his plan if the obstacle appeared and required an indirect trajectory. By comparison, monkey G did not form an initial plan; instead he waited until all information was available. Although G's neural population activity stabilized at the initial direction for obstacle-avoiding movements sooner than did H's, on catch trials the go cue occurred prior to the formation of a directional movement plan. Monkey G was also less accurate in the initial movement direction on catch trials, a possible behavioral correlate of the lack of directional plan activity. A similar difference between monkeys is also seen in the single-neuron properties (chapter 3), but without constructing a population-level model, the pattern of correlations between tuning across tasks is much harder to interpret.

The population vector analyses also indicated that during movement, hand position and velocity coding within the PMd population have different temporal leads relative to the movement. By using these results to inform simulations of kinematically-modulated firing rate data, artificial data were generated that reproduced key features of the real data when examined with the jPCA analysis framework (chapter 5). Failing to include parameters, or failing to use appropriate neural lead times for each parameter, degraded the performance of the simulations. In addition to the simulation results, the trajectories of the real neural data in state space appear to have orderly relationships to kinematic properties of the hand movements. This is perhaps unsurprising: if kinematic variables contribute to neural activity, and the hand kinematics are changing over the course of a reach, firing rates are expected to have complicated time-varying

patterns. It appears from these results that kinematic encoding can explain some portion of the observed rotational state space dynamics. To determine any additional intrinsic dynamical patterns in the cortical activity, it would be helpful (if not necessary) to account for these effects.

At the other end of the spectrum from the population analyses are the single-unit response properties, characterized in chapter 3. These analyses emphasize that many individual neurons have directionally modulated firing rates, during pre-movement delay periods and during movement execution. The contribution of any particular parameter to a single neuron's activity is typically small, but many neurons are modulated by more than one parameter. When a cell is tuned to a kinematic variable, the preferred direction remains similarly oriented for the course of the delay period and into the reaction time, and does not systematically change direction as the trial progresses. If care is taken to fit the data to the same parameter in a different task (and the monkey cooperates by preparing similarly), the PD is consistent across behaviors as well. Of course, these findings are limited to the types of tasks and movement conditions studied here. Learning novel associations (Mitz et al., 1991; Zach et al., 2008), changing the dynamics of the environment via externally-applied force fields (Xiao, 2005; Xiao et al., 2006), and many other manipulations have been shown to alter the tuning curves of some PMd neurons.

One particularly striking finding from the single-unit analysis is the subpopulation of neurons with cosine-tuning properties to movement direction *and* target direction during the preparatory period of obstacle-avoidance reaching. In these cells there is a strong negative correlation in the preferred directions to these two parameters. As was discussed in chapter 3, one hypothesis about this pattern of activity is that it reflects suppression or inhibition of a default, direct, hand movement. That these neurons are also tuned for direct movements in the opposite direction suggests that the circuitry used for planning simple reaches may also play a

role in more complex behaviors. A suppressive role for this type of cell is only a hypothesis at this point. The hypothesis predicts that a particular type of response would be seen in these cells during anti-reach tasks like Crammond and Kalaska (Crammond and Kalaska, 1994), where the spatial target instructs a reach in the opposite direction, or the mental rotation task (Georgopoulos, Lurito, et al., 1989). Rather than just a single angular relationship between target and movement directions, a range of angles could be tested in these tasks to examine tuning curves and interaction effects, as in the obstacle-avoidance task here. Inhibiting a motor response during NOGO tasks (Kalaska and Crammond, 1995) may engage this circuitry even though no movement is to be made. Ideally, single neurons would be tested in multiple such tasks in order to move beyond descriptions of what PMd does as an area, and instead determine the cortical mechanisms that unite these findings. In the future, long-term recordings from single neurons using chronically-implanted arrays would be helpful, since extensive behavioral testing on multiple tasks is exceedingly difficult in acute recording sessions. Optogenetic techniques may also be useful to help determine differential response characteristics of distinct cell types and to ensure consistent identification of individual units from day to day in the chronic array recordings.

The ability to withhold reaching directly for a potentially valuable target in favor of a different action is a critical component of behavior, and is disrupted by lesions to premotor cortex (Picton et al., 2007). The work presented in this thesis helps to clarify the properties of neural activity in PMd during one such behavior, indirect reaching in the presence of obstacles. Additionally, the results suggest a potential common mechanism for generating indirect trajectories, performing arbitrary stimulus-response mappings, and suppressing movement.

These observations provide a framework for future investigations of the cortical substrates of these behaviors.

7 References

Abe, M., Hanakawa, T., 2009. Functional coupling underlying motor and cognitive functions of the dorsal premotor cortex. Behav. Brain Res. 198, 13–23.

Aflalo, T.N., Graziano, M.S.A., 2006. Partial tuning of motor cortex neurons to final posture in a free-moving paradigm. Proc. Natl. Acad. Sci. U.S.A. 103, 2909–2914.

Aivar, M.P., Brenner, E., Smeets, J.B.J., 2008. Avoiding moving obstacles. Exp Brain Res 190, 251–264.

Ajemian, R., Bullock, D., Grossberg, S., 2001. A model of movement coordinates in the motor cortex: posture-dependent changes in the gain and direction of single cell tuning curves. Cereb. Cortex 11, 1124–1135.

Albright, T.D., 1984. Direction and orientation selectivity of neurons in visual area MT of the macaque. J. Neurophysiol. 52, 1106–1130.

Baldauf, D., 2011. Chunking movements into sequence: the visual pre-selection of subsequent goals. Neuropsychologia 49, 1383–1387.

Barbas, H., Pandya, D.N., 1987. Architecture and frontal cortical connections of the premotor cortex (area 6) in the rhesus monkey. J. Comp. Neurol. 256, 211–228.

Batista, A.P., Santhanam, G., Yu, B.M., Ryu, S.I., Afshar, A., Shenoy, K.V., 2007. Reference frames for reach planning in macaque dorsal premotor cortex. J. Neurophysiol. 98, 966–983.

Bauswein, E., Fromm, C., 1992. Activity in the Precentral Motor Areas After Presentation of Targets for Delayed Reaching Movements Varies with the Initial Arm Position. Eur. J. Neurosci. 4, 1407–1410.

Boussaoud, D., 2001. Attention versus intention in the primate premotor cortex. Neuroimage 14, S40–45.

Boussaoud, D., Jouffrais, C., Bremmer, F., 1998. Eye position effects on the neuronal activity of dorsal premotor cortex in the macaque monkey. J. Neurophysiol. 80, 1132–1150.

Busan, P., Barbera, C., Semenic, M., Monti, F., Pizzolato, G., Pelamatti, G., Battaglini, P.P., 2009. Effect of transcranial magnetic stimulation (TMS) on parietal and premotor cortex during planning of reaching movements. PLoS ONE 4, e4621.

Caminiti, R., Johnson, P.B., Galli, C., Ferraina, S., Burnod, Y., 1991. Making arm movements within different parts of space: the premotor and motor cortical representation of a coordinate system for reaching to visual targets. J. Neurosci. 11, 1182–1197.

Catalan, M.J., Honda, M., Weeks, R.A., Cohen, L.G., Hallett, M., 1998. The functional neuroanatomy of simple and complex sequential finger movements: a PET study. Brain 121 (Pt 2), 253–264.

Chang, S.W.C., Papadimitriou, C., Snyder, L.H., 2009. Using a compound gain field to compute a reach plan. Neuron 64, 744–755.

Churchland, M.M., Cunningham, J.P., Kaufman, M.T., Foster, J.D., Nuyujukian, P., Ryu, S.I., Shenoy, K.V., 2012. Neural population dynamics during reaching. Nature 487, 51–56.

Churchland, M.M., Cunningham, J.P., Kaufman, M.T., Ryu, S.I., Shenoy, K.V., 2010. Cortical preparatory activity: representation of movement or first cog in a dynamical machine? Neuron 68, 387–400.

Churchland, M.M., Shenoy, K.V., 2007a. Delay of movement caused by disruption of cortical preparatory activity. J. Neurophysiol. 97, 348–359.

Churchland, M.M., Shenoy, K.V., 2007b. Temporal Complexity and Heterogeneity of Single-Neuron Activity in Premotor and Motor Cortex. Journal of Neurophysiology 97, 4235–4257.
Churchland, M.M., Yu, B.M., Ryu, S.I., Santhanam, G., Shenoy, K.V., 2006. Neural Variability in Premotor Cortex Provides a Signature of Motor Preparation. J. Neurosci. 26, 3697–3712.
Cisek, P., Crammond, D.J., Kalaska, J.F., 2003. Neural activity in primary motor and dorsal premotor cortex in reaching tasks with the contralateral versus ipsilateral arm. Journal of neurophysiology 89, 922.
Cisek, P., Kalaska, J.F., 2004. Neural correlates of mental rehearsal in dorsal premotor cortex. Nature 431, 993–996.
Cisek, P., Kalaska, J.F., 2005. Neural correlates of reaching decisions in dorsal premotor cortex: specification of multiple direction choices and final selection of action. Neuron 45, 801–814.
Crammond, D.J., Kalaska, J.F., 1994. Modulation of preparatory neuronal activity in dorsal premotor cortex due to stimulus-response compatibility. J. Neurophysiol. 71, 1281–1284.
Crammond, D.J., Kalaska, J.F., 1996. Differential relation of discharge in primary motor cortex and premotor cortex to movements versus actively maintained postures during a reaching task. Exp Brain Res 108, 45–61.
Crammond, D.J., Kalaska, J.F., 2000. Prior information in motor and premotor cortex: activity during the delay period and effect on pre-movement activity. J. Neurophysiol. 84, 986–1005.
Dayan, P., Abbott, L., 2005. Theoretical Neuroscience. MIT Press.
di Pellegrino, G., Wise, S.P., 1993. Effects of attention on visuomotor activity in the premotor and prefrontal cortex of a primate. Somatosens Mot Res 10, 245–262.
Evarts, E.V., 1966. Pyramidal tract activity associated with a conditioned hand movement in the monkey. J Neurophysiol 29, 1011–1027.
Evarts, E.V., 1968. Relation of pyramidal tract activity to force exerted during voluntary movement. J. Neurophysiol 31, 14–27.
Fogassi, L., Gallese, V., di Pellegrino, G., Fadiga, L., Gentilucci, M., Luppino, G., Matelli, M., Pedotti, A., Rizzolatti, G., 1992. Space coding by premotor cortex. Exp Brain Res 89, 686–690.
Fu, Q.G., Flament, D., Coltz, J.D., Ebner, T.J., 1995. Temporal encoding of movement kinematics in the discharge of primate primary motor and premotor neurons. J Neurophysiol 73, 836–54.
Fu, Q.G., Suarez, J.I., Ebner, T.J., 1993. Neuronal specification of direction and distance during reaching movements in the superior precentral premotor area and primary motor cortex of monkeys. J. Neurophysiol. 70, 2097–2116.
Fujii, N., Mushiake, H., Tanji, J., 2000. Rostrocaudal distinction of the dorsal premotor area based on oculomotor involvement. J. Neurophysiol. 83, 1764–1769.
Gail, A., Klaes, C., Westendorff, S., 2009. Implementation of spatial transformation rules for goal-directed reaching via gain modulation in monkey parietal and premotor cortex. J. Neurosci. 29, 9490–9499.
Gallese, V., Fadiga, L., Fogassi, L., Rizzolatti, G., 1996. Action recognition in the premotor cortex. Brain 119 (Pt 2), 593–609.

Georgopoulos, A.P., Crutcher, M.D., Schwartz, A.B., 1989. Cognitive spatial-motor processes. 3. Motor cortical prediction of movement direction during an instructed delay period. Exp Brain Res 75, 183–194.
Georgopoulos, A.P., Kalaska, J.F., Caminiti, R., Massey, J.T., 1982. On the relations between the direction of two-dimensional arm movements and cell discharge in primate motor cortex. Journal of Neuroscience 2, 1527.
Georgopoulos, A.P., Lurito, J.T., Petrides, M., Schwartz, A.B., Massey, J.T., 1989. Mental rotation of the neuronal population vector. Science 243, 234–236.
Georgopoulos, A.P., Schwartz, A.B., Kettner, R.E., 1986. Neuronal population coding of movement direction. Science 233, 1416–9.
Godschalk, M., Lemon, R.N., Kuypers, H.G., van der Steen, J., 1985. The involvement of monkey premotor cortex neurones in preparation of visually cued arm movements. Behav. Brain Res. 18, 143–157.
Godschalk, M., Lemon, R.N., Nijs, H.G., Kuypers, H.G., 1981. Behaviour of neurons in monkey peri-arcuate and precentral cortex before and during visually guided arm and hand movements. Exp Brain Res 44, 113–116.
Graziano, M.S., Hu, X.T., Gross, C.G., 1997. Visuospatial properties of ventral premotor cortex. J. Neurophysiol. 77, 2268–2292.
Graziano, M.S., Reiss, L.A., Gross, C.G., 1999. A neuronal representation of the location of nearby sounds. Nature 397, 428–430.
Graziano, M.S.A., Taylor, C.S.R., Moore, T., 2002. Complex movements evoked by microstimulation of precentral cortex. Neuron 34, 841–851.
Gu, Y., Watkins, P.V., Angelaki, D.E., DeAngelis, G.C., 2006. Visual and nonvisual contributions to three-dimensional heading selectivity in the medial superior temporal area. J. Neurosci. 26, 73–85.
Hamilton, A.F. de C., Wolpert, D.M., 2002. Controlling the statistics of action: obstacle avoidance. J. Neurophysiol. 87, 2434–2440.
Hatsopoulos, N., Joshi, J., O'Leary, J.G., 2004. Decoding continuous and discrete motor behaviors using motor and premotor cortical ensembles. J. Neurophysiol. 92, 1165–1174.
Hocherman, S., Wise, S.P., 1991. Effects of hand movement path on motor cortical activity in awake, behaving rhesus monkeys. Exp Brain Res 83, 285–302.
Hoshi, E., Tanji, J., 2002. Contrasting neuronal activity in the dorsal and ventral premotor areas during preparation to reach. J. Neurophysiol. 87, 1123–1128.
Hoshi, E., Tanji, J., 2007. Distinctions between dorsal and ventral premotor areas: anatomical connectivity and functional properties. Curr. Opin. Neurobiol. 17, 234–242.
Kakei, S., Hoffman, D.S., Strick, P.L., 2001. Direction of action is represented in the ventral premotor cortex. Nat. Neurosci. 4, 1020–1025.
Kalaska, J.F., Crammond, D.J., 1992. Cerebral cortical mechanisms of reaching movements. Science 255, 1517–1523.
Kalaska, J.F., Crammond, D.J., 1995. Deciding not to GO: neuronal correlates of response selection in a GO/NOGO task in primate premotor and parietal cortex. Cereb. Cortex 5, 410–428.
Kass, R.E., Ventura, V., Brown, E.N., 2005. Statistical issues in the analysis of neuronal data. J. Neurophysiol. 94, 8–25.

Kaufman, M.T., Churchland, M.M., Santhanam, G., Yu, B.M., Afshar, A., Ryu, S.I., Shenoy, K.V., 2010. Roles of monkey premotor neuron classes in movement preparation and execution. J. Neurophysiol. 104, 799–810.
Kurata, K., Hoffman, D.S., 1994. Differential effects of muscimol microinjection into dorsal and ventral aspects of the premotor cortex of monkeys. J. Neurophysiol. 71, 1151–1164.
Kurata, K., Tanji, J., 1986. Premotor cortex neurons in macaques: activity before distal and proximal forelimb movements. J. Neurosci. 6, 403–411.
Kurata, K., Tsuji, T., Naraki, S., Seino, M., Abe, Y., 2000. Activation of the dorsal premotor cortex and pre-supplementary motor area of humans during an auditory conditional motor task. J. Neurophysiol. 84, 1667–1672.
Lebedev, M.A., Wise, S.P., 2001. Tuning for the orientation of spatial attention in dorsal premotor cortex. Eur. J. Neurosci. 13, 1002–1008.
Lu, M.T., Preston, J.B., Strick, P.L., 1994. Interconnections between the prefrontal cortex and the premotor areas in the frontal lobe. J. Comp. Neurol. 341, 375–392.
Messier, J., Kalaska, J.F., 2000. Covariation of primate dorsal premotor cell activity with direction and amplitude during a memorized-delay reaching task. Journal of neurophysiology 84, 152.
Mitchell, J.F., Sundberg, K.A., Reynolds, J.H., 2007. Differential attention-dependent response modulation across cell classes in macaque visual area V4. Neuron 55, 131–141.
Mitz, A.R., Godschalk, M., Wise, S.P., 1991. Learning-dependent neuronal activity in the premotor cortex: activity during the acquisition of conditional motor associations. J. Neurosci. 11, 1855–1872.
Moll, L., Kuypers, H.G., 1977. Premotor cortical ablations in monkeys: contralateral changes in visually guided reaching behavior. Science 198, 317–319.
Moran, D.W., Schwartz, A.B., 1999. Motor cortical representation of speed and direction during reaching. J. Neurophysiol 82, 2676–2692.
Muakkassa, K.F., Strick, P.L., 1979. Frontal lobe inputs to primate motor cortex: evidence for four somatotopically organized "premotor" areas. Brain Res. 177, 176–182.
Murray, E.A., Bussey, T.J., Wise, S.P., 2000. Role of prefrontal cortex in a network for arbitrary visuomotor mapping. Exp Brain Res 133, 114–129.
Nakayama, Y., Yamagata, T., Tanji, J., Hoshi, E., 2008. Transformation of a virtual action plan into a motor plan in the premotor cortex. J. Neurosci. 28, 10287–10297.
Ochiai, T., Mushiake, H., Tanji, J., 2002. Effects of image motion in the dorsal premotor cortex during planning of an arm movement. J. Neurophysiol. 88, 2167–2171.
Paninski, L., Fellows, M.R., Hatsopoulos, N.G., Donoghue, J.P., 2004. Spatiotemporal tuning of motor cortical neurons for hand position and velocity. J. Neurophysiol. 91, 515–532.
Pastor-Bernier, A., Tremblay, E., Cisek, P., 2012. Dorsal premotor cortex is involved in switching motor plans. Front Neuroeng 5, 5.
Pearce, T.M., Moran, D.W., 2012. Strategy-dependent encoding of planned arm movements in the dorsal premotor cortex. Science 337, 984–988.
Pesaran, B., Nelson, M.J., Andersen, R.A., 2006. Dorsal Premotor Neurons Encode the Relative Position of the Hand, Eye, and Goal during Reach Planning. Neuron 51, 125–134.
Pesaran, B., Nelson, M.J., Andersen, R.A., 2010. A relative position code for saccades in dorsal premotor cortex. The Journal of Neuroscience 30, 6527–6537.
Picard, N., Strick, P.L., 2001. Imaging the premotor areas. Curr. Opin. Neurobiol. 11, 663–672.

Picton, T.W., Stuss, D.T., Alexander, M.P., Shallice, T., Binns, M.A., Gillingham, S., 2007. Effects of focal frontal lesions on response inhibition. Cereb. Cortex 17, 826–838.
Quiroga, R.Q., Nadasdy, Z., Ben-Shaul, Y., 2004. Unsupervised spike detection and sorting with wavelets and superparamagnetic clustering. Neural Comput 16, 1661–1687.
Raos, V., Franchi, G., Gallese, V., Fogassi, L., 2003. Somatotopic Organization of the Lateral Part of Area F2 (Dorsal Premotor Cortex) of the Macaque Monkey. J Neurophysiol 89, 1503–1518.
Rathelot, J.-A., Strick, P.L., 2006. Muscle representation in the macaque motor cortex: an anatomical perspective. Proc. Natl. Acad. Sci. U.S.A. 103, 8257–8262.
Reina, G.A., Moran, D.W., Schwartz, A.B., 2001. On the relationship between joint angular velocity and motor cortical discharge during reaching. J. Neurophysiol. 85, 2576–2589.
Rizzolatti, G., Fogassi, L., Gallese, V., 2002. Motor and cognitive functions of the ventral premotor cortex. Current Opinion in Neurobiology 12, 149–154.
Sabes, P.N., Jordan, M.I., 1997. Obstacle avoidance and a perturbation sensitivity model for motor planning. J. Neurosci. 17, 7119–7128.
Sabes, P.N., Jordan, M.I., Wolpert, D.M., 1998. The role of inertial sensitivity in motor planning. J. Neurosci. 18, 5948–5957.
Salinas, E., Abbott, L.F., 1994. Vector reconstruction from firing rates. J Comput Neurosci 1, 89–107.
Santhanam, G., Ryu, S.I., Yu, B.M., Afshar, A., Shenoy, K.V., 2006. A high-performance brain-computer interface. Nature 442, 195–198.
Sawaguchi, T., Yamane, I., Kubota, K., 1996. Application of the GABA antagonist bicuculline to the premotor cortex reduces the ability to withhold reaching movements by well-trained monkeys in visually guided reaching task. J. Neurophysiol. 75, 2150–2156.
Schaal, S., Mohajerian, P., Ijspeert, A., 2007. Dynamics systems vs. optimal control--a unifying view. Prog. Brain Res. 165, 425–445.
Schwartz, A.B., Kettner, R.E., Georgopoulos, A.P., 1988. Primate motor cortex and free arm movements to visual targets in three-dimensional space. I. Relations between single cell discharge and direction of movement. J Neurosci 8, 2913–27.
Schwartz, A.B., Moran, D.W., Reina, G.A., 2004. Differential representation of perception and action in the frontal cortex. Science 303, 380–383.
Shadmehr, R., Wise, S.P., 2005. The Computational Neurobiology of Reaching and Pointing. MIT Press.
Shen, L., Alexander, G.E., 1997. Preferential representation of instructed target location versus limb trajectory in dorsal premotor area. J. Neurophysiol. 77, 1195–1212.
Simon, S.R., Meunier, M., Piettre, L., Berardi, A.M., Segebarth, C.M., Boussaoud, D., 2002. Spatial attention and memory versus motor preparation: premotor cortex involvement as revealed by fMRI. J. Neurophysiol. 88, 2047–2057.
Song, J.-H., McPeek, R.M., 2010. Roles of narrow- and broad-spiking dorsal premotor area neurons in reach target selection and movement production. J. Neurophysiol. 103, 2124–2138.
Stevenson, I.H., Cherian, A., London, B.M., Sachs, N.A., Lindberg, E., Reimer, J., Slutzky, M.W., Hatsopoulos, N.G., Miller, L.E., Kording, K.P., 2011. Statistical assessment of the stability of neural movement representations. J. Neurophysiol. 106, 764–774.

Thach, W.T., 1978. Correlation of neural discharge with pattern and force of muscular activity, joint position, and direction of intended next movement in motor cortex and cerebellum. J. Neurophysiol 41, 654–676.
Torres, E., Andersen, R., 2006. Space-time separation during obstacle-avoidance learning in monkeys. J. Neurophysiol. 96, 2613–2632.
Wang, W., Chan, S.S., Heldman, D.A., Moran, D.W., 2007. Motor Cortical Representation of Position and Velocity During Reaching. Journal of Neurophysiology 97, 4258 –4270.
Weinrich, M., Wise, S.P., 1982. The premotor cortex of the monkey. J. Neurosci. 2, 1329–1345.
Weinrich, M., Wise, S.P., Mauritz, K.H., 1984. A neurophysiological study of the premotor cortex in the rhesus monkey. Brain 107 (Pt 2), 385–414.
Wise, S.P., 1985. The primate premotor cortex: past, present, and preparatory. Annu. Rev. Neurosci. 8, 1–19.
Wise, S.P., Boussaoud, D., Johnson, P.B., Caminiti, R., 1997. PREMOTOR AND PARIETAL CORTEX: Corticocortical Connectivity and Combinatorial Computations 1. Annual review of neuroscience 20, 25–42.
Woltring, H.J., 1986. A Fortran package for generalized, cross-validatory spline smoothing and differentiation. Advances in Engineering Software (1978) 8, 104–113.
Xiao, J., 2005. Premotor neuronal plasticity in monkeys adapting to a new dynamic environment. Eur. J. Neurosci. 22, 3266–3280.
Xiao, J., Padoa-Schioppa, C., Bizzi, E., 2006. Neuronal correlates of movement dynamics in the dorsal and ventral premotor area in the monkey. Exp Brain Res 168, 106–119.
Yang, Y., Liu, S., Chowdhury, S.A., DeAngelis, G.C., Angelaki, D.E., 2011. Binocular disparity tuning and visual-vestibular congruency of multisensory neurons in macaque parietal cortex. J. Neurosci. 31, 17905–17916.
Zach, N., Inbar, D., Grinvald, Y., Bergman, H., Vaadia, E., 2008. Emergence of novel representations in primary motor cortex and premotor neurons during associative learning. J. Neurosci. 28, 9545–9556.